Synthesis and biological properties of synthetic methylene blue analogues

M Weyers

21653100

Dissertation submitted in fulfillment of the requirements for the degree *Magister Scientiae* in Pharmaceutical Chemistry at the Potchefstroom Campus of the North-West University

Supervisor:	Prof JP Petzer
Co-supervisor:	Prof A Petzer
Co-supervisor:	Prof BH Harvey
Assistant supervisor:	Mrs A Delport

November 2016

Preface

Research supported in part by the National Research Foundation (NRF) of South Africa. Grant specific unique reference numbers UID: 100363

Acknowledgment by grant holder that research expressed in any publication generated by NRF supported research are that of the authors, the NRF accepts no liability in this regard.

References were done according to:

NWU. 2012. NWU Referencing Guide. Potchefstroom: Library Services of North-West University, Potchefstroom Campus.

“What We Do In Life Echoes In Eternity” – Maximus (The Gladiator)

Abstract

Methylene blue (MB) has diverse medical applications. Among these, MB may act as an antimalarial agent and has demonstrated potential for the treatment of neurodegenerative disorders such as Alzheimer's disease. MB also possesses promising antidepressant and anxiolytic activity. While MB acts at numerous pharmacological targets, MB is a noteworthy inhibitor of monoamine oxidase A (MAO-A), exhibiting an *in vitro* IC_{50} value of 0.07 μM. MB is a much less potent MAO-B inhibitor with an IC_{50} value of 4.37 μM. While MB possesses an excellent safety profile, in combination with serotonergic agents such as serotonin reuptake inhibitors, MB can induce serotonin toxicity, which is a direct result of its ability to potently inhibit MAO-A. It may therefore be advantageous to "design-out" the MAO-A inhibition properties of MB in order to improve its safety profile. During this study, two new derivatives of MB were synthesized and their *in vitro* interactions with recombinant human MAO-A and MAO-B characterised. The MB analogues, compounds **1** and **2**, were synthesized by reacting phenothiazine with iodine to yield phenothiazin-5-ium tetraiodide hydrate. This intermediate was subsequently treated with an appropriate amine to yield the monosubstituted MB analogues. These new compounds were characterised by nuclear magnetic resonance (NMR) spectroscopy and mass spectrometry (MS). The two MB analogues were evaluated as potential inhibitors of human MAO-A and MAO-B. The results showed that compounds **1** and **2** are significantly weaker as MAO-A inhibitors compared to MB, but display more potent inhibition of the MAO-B isoform compared to MB. The analogues were also found to be reversible MAO inhibitors, although **2** may exhibit some tight-binding to MAO-B. Interestingly, the Lineweaver-Burk plots constructed for the inhibition of the MAOs by **1** and **2** are not typical of competitive inhibition. For the inhibition of MAO-A by **1**, the Lineweaver-Burk plots are indicative of non-competitive inhibition. A modelling study was carried out to propose potential binding orientations of the MB analogues in MAO-A and MAO-B. For this study it may be concluded that, compounds (such as **1**) that potently inhibit both MAO-A and MAO-B would be applicable for the treatment of Parkinson's disease where depression is a comorbidity. Since MAO-A is inhibited reversibly, the possibility of tyramine-induced hypertension is reduced. Serotonin toxicity, however, remain a concern of MB analogues that inhibit MAO-A.

***Key words*:** Depression, Inhibition, Methylene blue, Monoamine Oxidase.

Opsomming

Metileenblou (MB) het verskeie mediese toepassings. MB besit byvoorbeeld antimalaria aktiwiteit en kan moontlik vir die behandeling van neurodegeneratiewe siektes soos Alzheimersiekte aangewend word. MB het ook belowende antidepressant en angsiolitiese aktiwiteite. Alhoewel MB op verskeie farmakologiese teikens werk, is MB 'n merkwaardige inhibeerder van monoamienoksidase A (MAO-A) met 'n *in vitro* IC_{50} waarde van 0.07 µM. MB is 'n minder potente MAO-B-inhibeerder met 'n IC_{50} waarde van 4.37 µM. Alhoewel MB 'n goeie veiligheidsprofiel het, kan dit in kombinasie met serotonergiese middels, soos serotonien heropnameremmers, serotonientoksisiteit veroorsaak wat 'n direkte gevolg van MB se vermoë om MAO-A te inhibeer is. Om MB se veiligheidsprofiel te verbeter mag dit dus voordelig wees om MB-analoë te ontwerp wat nie MAO-A inhibeer nie. In hierdie studie is twee nuwe analoë van MB gesintetiseer en hul *in vitro* interaksies met rekombinante MAO-A en MAO-B gekarakteriseer. Die MB-analoë, verbindings **1** en **2**, is gesintetiseer deur fenotiasien met jodium te reageer om fenotiasien-5-ium tetrajodied hidraat te gee. Hierdie intermediêr is verder behandel met 'n toepaslike amien om die monogesubstitueerde MB-analoë te gee. Hierdie nuwe verbindings is deur kernmagnetieseresonans- (KMR) spektroskopie en massaspektrometrie (MS) gekarakteriseer. Die twee analoë is as potensiële inhibeerders van mens MAO-A en MAO-B geëvalueer. Die resultate wys dat verbindings **1** en **2** aansienlik swakker MAO-A-inhibeerders is as MB, maar as meer potente inhibeerders van die MAO-B-isoform optree vergeleke met MB. Daar is verder gevind dat die analoë omkeerbare MAO-inhibeerders is, alhoewel **2** stewige-binding aan MAO-B kan toon. Lineweaver-Burk grafieke wat vir die inhibisie van die MAO-ensieme deur verbindings **1** en **2** opgestel is, is nie kenmerkend vir kompeterende inhibisie nie. Vir die inhibisie van MAO-A deur verbinding **1**, is die Lineweaver-Burk grafieke aanduidend van nie-kompeterende inhibisie. 'n Moduleringstudie is uitgevoer om die moontlike bindingsoriëntasies van die MB-analoë in MAO-A en MAO-B voor te stel. Hierdie studie maak die gevolgtrekking dat verbindings (soos verbinding **1**) wat beide MAO-A en MAO-B inhibeer, geskik mag wees vir die behandeling van Parkinson se siekte wat met depressie geassosieer word. Omdat MAO-A omkeerbaar geïnhibeer word, is die waarskynlikheid vir tiramien-geïnduseerde hipertensie laag. Serotonientoksisiteit bly egter 'n bekommernis vir MB-analoë wat MAO-A inhibeer.

***Sleutelwoorde*:** Depressie, Inhibisie, Metileenblou, Monoamienoksidase.

Acknowledgements

I wish to express my sincere appreciation to the following people:

My supervisors, Prof. Jacques Petzer, Prof. Anél Petzer, Prof. Brian Harvey and Mrs. Anzelle Delport, thank you for your time and effort, your consistent support and motivation.

To my colleagues and friends, thank you for all your help and encouragement, as well as Prof. Wilna Liebenberg for help with the DSC thermograms.

Many thanks to Fresenius Kabi in aid for laboratory equipment, as well as the National Research Foundation (NRF) for funding.

Abbreviations and Acronyms

A

ACT	Artimisinin-based therapy
AChE	Acetylcholinesterase
ATP	Adenosine triphosphate
APCI	Atmospheric-pressure chemical ionization

B

BASF	Badische Anilin- und Soda-Fabrik
BuChE	Butyrylcholinesterase

C

CH_2	Methylene
CH_3	Methyl
$CuSO_4$	Copper(II)sulfate
cGMP	Cyclic guanosine monophosphate

D

DMSO	Dimethyl sulfoxide
DSC	Differential scanning calorimetry

E

EDRF	Endothelial-Derived Relaxing Factor
ETC	Ethylthioninium chloride

F

$FADH_2$	Flavin adenine dinucleotide
$FeCl_3$	Iron(III)chloride
FST	Forced swim test

H

HRMS	High resolution mass spectra
HCl	Hydrochloric acid
H_2SO_4	Sulphuric acid

I

I.V.	Intravenous
IC_{50}	Inhibitor concentration at 50% inhibition

K

K_2HPO_4	Potassium phosphate
K_i	Dissociation constant
KI	Potassium iodide

L

L-DOPA	Levodopa
LeucoMB	Leucomethylene blue

M

MAO	Monoamine oxidase
MAO-A	Monoamine oxidase isoform A
MAO-B	Monoamine oxidase isoform B
MB	Methylene blue
MS	Mass spectrometry
MG	Methylene green

N

NaCl	Sodium chloride
Na_2S	Sodium sulphide
NADPH	Nicotinamide adenine dinucleotide phosphate
$Na_2S_2O_3$	Sodium thiosulfate
$Na_2Cr_2O_7$	Sodium dichromate
NMR	Nuclear magnetic resonance
NO	Nitric oxide
NOS	Nitric oxide synthases
NO-cGMP	Nitric oxide-cyclic guanosine monophosphate
NRF	National Research Foundation

P

PBS	Phosphate-buffered saline
ppm	Parts per million
pH	Potential of hydrogen
pKa	Acid dissociation constant

R

Rf	Retardation factor
ROS	Reactive oxygen species

S

SD	Standard deviation
SERT	Serotonin transporter
SI	Selectivity index
SRIs	Serotonin reuptake inhibitors
ST	Serotonin toxicity

T

TCA	Tricyclic antidepressant
TLC	Thin layer chromatography

Table of Contents

List of Figures

List of Tables

Chapter 1
Introduction

1.1 Research problem

MB has multiple pharmacological actions:

Methylene blue (MB) (Figure 1.1) is considered to have diverse medical applications. In recent years the focus has shifted to MB as a potential antimalarial agent and as a potential treatment of neurodegenerative disorders such as Alzheimer's disease, possibly through its inhibition of the aggregation of tau protein and enhancement of mitochondrial respiration (Schirmer *et al*., 2011; Oz *et al*., 2009). Although the tricyclic structure of MB bears a strong resemblance to the tricyclic antidepressants (TCAs), it has other unique physicochemical attributes, including an ionic charge (Oz *et al*., 2011). MB possesses promising antidepressant (Harvey *et al*., 2010) and anxiolytic (Eroğlu & Cağlayan, 1997) activity in pre-clinical models and has shown promise in clinical trials for bipolar disorder and depressive illness (Naylor *et al*., 1987). MB is a noteworthy inhibitor of monoamine oxidase A (MAO-A), inhibiting recombinant human MAO-A *in vitro* with an IC_{50} value of 0.07 μM (Harvey *et al*., 2010; Ramsay *et al*., 2007). MB is a much less potent MAO-B inhibitor with an IC_{50} value of 4.37 μM (Harvey *et al*., 2010). MAO-A inhibition is a well-established mechanism of action for the MAO inhibitor class of antidepressants, of which the selective MAO-A inhibitor moclobemide is the best known (Brunton *et al*., 2010). MAO-B inhibitors, in turn, are established as treatment for Parkinson's disease.

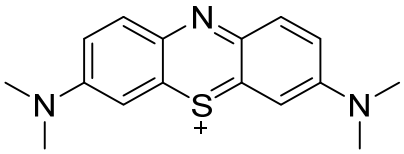

Figure 1.1. The structure of MB (Oz *et al*., 2009).

*MB and other MAO-A inhibitors interact with tyr*amine:

Irreversible MAO-A inhibitors may cause a potentially fatal adverse effect, termed the "cheese reaction" that occurs when MAO-A inhibitors are combined with tyramine-containing food such as cheese and wine. MAO-A inhibitors prevent the metabolism of tyramine in the gastrointestinal mucosa and hepatic tissues leading to high systemic concentrations of tyramine and an elevation in blood-pressure (Da Prada *et al*., 1988; Flockhart, 2012). Because

of concern for a hypertensive crisis due to the interaction between inhibitors of MAO-A with tyramine and other monoamine-releasing compounds (Brunton *et al*., 2010), MAO inhibitors are used more restrictively in the clinic and are reserved for the treatment of resistant forms of depression (Gillman, 2011). Although the reversible MAO-A inhibitor, moclobemide, is less prone to causing this potentially lethal drug interaction, it is markedly less potent than irreversible MAO inhibitors such as tranylcypromine (Gillman, 2011). Despite these concerns, there is a growing interest in the clinical benefit and utility of MAO inhibitors in the treatment of depression (Gillman, 2011). There would thus be great value in developing a high potency but reversible MAO-A inhibitor for the treatment of depression. Moreover, due to the increasing use of MB as an antioxidant for treating methaemoglobinemia, ifosfamide-induced encephalopathy, malaria and the prevention of urinary tract infections (Coulibaly *et al*., 2009; Querfurth & LaFerla, 2010; Singh *et al*., 2012), as well as increased interest in its use for treating Alzheimer's disease and bipolar disorder noted earlier, MB analogues with an improved safety profile with respect to the inhibition of MAO-A may be of value.

MB and serotonin toxicity:

Another disadvantage of MB as a drug is that, in combination with serotonergic agents such as serotonin reuptake inhibitors (SRIs), MB can induce serotonin toxicity (ST), which is a direct result of its ability to potently inhibit MAO-A. It may therefore be advantageous to "design-out" the MAO-A inhibition properties of MB in order to improve its safety profile (Petzer *et al*., 2012; Ramsay *et al*., 2007). In this study we propose to design and synthesise new derivatives of MB and to characterise their interactions with human MAO-A and MAO-B. Many of MB's effects are, however, mediated by its effect on mitochondrial function (Atamna *et al*., 2008; Louters *et al*., 2006), by acting as an alternative electron acceptor/donor MB improves neuronal energy production and inhibits the formation of superoxide, effects which also may contribute to its antidepressant activity (Atamna *et al*., 2008; Petzer *et al*., 2012). Because of the great interest in MB, this study will synthesise additional MB analogues with the aim to establish how structural modification of MB affects its MAO inhibition properties. The charged structure of MB will be retained in the analogues since this is key to MB's unique redox properties and mitochondrial respiration enhancing effects (Harvey *et al*., 2010).

MB analogues as antidepressants and therapy for Parkinson's disease:

MB analogues that potently inhibit MAO-A with a reversible mode of action would be suitable as antidepressant agents. As mentioned above, such compounds are less likely to lead to tyramine-induced adverse effects than irreversible acting MAO-A inhibitors. Potent MAO-A inhibitors, whether acting reversibly or irreversibly, however, may cause

ST when combined with serotonergic drugs. MB analogues with potent MAO-B inhibition activity would also be of great interest for the treatment of Parkinson's disease. In the central nervous system, MAO-B is a major catabolic enzyme of dopamine, and inhibition of this enzyme conserves the central dopamine supply (Youdim & Bakhle, 2006). MAO-B inhibitors are thus used to alleviate the central dopamine deficiency that underlies the motor symptoms of Parkinson's disease. L-Dopa, the metabolic precursor of dopamine, is the treatment of choice for Parkinson's disease. L-Dopa is frequently combined with MAO-B inhibitors with the aim of further enhancing central dopamine levels (Finberg *et al*., 1998). In early Parkinson's disease, monotherapy with MAO-B inhibitors may delay the necessity for L-Dopa therapy (Pålhagen *et al*., 1998). Currently two irreversible MAO-B inhibitors, selegiline [(R)-deprenyl] and rasagiline, are employed in the clinic for the treatment of Parkinson's disease. An MB analogue with high potency MAO-B inhibition would be of value for symptomatic treatment of Parkinson's disease, particularly in combination with L-Dopa. Since Parkinson's disease has been associated with mitochondrial dysfunction and oxidative stress, the potential mitochondrial respiration enhancing effects of MB analogues may be of further value in Parkinson's disease and may slow the degenerative process (Atamna *et al*., 2008; Louters *et al*., 2006). As mentioned, MB analogues that potently inhibit MAO-B, but exhibit low MAO-A inhibition would also be considered useful since such compounds would have a low risk of causing ST. Depression is highly comorbid in patients with Parkinson's disease (Rana *et al.*, 2016). However, many of the most popular antidepressants, in particular the serotonin reuptake inhibitors (SRI), may suppress striatal dopamine release and worsen the motor symptoms of the disease (Harvey *et al*., 1999). Thus MB-related analogues may represent a novel therapeutic option that will adequately address both illnesses.

1.2 Aim and objectives

The aim of this study:

In the present study selected MB analogues will be synthesized and characterised by nuclear magnetic resonance (NMR) spectroscopy and mass spectrometry (MS). The successfully synthesized MB analogues will subsequently be evaluated as potential inhibitors of human MAO-A and MAO-B.

The objectives of this study are:

1. Selected MB analogues will be synthesized by firstly reacting phenothiazine with iodine to yield phenothiazin-5-ium tetraiodide hydrate. Phenothiazin-5-ium tetraiodide hydrate will, in turn, be treated with a selected amine to yield the MB analogues (Strekowski *et al*., 1993).

2. The synthesized MB analogues will be evaluated as inhibitors of human MAO-A and MAO-B, and the inhibition potencies will be expressed as the corresponding IC_{50} values. Structure-activity relationships may be derived by comparing these IC_{50} values with those reported for MB.
3. For those MB analogues that inhibit the human MAOs, the reversibility of MAO inhibition will be examined by dialysis.
4. For reversible interaction with the MAOs, the enzyme-inhibitor dissociation constants (K_i values) will be measured. For this purpose Lineweaver-Burk (double-reciprocal) and Michaelis-Menten plots will be constructed.
5. MB and the MB analogues will be computationally docked into active site models of human MAO-A and MAO-B in order to determine potential binding modes and interactions of the analogues with the enzymes.

1.3 Research hypothesis

This study hypothesises that selected MB analogues will act as inhibitors of human MAO-A and MAO-B. This hypothesis is based on the observation that MB is an inhibitor of human MAO-A with an IC_{50} value of 0.07 μM (Harvey *et al*., 2010). MB's principal metabolite, azure B (Figure 1.2) is an even more potent inhibitor of human MAO-A with an IC_{50} value of 0.01 μM (Petzer *et al*., 2012). Other structural analogues, such as ethylthioninium chloride (ETC), also inhibit the human MAOs. With ETC the dimethylamine groups of MB were replaced by diethylamine groups to yield a structure with more steric bulk. Larger compounds are less likely to fit within the MAO-A active site, and should be lower potency MAO-A inhibitors. This compound indeed inhibited MAO-A (IC_{50} = 0.510 μM) with lower potency compared to MB (IC_{50} = 0.07 μM) and azure B (IC_{50} = 0.01 μM) (Delport *et al*., 2014). ETC also inhibits MAO-B with an IC_{50} value of 0.592 μM (Delport *et al*., 2014). In this instance, the increased steric bulk of ETC enhanced MAO-B inhibition compared to MB (IC_{50} = 4.37 μM) and azure B (IC_{50} = 0.968 μM).

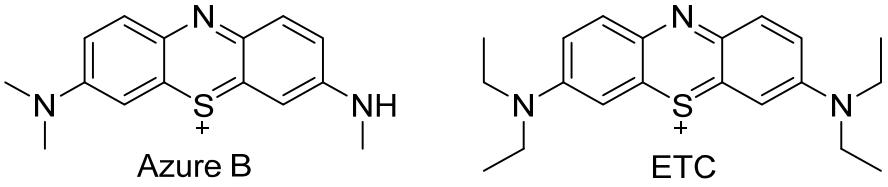

Figure 1.2. The structures of azure B and ETC (Delport *et al*., 2014; Petzer *et al*., 2012).

Based on the outcome of the MAO inhibition studies of the current study, the following may be observed:

- Compounds that are devoid of MAO-A inhibition, or that exhibit a very low degree of inhibition, while acting as potent MAO-B inhibitors will be particularly appealing for the treatment of Parkinson's disease. Such compounds will possess a very low probability of causing ST or tyramine-induced hypertension, adverse effects that are linked to the inhibition of MAO-A.
- Compounds that potently inhibit MAO-A (but not MAO-B), but with a reversible mode of action would be useful as potential antidepressant agents. Such compounds would be less likely to cause tyramine-induced hypertension than irreversible MAO-A inhibitors, but ST may still occur.
- Compounds that potently inhibit both MAO-A and MAO-B would be applicable for the treatment of Parkinson's disease where depression is a comorbidity. In this instance, MAO-A should be inhibited reversibly to reduce the possibility of tyramine-induced hypertension. Since MB, azure B and ETC are reversible MAO inhibitors, it is anticipated that other MB analogues will also exhibit a reversible mode of inhibition (Delport *et al*., 2014; Harvey *et al*., 2010; Petzer *et al*., 2012).
- Compounds that are devoid of MAO inhibition may be evaluated in future studies for activity at other targets relevant to MB such as enhancement of mitochondrial respiration, reduction of oxidative stress and inhibition of nitric oxide synthase (NOS).

1.4 MB analogues that were synthesized in this study

As will be discussed in Chapter 3, the synthesis of MB analogues is challenging and often yields mixtures of products that are difficult to separate by chromatography. Traditional synthetic protocols employ metals as reactants which represent a major disadvantage since MB and its analogues are known to form metal chelates. It's challenging to separate the final MB analogues from the metal ions, which affects the recording of NMR spectra and may even impact on the results of biological studies.

The most convenient route to MB analogues is that first reported by Strekowski *et al.* (1993). In this protocol, phenothiazine is reacted with iodine to yield phenothiazin-5-ium tetraiodide hydrate. The intermediate is subsequently treated with an appropriate amine to yield the disubstituted or monosubstituted MB analogue, depending on the stoichiometry of the amine and phenothiazinium reactants. After considerable experimentation with various amine substrates, and trial-and-error with respect to the synthetic procedure, two MB analogues were successfully synthesized in this study. Their structures are shown in figure 1.3. As will be

discussed in subsequent chapters, the MAO inhibition studies and physicochemical characterisations were carried out with these MB analogues.

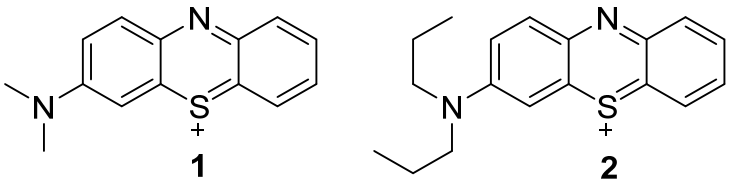

Figure 1.3. The structures of the MB analogues that were synthesized in this study.

Chapter 2
Literature background

2.1 General background and history

The phenothiazine structure has featured in medical applications for more than 100 years and is the most recurrent pharmaceutical chemical compound of all time. It is used in multiple spectrums of disorders and physiological diseases (Wainwright & Crossley, 2002). MB is a heterocyclic aromatic compound composed of the phenothiazine nucleus and is considered to be one of the most useful lead structures of the 20th century (Ohlow & Moosmann, 2011). In 1876, MB was synthesized for the first time by Heinrich Caro of Badische Anilin- und Soda-Fabrik (BASF) for use as a potential cotton stain (Caro, 1877). In that time it was also discovered that, with different dyes, one can stain cellular structures as well as selectively inactivate microbial species. This led to the proposal that MB may act as a medicine and MB was subsequently used for the first time for the treatment of malaria by Guttmann and colleagues in 1891 (Coulibaly *et al*., 2009). MB is not only the first synthetic drug against malaria, but also the first ever synthetic compound to be used therapeutically as an antiseptic clinical dye (Schirmer *et al*., 2003). Soon after this, MB was used for a variety of conditions including psychiatric disorders, and ultimately in this manner, the antidepressant and psychotropic effects of MB were discovered (Harvey *et al*., 2010). MB also served as the lead compound for drugs such as chlorpromazine and the tricyclic antidepressants, drugs which have been used in clinical practise for many years.

In recent years, interest in MB has been renewed, especially since previously unknown pharmacological actions of MB have been discovered (Schirmer *et al*., 2003). For example, MB has been demonstrated to be a MAO-A and MAO-B inhibitor with an IC_{50} value of 0.07 µM for the inhibition of MAO-A (Aeschlimann *et al*., 1996; Harvey *et al*., 2010) and an IC_{50} value of 4.37 µM for the inhibition of MAO-B (Harvey *et al*., 2010; Ramsay *et al*., 2007). Many of MB's effects are, however, mediated by its effect on mitochondrial function (Atamna *et al*., 2008; Louters *et al*., 2006). By acting as an alternative electron acceptor/donor, MB improves neuronal energy production and inhibits the formation of superoxide, effects which also may contribute to its antidepressant activity (Atamna *et al*., 2008; Narsapur & Naylor; 1983, Petzer *et al*., 2012). Also closely associated with its effect on mitochondrial function is the ability of MB to scavenge reactive oxygen species (ROS), an effect which may play an important role in the neuroscience of depression and treatment of psychiatric disorders (Bernstein *et al*., 1998; Harvey, 1996; Harvey *et al*., 2010). MB is a non-selective nitric oxide

synthase (NOS) and guanylate cyclase inhibitor (Moore & Handy, 1997), which suggests that MB has the ability to alter the nitric oxide-cyclic guanosine monophosphate (NO-cGMP) pathway (Garthwaite, 1991). Modulation of the nitric oxide-cGMP pathway is now widely recognised as a potentially novel target for psychotropic drug action (Brink *et al.*, 2008; Harvey *et al*., 1994; Harvey, 1996; Harvey *et al.*, 2010; Liebenberg *et al.*, 2010; Wegener *et al.*, 2010). These mechanisms of action (MAO-A inhibition, modulation of the NO-cGMP pathway, enhancement of mitochondrial function and scavenging of ROS) are closely related to MB's anxiolytic and antidepressant effects (Harvey *et al.*, 2010).

As mentioned, MB possesses antimalarial activity (Akoachere *et al*., 2005). MB may exert its action by interacting with parasite disulphide reductase enzymes (Buchholz *et al.,* 2008). This ultimately results in the increased production of ROS and subsequently parasite death. Although artemisinin-based therapy (ACT) is highly effective against malaria in several field trails, the drug is expensive in the Sub-Saharan Africa setting (Kouyaté *et al*., 2007; Wiseman *et al*., 2006). In recent studies MB has demonstrated the potential to eradicate parasites in combination with artemisinin-based therapy, and closer attention must be paid to MB as a drug against malaria (Zoungrana *et al*., 2008). MB used in combination with other antimalarial drugs may serve as an effective and viable treatment of malaria. Furthermore, evidence of MB synergy with artemisinin derivatives against malaria was observed in *in vitro* studies (Akoachere *et al*., 2005).

Besides its potential as treatment for affective disorders and malaria, MB has other therapeutic applications. A common clinical application of MB is the treatment of methemoglobinemia (Cawein *et al*., 1964). MB is also used for the treatment of isofosfamide-induced encephalopathy (Aeschlimann *et al*., 1996; Alici-Evcimen & Breitbart, 2007). In recent years, MB has been proposed as a potential treatment for Alzheimer's disease, in part because of its action as a mitochondrial metabolic enhancer and an inhibitor of the enzyme, acetylcholinesterase (AChE) (Cawein *et al*., 1964; Louters *et al*., 2006). Because of the significant interest in MB, this study will synthesise MB analogues with the aim of establishing how structural modification of MB affects selected pharmacological properties.

2.2 Select physicochemical properties of MB

Physicochemical properties:

MB (tetramethylthionine, $C_{16}H_{18}N_3S$) is an aromatic and cationic heterocyclic phenothiazine compound which has a molecular weight of 284.399 g/mol (Wainwright & Crossley, 2002). Crystalline MB is available as the chloride salt.

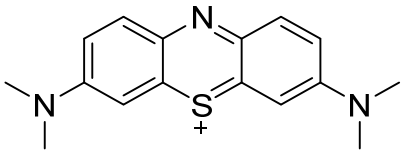

Figure 2.1. The structure of MB (Oz *et al.*, 2009).

MB is soluble in water and interestingly also dissolves in certain organic solvents such as chloroform. In the solid state, MB is an odourless dark blue to green crystal, and yields a blue solution when dissolved in water (Ramsay *et al*., 2007; Wagner *et al*., 1998). In the oxidised state, MB solutions has a blue colour, which is due to the fact that the phenothiazinium molecule absorbs visible light strongly in the region of 600–700 nm, thus allowing for the remainder of the visible spectrum (350–600 nm) to be transmitted (Ramsay *et al*., 2007). MB's conversion to its reduced form, leuco-methylene blue (leucoMB), as demonstrated below in Figure 2.2, is caused by reducing agents such as nicotinamide adenine dinucleotide phosphate (NADPH) (Schirmer *et al*., 2011).

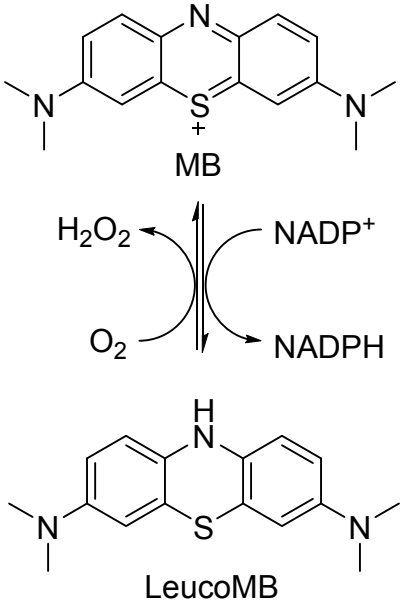

Figure 2.2. The reduction of MB to leucoMB (Schirmer *et al*., 2011).

LeucoMB is colourless and does not absorb light in the visible region (Ramsay *et al*., 2007). MB shows a redox potential of 11 mV, indicating that MB cycles efficiently between the oxidised and reduced forms. A reducing agent such as NADPH thus has the ability to reduce MB to leucoMB. LeucoMB can be reoxidised to yield MB in the presence of O_2 as well as other electron acceptors such as cytochrome *c* and heme proteins (McCord & Fridovich, 1969).

Brain penetration:

MB has been demonstrated to cross the blood-brain barrier (Sweet & Standiford, 2007). Although MB is ionised, the charge is dispersed and distributed throughout the molecule. This property may facilitate MB's entry into the brain (Wagner *et al*., 1998). In this respect, MB's charge in not localised on the nitrogen and sulphur atoms, but is rather distributed equally on the surface of the molecule (Wagner *et al*., 1998). Another factor that determines the membrane penetration of MB is the difference in ionisation state and lipophilicity between LeucoMB and MB. In the pH range of 1–8, MB is completely ionised since it displays a pKa value of approximately 0–1 (DiSanto & Wagner, 1972). Given MB's positive charge it is expected to be hydrophilic and should not be able to pass through the lipid bilayers of membranes. Positively charged MB is, however, reduced to leucoMB by redox reaction systems in peripheral tissue. Since leucoMB is neutral, this compound may cross membranes and are taken up by cells (Clifton & Leikin, 2003; DiSanto & Wagner, 1972; Lorke *et al*., 2008). LeucoMB displays a pKa of 5.8, which suggests that at least a fraction exists as the unionised form at physiological pH. Since leucoMB is approximately 20-fold more lipophilic than MB the unionised fraction of leucoMB is expected to readily penetrate biological membranes (Müller, 1998, 2000). It has therefore been suggested that, by the action of reducing agents such as NADPH, MB is reduced to the uncharged leucoMB, which rapidly enters cells and tissues. Once in the intracellular compartment leucoMB is reoxidised to MB (Müller, 1998, 2000). At high concentrations (e.g. 10 mM) MB forms dimers and may accumulate in cellular organelles, which may lead to cell toxicity (Clifton & Leikin, 2003).

Pharmacokinetic properties:

As mentioned, after MB is taken up by cells, it may dimerise in the cytoplasmic organelles, and lead to DNA damage and cellular toxicity (Clifton & Leikin, 2003; Wagner *et al*., 1998). MB forms dimers at concentrations higher than 10 mM with a dissociation constant of 170 mM (Buchholz *et al*., 2008; Wagner *et al*., 1998) and induces cell toxicity. Such toxicity has for example been demonstrated *in vitro* using MB and ETC (Delport *et al*., 2014). The accumulation of MB in various cellular tissues is a complex process and is dependent on the reduction of MB to leucoMB. This in turn is determined by the oxidant status of the cellular tissue (Bongard *et al*., 1994; Wagner *et al*., 1998). After oral administration of 100 mg MB,

whole blood MB concentrations in healthy individuals were shown to be one order of magnitude lower than after intravenous (I.V.) administration of the same dosage regime (Peter *et al*., 2000). However, by comparing the administration of single doses of MB (50 mg I.V. versus 500 mg orally) a recent study indicated that the absolute bioavailability of MB after oral administration was 72.3% (Walter-Sack *et al*., 2009). The conflicting observations between these studies demonstrate aspects such as different methodologies and cellular uptake, mode of application as well as blood versus plasma measurements (Walter-Sack *et al*., 2009). When MB is administered I.V. it displays a terminal plasma half-life of 5–7 h with multi-compartmental pharmacokinetics (Peter *et al*., 2000). The organ distribution of MB differs remarkably when comparing oral with I.V. administration. Oral MB results in higher intestinal and liver concentrations while I.V. administration results in higher cerebral concentrations (Peter *et al*., 2000).Total urinary recovery of MB ranges from 53 to 97% of its oral dose (DiSanto & Wagner, 1972). The colour of the urine following oral administration of MB was shown to be unrelated to the amount absorbed, since a considerable percentage of the dye (33–78%) recovered in the urine was excreted as stabilised leucoMB (DiSanto & Wagner, 1972; Peter *et al*., 2000). In clinical applications, MB usually produces blue-green urine, blue sclera and stained clothing. This benign discoloration can be alarming to patients, although it is self-limiting and disappears within a few days of discontinuing the drug.

2.3 The metabolism of MB

It has been demonstrated that MB is metabolised to N-demethylated metabolites in humans, with azure B as the major metabolite and azure A as the secondary metabolite (Figure 2.3) (Warth *et al*., 2009). The examination of autopsied peripheral organs of a patient receiving I.V. MB has demonstrated that the concentrations of MB in the tissues of these peripheral organs are 74–208 ng/g, while the concentrations of azure B (475–2943 ng/g) are significantly higher (Warth *et al*., 2009). Although azure B has been reported to possess pharmacological effects, with the exception of recent studies by Petzer *et al*. (2012; 2014), these actions have not been studied in any detail. Importantly, azure B possesses superior activities compared to MB at a variety of biochemical targets, such as inhibiting Aβ-peptide aggregation, inhibiting MAO-A, and in certain instances azure B has been found to elicit improved therapeutic responses in animal models such as protecting mice from endotoxic shock as well as antidepressant-like effects (Culo *et al*., 1991; Delport *et al*., 2014; Taniguchi *et al*., 2005).

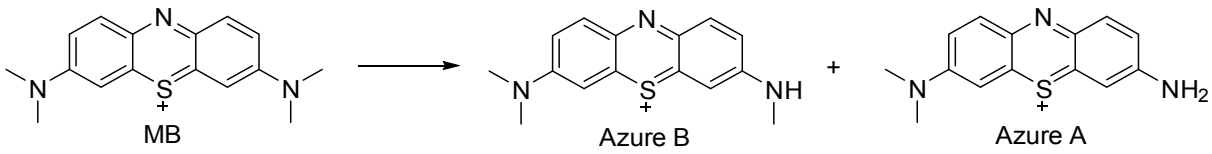

Figure 2.3. The metabolism of MB to yield azure A and azure B (Warth *et al*., 2009).

2.4 Neurohistology of MB

The first staining of nervous tissue with MB by I.V. administration to a living animal was carried out in 1886 by Paul Ehrlich (Coulibaly *et al*., 2009). Following Ehrlich, numerous studies and various methods where developed and employed for vital and supra-vital neuronal structure staining with MB (Barbosa & Peters, 1971). MB has also been used for locating cutaneous nerve motor endings (Cheng, 1954; Volke *et al*., 1999; Wegener *et al*., 2000) and it has been demonstrated that MB has a high affinity for binding to nervous tissue and autonomous nerve fibres (Imaizumi *et al*., 1959).

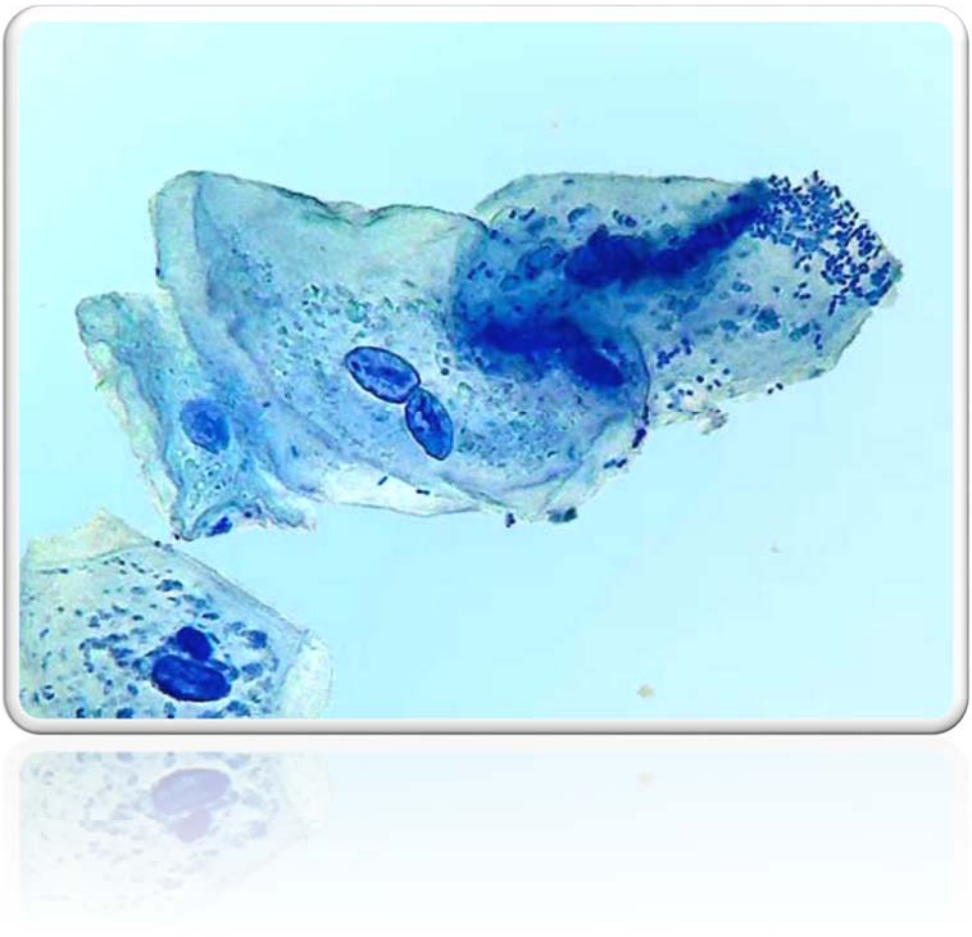

Figure 2.4. An example of tissue stained by MB (Dioni, 2011).

2.5 The biochemistry of MB

2.5.1 Inhibition of AChE

Acetylcholine plays an important role in cognitive functions (Giacobini, 2003; Holzgrabe *et al*., 2007). The enzyme acetylcholine esterase (AChE) hydrolyses acetylcholine and thus terminates the action of acetylcholine at synapses (Deiana *et al*., 2009). MB is a notable inhibitor of AChE (Pfaffendorf *et al*., 1997; Petzer *et al*., 2014) and may thus find application in the treatment of Alzheimer's disease. Laboratory evidence suggests that the degeneration of cholinergic neurons in the basal forebrain results in a reduction of acetylcholine levels, which is associated with Alzheimer's disease (Holzgrabe *et al*., 2007; Nordberg, 2006). The cholinergic system is thus an important target for drug design directed towards the treatment of Alzheimer's disease (Deiana *et al*., 2009) and inhibitors of AChE will indirectly enhance the reduced cholinergic neurotransmission seen in Alzheimer's disease (Deiana *et al*., 2009; Holzgrabe *et al*., 2007; Pfaffendorf *et al*., 1997). AChE inhibitors are currently used in Alzheimer's disease patients as long-term symptomatic treatment (Holzgrabe *et al*., 2007). The potential of MB in Alzheimer's disease has been demonstrated on several occasions. For example, the cognitive deficits induced by a potent muscarinic receptor antagonist, scopolamine, was reversed by MB in mice (Deiana *et al*., 2009). A second enzyme responsible for the metabolism of acetylcholine namely butyrylcholinesterase (BuChE), is also inhibited by MB (Pfaffendorf *et al*., 1997). It has been suggested that mixed AChE and BuChE inhibitors such as MB, may be more effective in the treatment of Alzheimer's disease (Abi-Gerges *et al*., 1997).

2.5.2 Monoamine oxidase

MAO is an enzyme that is attached to the outer mitochondrial membrane. MAO is a flavin-containing enzyme and consists of two isoforms, namely MAO-A and MAO-B (Edmondson *et al*., 2007). These enzymes are drug targets for the development of antidepressant drugs and drugs for the treatment of neurodegenerative disorders such as Parkinson's disease (Binda *et al*., 2002). The principal function of the MAOs is the metabolism of catecholamine neurotransmitters (Ghaemi *et al*., 2001). MAO-A is mainly responsible for metabolism of serotonin and noradrenaline and inhibitors of MAO-A have been used as antidepressant drugs in the clinic (Tariot *et al*., 1987). MAO-B is mainly responsible for the metabolism of dopamine in the brain and inhibitors of MAO-B have been used as therapy for Parkinson's disease (Glover *et al*., 1977). Recent studies have shown that MB inhibits the MAO enzymes (Oxenkrug *et al*., 2007; Ramsay *et al*., 2007). MB is a potent *in vitro* inhibitor of human MAO-A with an IC_{50} value of 0.07 μM, and this inhibitory effect of MAO-A may, at least in part, explain the antidepressant effects of MB (Aeschlimann *et al*., 1996; Harvey *et al*., 2010;

Ramsay *et al*., 2007). MB also inhibits MAO-B, but with lower potency compared to MAO-A. MB inhibits MAO-B with an IC_{50} value of 4.37 μM (Harvey *et al*., 2010; Ramsay *et al*., 2007). MB's principal metabolite, azure B, also is a MAO inhibitor and displays an IC_{50} value of 0.11 μM and 968 μM for the inhibition of MAO-A and MAO-B, respectively (Delport *et al*., 2014; Harvey *et al*., 2010; Petzer *et al*., 2012).

2.5.3 MB inhibits the nitric oxide-cGMP pathway

Nitric oxide (NO), originally termed Endothelial-Derived Relaxing Factor (EDRF) before it was identified as NO, fulfil important physiological roles within the cardiovascular, immune and central and peripheral nervous systems (Hibbs *et al*., 1987; Oosthuizen *et al*., 2005; Palmer *et al*., 1987). NO is produced in neurons from the amino acid, L-arginine, by action of the enzyme, nitric oxide synthase (NOS). Guanylate cyclase is one of the main targets of NO, and by binding to the heme part of this enzyme, NO activates soluble guanylate cyclase. This activation leads to an increase in cyclic guanosine monophosphate (cGMP) formation (Dawson & Snyder, 1994). It is generally accepted that NO exerts its effects through the production of cGMP (Moncada *et al*., 1991).

MB, by oxidation of the enzyme-bound ferrous iron, directly inhibits and inactivates constitutive and inducible forms of NOS (Mayer *et al*., 1993; Volke *et al*., 1999). Furthermore, MB also inhibits guanylate cyclase activity (Lo *et al*., 2014). The inhibition of NOS and guanylate cyclase reduces cGMP formation and in this way MB modulates NO-cGMP signalling. MB may also directly react and inactivate NO (Mayer *et al*., 1993; Volke *et al*., 1999). These pharmacological properties of MB may find application in disorders such as depression (Krass *et al*., 2011). In animal models, NOS inhibitors display antidepressant-like effects (Harkin *et al*., 1999), while plasma nitrite concentrations, an index of NO production, is increased in patients with depression which suggests that elevated levels of NO may contribute to the neurochemistry and neuropathology of depression (Suzuki *et al*., 2001; Taniguchi *et al*., 2005).

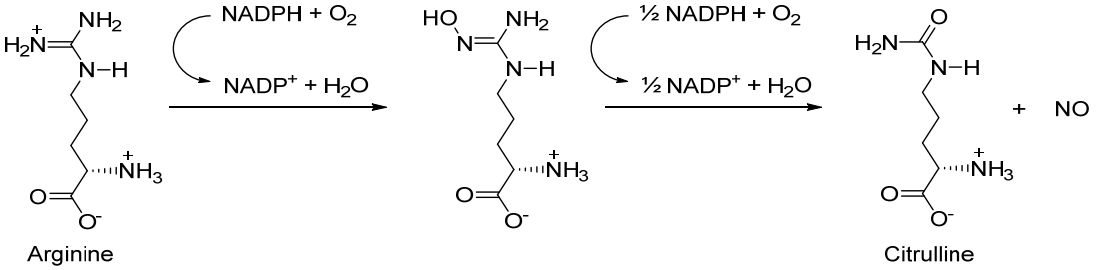

Figure 2.5. The production of NO by the action of NOS on L-arginine. The NOS enzyme uses 3/2 equivalents of NADPH to reduce arginine to citrulline, with the formation of NO (Dawson & Snyder, 1994).

2.5.4 MB enhances mitochondrial respiration

The enhancement of cognitive function in Alzheimer's disease with MB has been linked to it's ability to enhance the function of the mitochondrial respiratory chain (Rojas *et al*., 2012). By acting as an oxidation/reduction couple, MB and leucoMB can interact directly with the mitochondrial respiratory chain. MB may oxidise reduced coenzyme Q while leucoMB may possibly reduce cytochrome C (Scott & Hunter, 1966). This increases the activity of cytochrome oxidase and as a result, mitochondrial respiration. MB thus increases oxygen consumption and enhances the production of adenosine triphosphate (ATP) (Wong-Riley, 1989; Zhang *et al*., 2006). The effect of MB on mitochondrial respiration is relevant in states of impaired function of the respiratory chain. These include Alzheimer's disease and depression. For example, in depressive patients muscle mitochondria produce lower amounts of ATP and the function of complexes I + III and II + III are impaired (Gardner *et al*., 2003). Indeed, depression has been proposed to represent a form of encephalopathy where disordered mitochondrial and redox status may underlie many of the more well-described disturbances recognised in mood disorders, in particular disordered monoamines (Harvey, 2008). In Alzheimer's disease, reduced mitochondrial respiration has been linked to memory deficits and neurodegeneration (Bennett *et al*., 1992; Gonzalez-Lima & Bruchey, 2004). Tissues such as neuronal tissue with high metabolic demands will benefit most from the respiration enhancing effects of MB.

2.5.5 MB reduces oxidative stress

MB is a potent antioxidant since it can accept electrons directly from the electron transport chain. This is particularly relevant in conditions where mitochondrial respiration is impaired. In conditions of impaired mitochondrial respiration, oxygen (O_2) accepts electrons "leaking" from the electron transport chain to yield superoxide. MB may reduce superoxide production by scavenging these electrons "leaking" from the electron transport chain. The reduced formation of superoxide will decrease oxidative stress in conditions of impaired mitochondrial respiration. In support of this view, MB significantly increases the rate of ATP production by mitochondria inhibited by complex I or complex III inhibitors, with no increase in superoxide noticed (Tretter *et al*., 2014). Because of its ability to readily undergo reduction to leucoMB, MB may scavenge electrons in all cell compartments and not only in mitochondria. MB may be viewed as a general cellular antioxidant (Rojas *et al*., 2012; Salaris *et al*., 1991).

2.5.6 MB as redox active compound in malaria

MB's ability to undergo reduction to leucoMB and reoxidation to MB plays an important role in its antimalarial activity. MB has been demonstrated to interact with parasite disulphide reductase flavoenzymes, such as glutathione reductase and thioredoxin reductase (Buchholz

et al., 2008; Haynes *et al*., 2010). The reduction of MB by reduced flavin adenine dinucleotide ($FADH_2$), the reduced flavoenzyme cofactor, yields leucoMB. MB is regenerated from leucoMB via oxidation by oxygen, with concomitant formation of ROS (Buchholz *et al*., 2008). Reduced NADPH, which is required for reduction of FAD to $FADH_2$, is subsequently depleted in a cycle involving reduction of MB to leucoMB. This in turn greatly impairs the disulphide reductase function and capacity to counter enhanced oxidative stress in the malarial parasite. In the presence of MB, parasite death is thus caused by oxidative stress, particularly the inability of the parasite to counter oxidative stress normally encountered in its environment.

2.5.7 MB as a photosensitizer

Photosensitizers are used in the treatment of cancer and may possibly also be used for microbial infections. A photosensitizer acts by absorbing light and in return produces reactive oxygen species (ROS). The ROS are then responsible for initiating cell death. MB acts as a photosensitizer and produces superoxide (from oxygen) when irradiated by light. MB absorbs light in the 600-660 nm region, the appropriate wavelength region for photodynamic therapy (Gorman *et al*., 2006; Tardivo *et al*., 2005; Wainwright *et al*., 2009).

2.6 Clinical use and potential applications of MB

2.6.1 MB and isofosfamide-encephalopathy

MB is well-known for the treatment of ifosfamide-induced encephalopathy (Ajithkumar *et al*., 2007; Oz *et al*., 2011; Querfurth & LaFerla, 2010). Isofosfamide is used in a wide range of tumours and hematologic malignancies as an alkylating agent. However, its use may result in neuropsychiatric toxicity, which is known as isofosphamide-induced encephalopathy (Aeschlimann *et al*., 1996; Alici-Evcimen & Breitbart, 2007). Oral and I.V. administrations of MB prevent and reverse the effects of isofosphamide-induced encephalopathy and for this reason MB is used as a prophylactic drug (Aeschlimann *et al*., 1996; Di Cataldo *et al*., 2009). Although the mechanism of toxicity of ifosfamide-induced encephalopathy is not well understood, MB may act by restoring the low nicotinamide adenine dinucleotide (NAD^+) to NADH ratio by acting as an alternative electron acceptor of the mitochondrial respiratory chain (Ajithkumar *et al*., 2007; Oz *et al*., 2011).

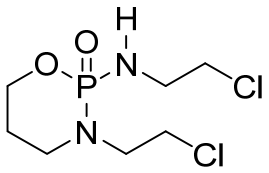

Figure 2.6. The structure of ifosfamide (Aeschlimann *et al*., 1996)

2.6.2 MB and methemoglobinimia

MB is used for the treatment of methemoglobinemia (MetHb). The biochemical mechanism for this effect involves the reduction of methemoglobin (MetHb) by leucoMB to yield haemoglobin (Hb) (Cawein *et al*., 1964; Querfurth & LaFerla, 2010). MetHb is the product formed when normal ferrous ion oxidises to ferric ion in the heme complex of Hb. The ferric state cannot bind to oxygen, and the decreased oxygen carrying and unloading from MetHb induces tissue hypoxia (Cawein *et al*., 1964; Do Nascimento *et al*., 2008; McCord & Fridovich, 1969; Singh *et al*., 2012). In the treatment of methemoglobinemia by MB, sufficient reduced NADPH within the red blood cells should be available to ensure the supply of leucoMB required for the reduction of MetHb (Do Nascimento *et al*., 2008; Singh *et al*., 2012).

2.6.3 MB and malaria

Interest in MB as an antimalarial drug was recently renewed, particularly for the treatment of uncomplicated malaria in children under the age of 5. In this respect, MB is not only readily accessible and available, but also affordable (Coulibaly *et al*., 2009; Müller, 1996, 1998; Peter *et al*., 2000). MB has been demonstrated to be active against *in vitro* and *in vivo* malaria, and also against the gametocytes of *Plasmoduim falciparum*, which is directly related to disease transmission from patient to mosquito (Coulibaly *et al*., 2009; Vennerstrom *et al*., 1995). In the clinic, two doses of 12 mg MB per kg body weight are administered orally for 3 days, which is equivalent to a total of 72 mg/kg for the duration of therapy (Zoungrana *et al*., 2008). MB-based therapy has been demonstrated to be safe and effective for children with glucose-6-phosphate dehydrogenase deficiency (G6PD deficiency). In West Africa, 15% of the male population is affected by G6PD deficiency. Despite the blue discoloration of urine, MB-based therapy is mostly accepted by communities. Patient compliance is apparent to health workers and caregivers where blue washable spots in clothes or diapers are indicative of MB treatment (Coulibaly *et al*., 2009; Müller, 1996, 1998; Peter *et al*., 2000).

As mentioned, the mechanism of MB's action in malaria involves the interaction with parasite flavoenzymes (Buchholz *et al*., 2008; Haynes *et al*., 2010). MB is firstly reduced to yield leucoMB by the flavoenzymes. With the re-oxidation of leucoMB to MB, oxygen is reduced to form superoxide. This process leads to oxidative stress in the parasite (Buchholz *et al*., 2008). Reduced NADPH, which is required for reduction of the flavoenzymes, is subsequently depleted which greatly impairs disulphide reductase function in the parasite and impairs the capacity to oppose the enhanced oxidative stress.

2.6.4 MB and Alzheimer's disease

Alzheimer's disease is a neurodegenerative disorder which arises from a complex pathological profile. Although the specific mechanism leading to Alzheimer's disease remains unknown, extracellular amyloid beta (Aβ) protein deposition has been postulated to be a central cause of the disease (Mudher & Lovestone, 2002). A second hypothesis proposes that in Alzheimer's disease, the microtubule associated protein tau, which is responsible for stabilisation of microtubules and is expressed in axons, becomes highly phosphorylated and aggregates into abnormal tangles. This in turn will impair the function of tau causing tangles to accumulate in the neuron, and may result in neuronal death (Mudher & Lovestone, 2002).

In clinical studies it has been demonstrated that MB may decelerate the cognitive decline in Alzheimer's disease (Luna-Muñoz *et al*., 2008; Sullivan, 2008). As mentioned, MB is a notable inhibitor of AChE (Pfaffendorf *et al*., 1997; Petzer *et al*., 2014). While the inhibition of AChE may contribute to its beneficial effect in Alzheimer's disease, MB may also influence other neuropathogenic events associated with Alzheimer's disease such as inhibition of aggregation and filament formation of tau. MB may also inhibit Aβ protein oligomerisation (Necula *et al*., 2007; Taniguchi *et al*., 2005; Wischik *et al*., 1996). MB also inhibits the second major form of cholinesterase, known as BuChE (Pfaffendorf *et al*., 1997; Petzer *et al*., 2014). Inhibitors of this enzyme demonstrate improved learning performance in rats with reduced Aβ protein levels, and based on this, BuChE may also play a role in the therapy of Alzheimer's disease (Grieg *et al*., 2014).

MB's enhancement of cognitive function is closely linked to its ability to enhance the function of the mitochondrial respiratory chain (Rojas *et al*., 2012). The MB/leucoMB oxidation/reduction system serves a direct interaction with the mitochondrial respiratory chain by oxidising reduced coenzyme Q and possibly reducing cytochrome C (Scott & Hunter, 1966). This in turn will increase mitochondrial oxidative metabolism. Memory deficits has been linked to neuronal degeneration and impaired mitochondrial oxidative metabolism, similar to those observed in Alzheimer's disease (Bennett *et al*., 1992; Gonzalez-Lima *et al*., 1997).

2.6.5 MB and shock

The cardiovascular response to shock involves the insufficient delivery of oxygen to tissues and organs due to low blood perfusion to the cells. This results in cellular injury and death (Lo *et al*., 2014). MB increases blood pressure in shock states by inhibiting guanylate cyclase. This inhibition reduces cGMP formation and subsequently counters vasodilation. Based on this analysis, MB may be useful in the treatment of various shock states (Lo *et al*., 2014). MB is also a NOS inhibitor (Griscavage *et al*., 1994). NO produced by NOS is released from the vascular endothelium and activates guanylate cyclase, which increases intracellular cGMP.

This action induces relaxation of vascular smooth muscle and causes vasodilatation. Since MB also inhibits NOS and thus reduces NO formation, blood pressure is increased. This provides an additional rationale of MB for the treatment of shock (Schneider *et al*., 1992).

2.6.6 MB and depression

MB has been used in treatment for neuropsychiatric illnesses from as early as 1899 (Coulibaly *et al*., 2009). Among these illnesses is depression, a serious psychiatric condition due to its recurrent nature (Narsapur & Naylor, 1983; Oz *et al*., 2012; Reif *et al*., 2006). Clinical depression data in the United States shows that one in every six individuals will develop the condition during their life time (Kessler *et al*., 2005).

Eroğlu and Cağlayan were first to evaluate MB's antidepressant and anxiolytic effects in behavioural animal models (Eroğlu & Cağlayan, 1997). In behavioural tests such as the elevated plus-maze test and the forced swim test (FST), it has been demonstrated that MB exhibits both antidepressant and anxiolytic effects (Eroğlu & Cağlayan, 1997; Harvey *et al*., 2010). Further studies have supported the antidepressant-like properties of MB in rats. MB as well as methylene green (MG) present with antidepressant-like effects during acute and sub-chronic treatment in the FST (Harvey *et al*., 2010). The observation that MG, a structural analogue of MB, showed antidepressant-like effects in the FST encouraged the idea to synthesise structurally related MB analogues and to evaluate these as potential antidepressant agents. Azure B, MB's major metabolite, was also evaluated for antidepressant-like behaviour in the FST (Delport *et al*., 2014). Delport and colleagues synthesized a structural analogue of MB, known as etylthioninium chloride (ETC), which was evaluated with azure B in the acute FST (Delport *et al*., 2014). Both ETC and azure B were administered to male Spraque-Dawley rats and the results showed a decrease in the immobility time in the FST, demonstrating antidepressant-like properties. Bio-behavioural studies in rodents established the structural requirements for a MB analogue to induce an antidepressant-like response, especially the presence of the charged sulphur moiety and the dimethylamino substituent (Harvey *et al*., 2010). This finding has subsequently been confirmed in more recent work by the Petzer group (Petzer *et al*., 2012; Delport *et al*., 2014).

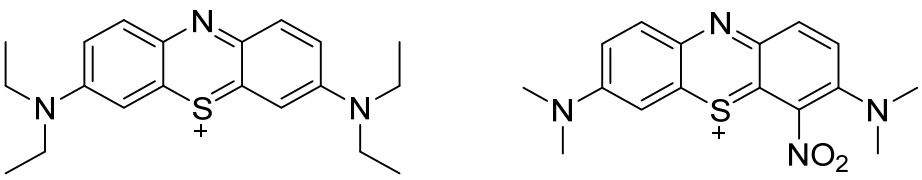

ETC Methylene green

Figure 2.7. The structure of ETC and methylene green (Delport *et al*., 2014; Harvey *et al*., 2010).

Narsapur and Naylor (1983) was first to note the antidepressant properties of MB in humans. MB was added as a treatment for manic depressive psychosis in 22 patients. These patients received 100 mg MB orally twice or three times daily and 16 patients showed definite improvement. The effect of MB in manic depressive patients was also evaluated in 31 patients treated with either 15 mg/day or 300 mg/day MB (Naylor *et al*., 1986) in a cross-over design. The results showed that in the year that the patients received 300 mg/day MB they were less depressed than during the year they received 15 mg/day MB. In a follow-up study the effect of 15 mg/day MB in severe depressive illness was evaluated (Naylor *et al*., 1987). The results showed that patients receiving MB showed significant improvement compared to the placebo treated patients. It was concluded that 15 mg/day MB has adequate antidepressant activity in severely depressed patients.

2.7 Adverse effects of MB

While MB is considered to be safe and relatively free of adverse effects, large dosages of MB (47 mg/kg) have been reported to cause nausea, chest pain, abdominal pain, sweating, dizziness, cyanosis, confusion, methemoglobinemia and headache in adults when administrated intravenously (Oz *et al*., 2011). MB easily crosses the blood-milk barrier and for this reason, administration during breast feeding is discouraged (Ziv & Heavner, 1984). In neonates MB toxicity presents as respiratory distress, haemolytic anaemia and photo-toxicity (Albert *et al*., 2003; Oz *et al*., 2011).

Serotonin toxicity:

MB causes serotonin toxicity or serotonin syndrome, which is characterised by dizziness, disorientation, headache, tremors and seizures. Serotonin toxicity is caused by excessive extra-neuronal levels of serotonin in the central nervous system and occurs when MB is administrated simultaneously with serotonin reuptake inhibitors (SRI) such as duloxetine and fluoxetine (Bach *et al*., 2004). For this reason, the clinical use of MB in patients taking serotonin re-uptake inhibitors is contraindicated (Oz *et al*., 2012). The serotonin transporter, known as SERT, is an integral membrane protein which regulates synaptic reuptake of released serotonin (Amara & Kuhar, 1993). The extracellular serotonin concentrations in the central nervous system are primarily regulated by SERT and the metabolism of serotonin by MAO-A. MB-related serotonin toxicity was first described in a patient receiving SRI's (Ramsay *et al*., 2007). It is currently believed that MB elicit serotonin toxicity by acting as a potent inhibitor of MAO-A in the central nervous system.

The cheese reaction:

Another adverse effect that should be considered is the so-called "cheese effect". In clinical practice, MAO-A inhibitors are used restrictively due to blood pressure changes that may occur

with the combined usage of MAO-A inhibitors with the dietary amine known as tyramine, which is present in fermented products, wine and cheese (Da Prada *et al*., 1988). Intestinal as well as peripheral MAO-A act as a metabolic barrier for dietary tyramine, and reduces the amount of tyramine which reaches the systemic circulation. Inhibitors of MAO-A blocks the metabolism of tyramine, which leads to increased systemic tyramine concentrations. Tyramine, an indirect sympathomimetic agent, releases noradrenaline from peripheral neurons which may induce a severe and potentially fatal hypertensive response. Irreversible MAO-A inhibition is mostly associated with the "cheese effect". The newer generation reversible inhibitors such as moclobemide and toloxatone appear not to provoke this effect (Bonnet, 2003; Provost *et al*., 1992). However MB is unlikely to cause tyramine-induced hypertension since it is a reversible MAO-A inhibitor. No reports have linked MB to the occurrence of the "cheese effect".

2.8 Approaches to the synthesis of MB analogues

In literature a number of routes for the synthesis of MB derivatives have been reported (Wischik *et al*., 2006). In one protocol N,N-dialkyl-*p*-phenylenediamine (**A**) is treated with sodium thiosulfate ($Na_2S_2O_3$) in the presence of sodium dichromate ($Na_2Cr_2O_7$). This reaction yields the thiosulfonic acid intermediate (**B**). In the subsequent step intermediate **B** is reacted with N,N-dialkylaniline in the presence of $Na_2Cr_2O_7$ and sulphuric acid (H_2SO_4) to yield the imine derivative, **C**. The target MB derivative (**D**) may be obtained after reaction of **C** with copper(II)sulfate ($CuSO_4$) (Wischik *et al*., 2006). The chloride or iodide salt of the MB derivative (**E**) may be obtained by treating **D** with sodium chloride (NaCl) and potassium iodide (KI), respectively, and recrystallising the product from ethanol.

In a second protocol, the hydrochloric acid (HCl) salt of N,N-dialkyl-*p*-phenylenediamine (**A**) is treated with sodium sulphide (Na_2S) and iron(III)chloride ($FeCl_3$) to yield the target MB derivative (**E**) as the chloride salt (Wischik *et al*., 2006). This procedure has previously been used by Delport and colleagues to synthesise ETC (Delport *et al*., 2014). The use of metals in these protocols is a major disadvantage since MB and its analogues are known to form metal chelates. This makes it challenging to separate the final MB analogues from the metal ions. The presence of metals will affect the recording of NMR spectra and may affect the biological evaluations of these compounds.

The most convenient route to MB analogues is that first reported by Strekowski and colleagues (1993). In the protocol, phenothiazine (**F**) is dissolved in chloroform, and reacted with iodine to yield phenothiazin-5-ium tetraiodide hydrate (**G**). The intermediate is dissolved in methanol, and treated dropwise with an appropriate amine. Depending on the reaction stoichiometry, monosubstituted or disubstituted analogues are obtained. Often the monosubstituted analogues (**H**) are prepared in the first step, and the disubstituted analogues (**I**) in the

subsequent reaction. A disadvantage of this procedure is that the iodide salts of the MB analogues are obtained as end-products instead of the more desirable chloride salts. To transform the iodide salts to chloride salts, anion-exchange resin is employed (Felgenträger *et al*., 2013; Lu *et al*., 2011). Another disadvantage of the Strekowski protocol is that it works well for only certain amine substrates, which limits the scope of potential MB analogues that can be synthesized.

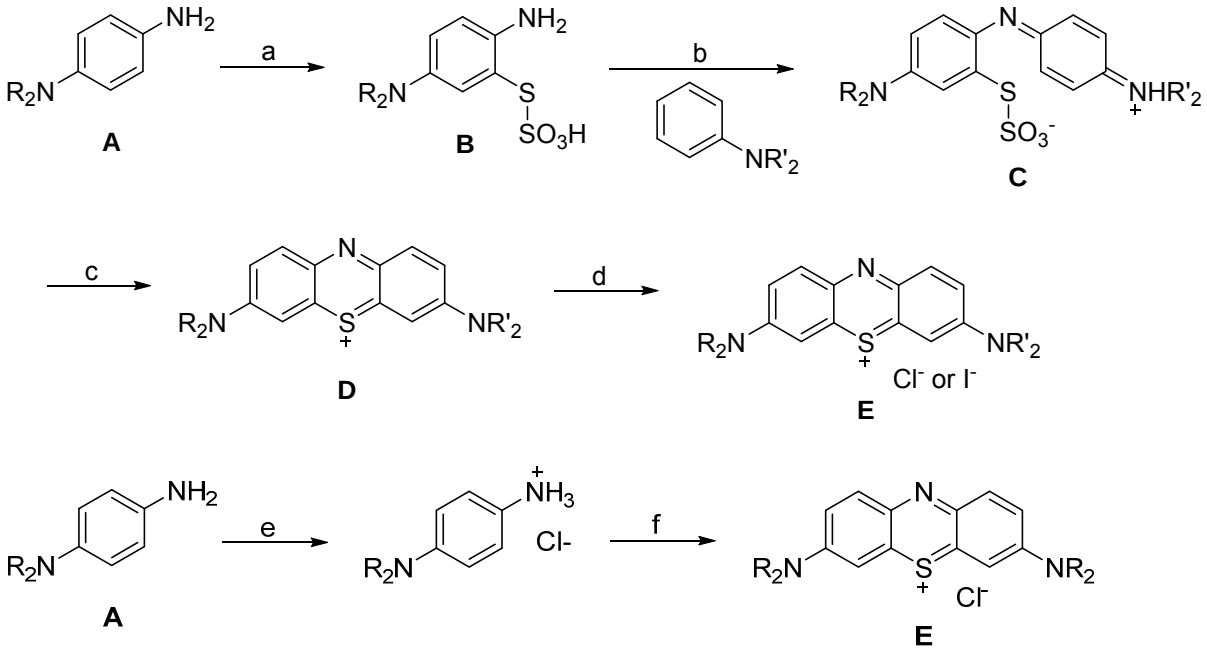

Figure 2.8. The synthesis of MB analogues from N,N-dialkyl-p-phenylenediamine (**A**). Key: (a) HCl, $Na_2S_2O_3$, $Na_2Cr_2O_7$; (b) $Na_2Cr_2O_7$, H_2SO_4; (c) $CuSO_4$, HCl; (d) KI; (e) HCl, Et_2O; (f) Na_2S, $FeCl_3$; HCl (Felgenträger *et al*., 2013; Lu *et al*., 2011).

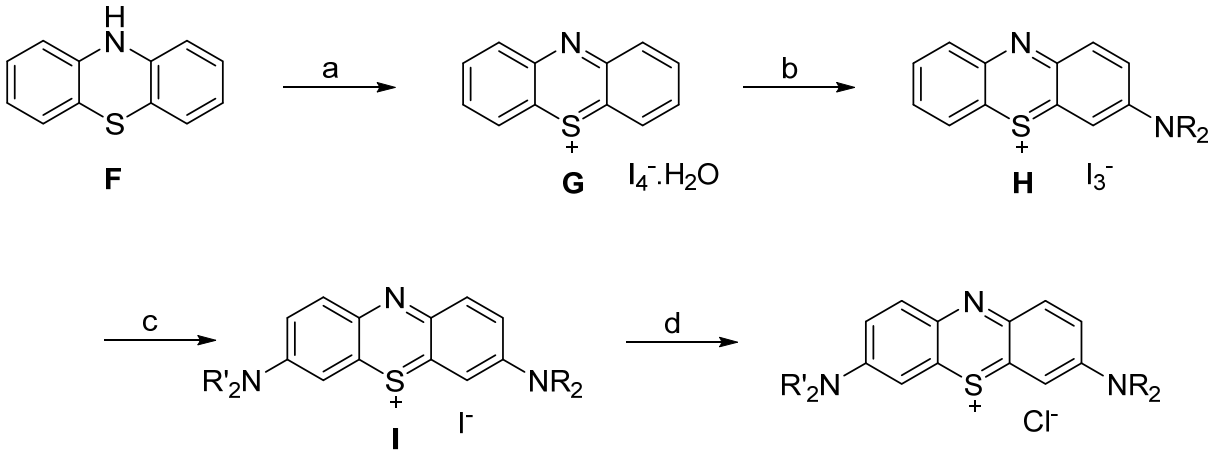

Figure 2.9. The synthesis of MB analogues from phenothiazine (**F**). Key: (a) I_2/CH_3Cl; (b) HNR_2, 2 equiv.; (c) HNR'_2, 6 equiv.; (d) Anion exchange (Felgenträger *et al*., 2013; Lu *et al*., 2011).

2.9 Conclusion

MB has been used as a drug for more than a century and is a well-known treatment of methemoglobinemia and isofosphamide-induced encephalopathy. MB has also received much attention as an antimalarial drug, particularly for children. Recently the potential roles of MB in depression and Alzheimer's disease have been emphasised (Harvey *et al*., 2010; Petzer *et al*., 2012; Querfurth & LaFerla, 2010; Ramsay *et al*., 2007). MB exerts its biochemical actions by several mechanisms, which include MAO-A inhibition, AChE inhibition, modulation of the NO-cGMP signalling pathway, enhancement of mitochondrial respiration and reducing oxidative stress. The unique redox chemistry of MB is central to many of these biochemical mechanisms (Garthwaite *et al*., 1989; Petzer *et al*., 2012). Based on the significant interest in MB and its many potential therapeutic applications, the current study will attempt to synthesise MB analogues, and to investigate select pharmacological properties of the resulting analogues. The experimental data obtained will be compared to those of MB and conclusions may be drawn regarding the effects of structural modification on these selected pharmacological properties.

Chapter 3
Synthesis of MB analogues

3.1 Introduction

Although MB has multiple pharmacological actions and has been used as drug for more than a century, few studies have investigated the structure-activity relationships of MB at selected targets. Of importance to this study is the discovery that MB is a potent inhibitor of human MAO-A with an IC_{50} value of 0.07 μM (Harvey *et al*., 2010). MB's principal metabolite, azure B, also acts as a potent inhibitor of MAO-A with an IC_{50} value of 0.01 μM (Harvey *et al*., 2010; Petzer *et al*., 2012). ETC, a structural analogue of MB, is a lower potency MAO-A inhibitor with an IC_{50} value of 0.510 μM. Interestingly, ETC inhibits human MAO-B (IC_{50} = 0.592 μM) more potently than MB (IC_{50} = 4.37 μM) and azure B (IC_{50} = 0.968 μM) (Delport *et al*., 2014). The current study aims to contribute to the structure-activity relationships of MAO inhibition by MB analogues. For this purpose selected MB analogues will be synthesized and characterised as human MAO inhibitors. The MAO inhibition properties of the synthetic analogues will be compared to that of MB.

As discussed in Chapter 1, the synthesis of MB analogues is challenging and the available synthetic routes are limited. In addition, most synthetic procedures employ metals which are difficult to separate from the target MB analogues due to chelation. The most convenient synthetic route remains that of Strekowski *et al*. (1993). Unfortunately this procedure works well for only certain amine substrates, which limits the scope of potential MB analogues that can be synthesized. Through considerable trial-and-error this study successfully synthesized two MB analogues by following the protocol by Strekowski *et al*. (1993). The structures of these MB analogues are given in Figure 3.1. The MB analogues are monosubstituted while MB is disubstituted. The MB analogues incorporate the dimethylamine (**1**) and dipropylamine (**2**) functional groups, respectively.

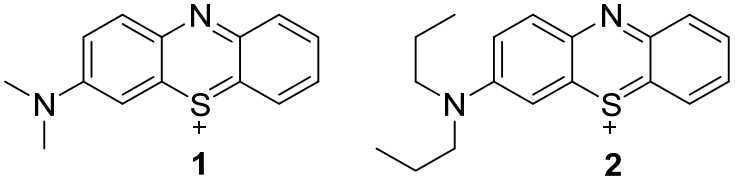

Figure 3.1. The structures of the MB analogues that were synthesized in this study.

This chapter will provide a detailed description of the synthesis of MB analogues **1**–**2**, and discuss the relevant spectroscopic data that supports the structure assignment. This chapter will also discuss, as example, the attempted synthesis of a disubstituted MB analogue, compound **3**.

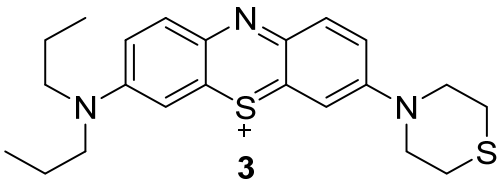

3

Figure 3.2. The structure of compound **3**.

3.2 General synthetic approach

As discussed in Chapter 2 the most convenient protocol to synthesise MB analogues was reported by Strekowski *et al*. (1993). Commercially available phenothiazine (**F**) is firstly dissolved in chloroform. Iodine is added and after reaction with phenothiazine, phenothiazin-5-ium tetraiodide hydrate (**G**) is obtained. The intermediate is in turn dissolved in methanol, and slowly treated with an amine. Depending on the stoichiometry of phenothiazin-5-ium tetraiodide (**G**) and the amine either the monosubstituted or disubstituted MB analogues are obtained. In the Strekowski protocol the monosubstituted analogues (**H**) are usually prepared in the first step, and the disubstituted analogues (**I**) in the subsequent reaction.

Following this procedure, the MB analogues are obtained as the iodide salts instead of the more desirable chloride salts. To convert the iodide salts to chloride salts, anion-exchange resin may be employed (Felgenträger *et al*., 2013; Lu *et al*., 2011).

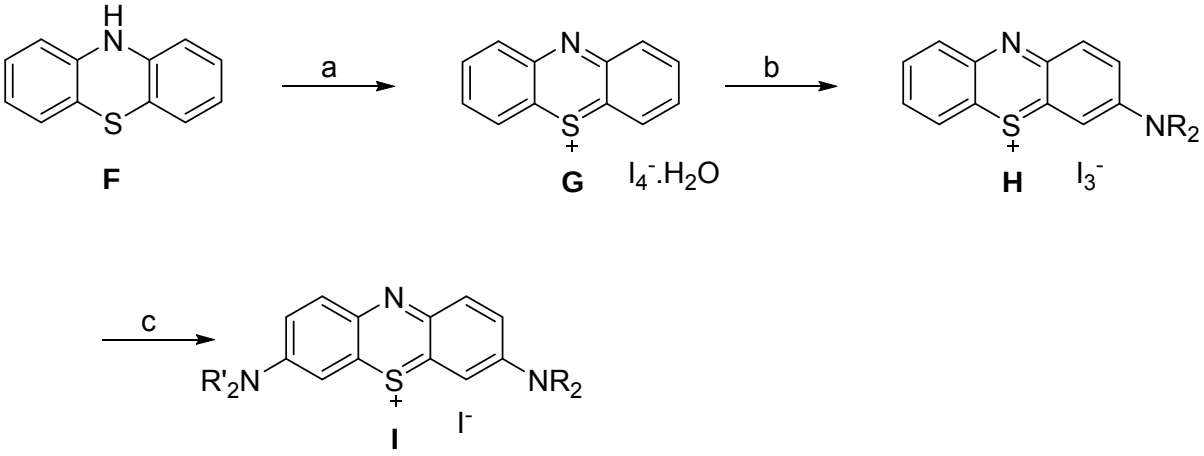

F **G** **H** **I**

Figure 3.3. The synthesis of MB analogues from phenothiazine (**F**). Key: (a) I_2/CH_3Cl; (b) HNR_2, 2 equiv.; (c) HNR'_2, 6 equiv.

3.3 Materials and Instruments

3.3.1 Materials

Reagents and solvents were obtained from Sigma-Aldrich (St. Louis, MO, USA) and used without further purification. The reagents for the synthetic work were phenothiazine, iodine, dimethylamine, thiomorpholine and dipropylamine.

3.3.2 Thin layer chromatography (TLC)

TLC was used to determine if the reactions proceeded to completion and to evaluate the purity of the MB analogues that were synthesized. TLC was carried out using silica gel 60 (Merck, Darmstadt, Germany) with UV_{254} fluorescent indicator. The mobile phase consisted of 85% methanol, 15% water and 3% ammonium acetate. The developed sheets were investigated visually since the MB analogues appear as intense blue spots. The R*f* values of the MB analogues were calculated and are given in the results section.

3.3.3 Nuclear magnetic resonance (NMR)

Proton (^{1}H) and carbon (^{13}C) NMR spectra were recorded on a Bruker Avance III 600 spectrometer (Karlsruhe, Germany) at frequencies of 600 MHz and 151 MHz, respectively. All NMR measurements were carried out in DMSO-d_6 as NMR solvent. The chemical shifts are given in parts per million (δ) and were referenced to the residual solvent signal. The spin multiplicities are given as s (singlet), d (doublet), dd (doublet of doublets), t (triplet) or m (multiplet).

3.3.4 Mass spectrometry (MS)

High resolution mass spectra (HRMS) were recorded with a Bruker micrOTOF-Q II mass spectrometer (Karlsruhe, Germany) functioning in atmospheric-pressure chemical ionization (APCI) mode (positive mode).

3.3.5 Melting points (mp) and differential scanning calorimetry (DSC)

Melting points (mp) were measured with a Buchi B-545 melting point apparatus (Büchi Labortechnik, Flawil, Switzerland) and are uncorrected. A Mettler TGA/DSC 3+ STARe system (Mettler Toledo, Greifensee, Switzerland) instrument was used to record the DSC thermograms. Samples, weighing approximately 3 - 5 mg was placed in aluminium 100 µl cells and heated to 300 °C with a heating rate of 10°C/min, with a nitrogen gas flow of 35 ml/min.

3.4 Detailed synthetic procedures

3.4.1 Synthesis of phenothiazin-5-ium tetraiodide hydrate (G)

Phenothiazine (**F**; 2.13 g, 11 mmol) was added to chloroform (75 ml) at 5 °C and stirred for 30 min to obtain a complete solution. Iodine (8.38 g, 33 mmol) was similarly added to chloroform (175 ml) and stirred for 90 min at 5 °C. During this time most of the iodine dissolved in the chloroform. The mixture of iodine and chloroform was filtered and the filtrate was added over a period of 90 min to the reaction containing the phenothiazine reagent. During this time the reaction was incubated in an ice bath. Stirring was continued for 30 min in the ice bath and the dark precipitate that formed was collected by filtration. The precipitate was washed with chloroform (150 ml) and air dried for 48 h (Felgenträger *et al*., 2013; Strekowski *et al*., 1993).

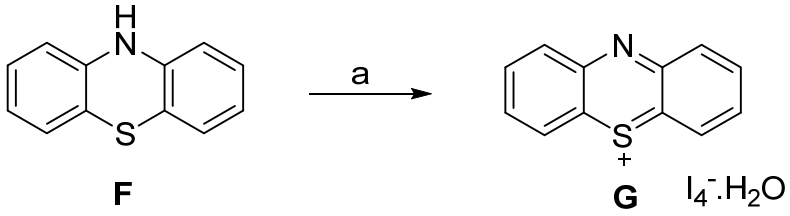

Figure 3.4. The synthesis of phenothiazin-5-ium tetraiodide hydrate (**G**). Key: (a) I_2/CH_3Cl (yield = 93%).

3.4.2 Synthesis of 3-dialkylaminophenthiazin-5-ium triiodide analogues 1 and 2

Phenothiazin-5-ium tetraiodide hydrate (**G**; 7.23 g, 10 mmol) was dissolved in 500 ml dichloromethane and a solution of the dialkylamine (20 mmol) in methanol (10 ml) was added dropwise over a period of 4 h. The reaction mixture was incubated overnight at room temperature and the solvent was subsequently removed by rotary evaporation, taking care that the temperature does not exceed 40 °C. Methanol (30 ml) was added to the liquid residue and the resulting mixture was incubated for a further 48 h. The solvent was again removed by decantation and another portion of methanol (25 ml) was added. After removal of the methanol phase by rotary evaporation, 20 ml dicholoromethane was added and the resulting solution was incubated at 5 °C for 21 days. The target monosubstituted MB analogue recrystallized to give a dark-green/blue solid. (Felgenträger *et al*., 2013; Strekowski *et al*., 1993). Following this procedure and employing dimethylamine and dipropylamine, respectively, as amine substrates, MB analogues **1** and **2** were synthesized.

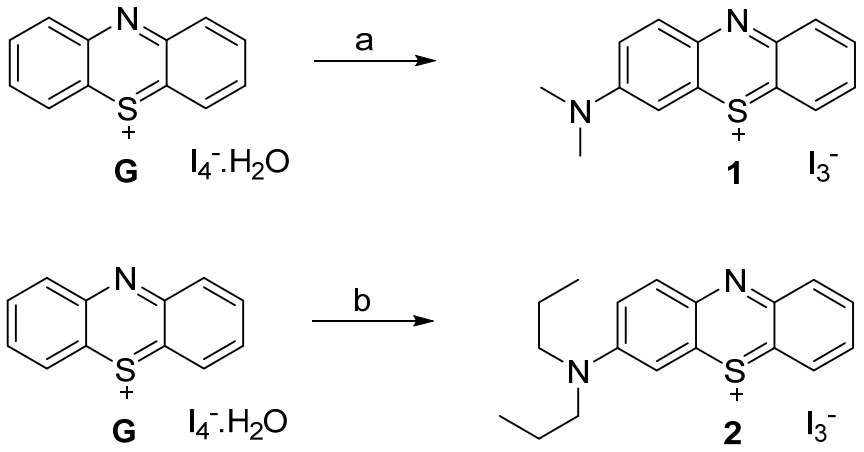

Figure 3.5. The synthesis of 3-dialkylaminophenthiazin-5-ium triiodide analogues **1** and **2**. Key: (a) Dimethylamine, 2 equiv. (yield = 16.5%); (a) Dipropylamine, 2 equiv. (yield = 20.2%).

3.4.3 The attempted synthesis of 3,7-disubstituted phenthiazin-5-ium iodide analogues

3-(Dipropylamino)phenthiazin-5-ium triiodide (**2**; 1.24 g, 2 mmol) was dissolved in dichloromethane (360 ml) and the resulting solution was treated dropwise with a solution of thiomorpholine (12 mmol) in dichloromethane (40 ml) over a period of 1 h. The reaction mixture was stirred overnight at room temperature and was subsequently washed with water (1 x 200 ml). The organic layer was dried over anhydrous $MgSO_4$ (5 g) and the solvent was removed with a rotary evaporator. The residue was dissolved in dichloromethane (10 ml) and precipitated with the addition of diethyl ether (50 ml). The dark blue precipitate was collected by filtration (Felgenträger *et al*., 2013; Strekowski *et al*., 1993).

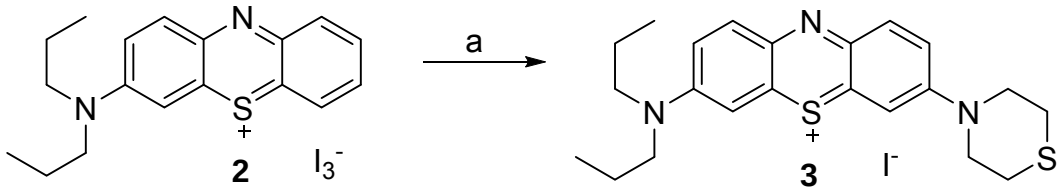

Figure 3.6. The attempted synthesis of 3-(thiomorpholino)-7-(dipropylamino)phenthiazin-5-ium iodide (**3**). Key: (a) Thiomorpholine, 6 equiv. (yield = 55.8%).

3.5 Results

3.5.1 Interpretation of the TLC

TLC was used to (1) determine whether the synthetic reactions proceeded to completeness and (2) to estimate the purity of the synthesized MB analogues. TLC sheets were developed for each of the three MB analogues synthesized. TLC was carried out using silica gel 60 with UV_{254} fluorescent indicator. The mobile phase consisted of 85% methanol, 15% water and 3% ammonium acetate. The developed TLC sheets were visually observed as the MB analogues

appear as blue spots on the sheets. Figure 3.7 provides examples of TLC sheets for MB analogues **1**–**3**. The R*f* value of each analogue was calculated employing equation 3.1 and the values are tabulated in Table 3.1. Since only one spot is visible for each MB analogue it may be concluded that the compounds are pure. This will be confirmed by the absence of signals of impurities in the NMR spectra.

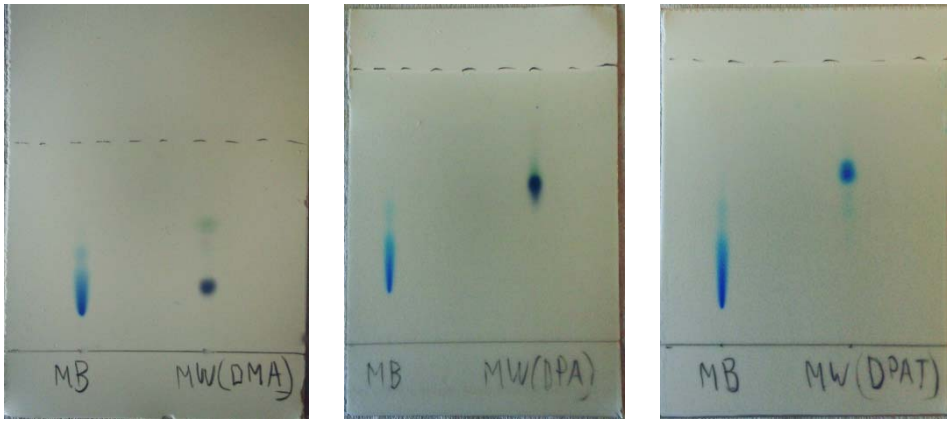

1 **2** **3**

Figure 3.7. The developed TLC sheets for MB analogues **1**–**3** (spots on the right). The position of MB (spot on the left) is also shown.

$$Rf = \frac{[Analyte]_{Distance\ of\ migration}}{[Solvent]_{Distance\ of\ migration}}$$

Equation 3.1. The equation for the calculation of R*f* values.

Table 3.1. The R*f* values of MB analogues **1**–**3** as well as that of MB.

	R*f* values
1	0.30
2	0.57
3	0.59
MB	0.19

3.5.2 Interpretation of mass spectra

The MB analogues **1**–**2** were characterised by high resolution mass spectrometry. The calculated and experimentally determined molecular weights of the MB analogues are given in Table 3.2 and show that, for all analogues, the calculated and experimental values

correspond well. The differences between the calculated and experimentally determined molecular weights may be evaluated by calculating the parts per million (ppm) value according to equation 3.2. In general, a ppm difference smaller than 5 is considered to indicate good agreement between the calculated and experimental values. The mass spectra for MB analogues **1**–**2** are given in Figure 3.8 and 3.9

$$ppm = \frac{[Found\ -Calculated]}{[Calculated]} \times 10^6$$

Equation 3.2. The equation for the calculation of ppm values as indication of the difference between calculated and experimentally determined molecular weights.

Table 3.2. The calculated and experimentally determined high resolution masses of the MB analogues.

	Calculated	**Found**	**Formula**	**ppm**
1	241.0794	241.0795	$C_{14}H_{13}N_2S$	0.41
2	297.1420	297.1416	$C_{18}H_{21}N_2S$	-1.3

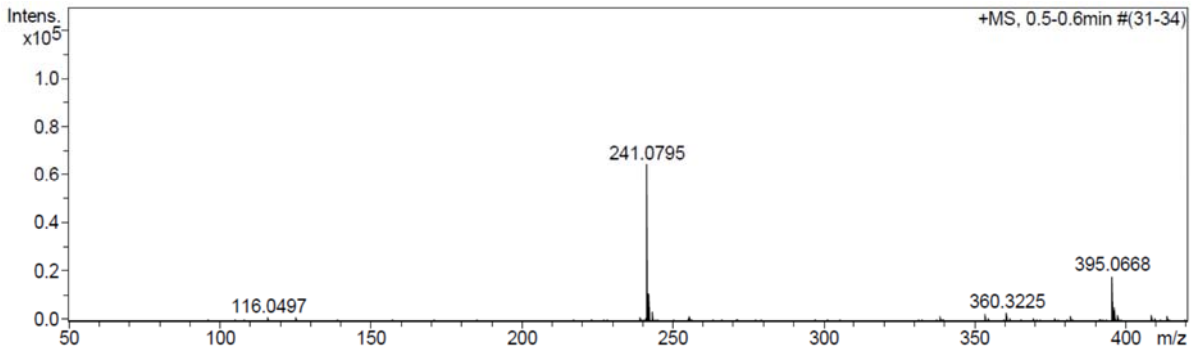

Figure 3.8. The high resolution mass spectrum of MB analogue **1**.

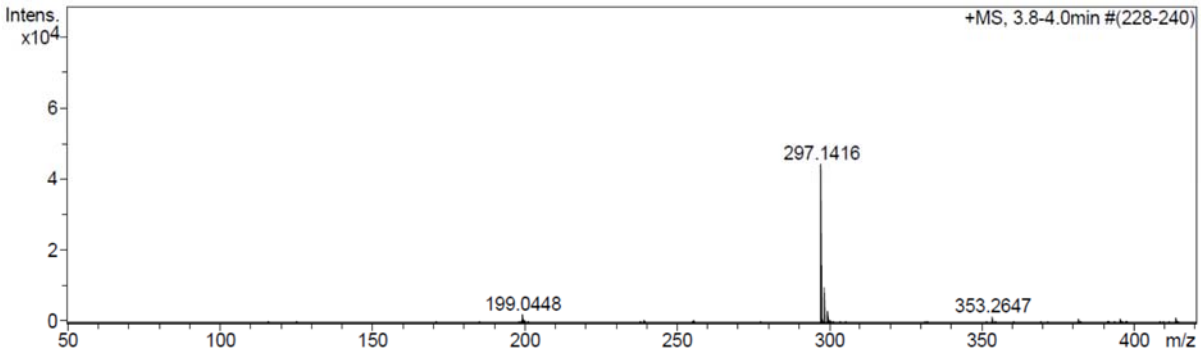

Figure 3.9. The high resolution mass spectrum of MB analogue **2**.

3.5.3 Interpretation of NMR spectra

The MB analogues **1**–**2** were characterised by ^{1}H NMR and ^{13}C NMR spectra. The spectra and notation are given below (Figures 3.10 and 3.11). For comparison, the NMR spectra of MB are also given (Figure 3.12).

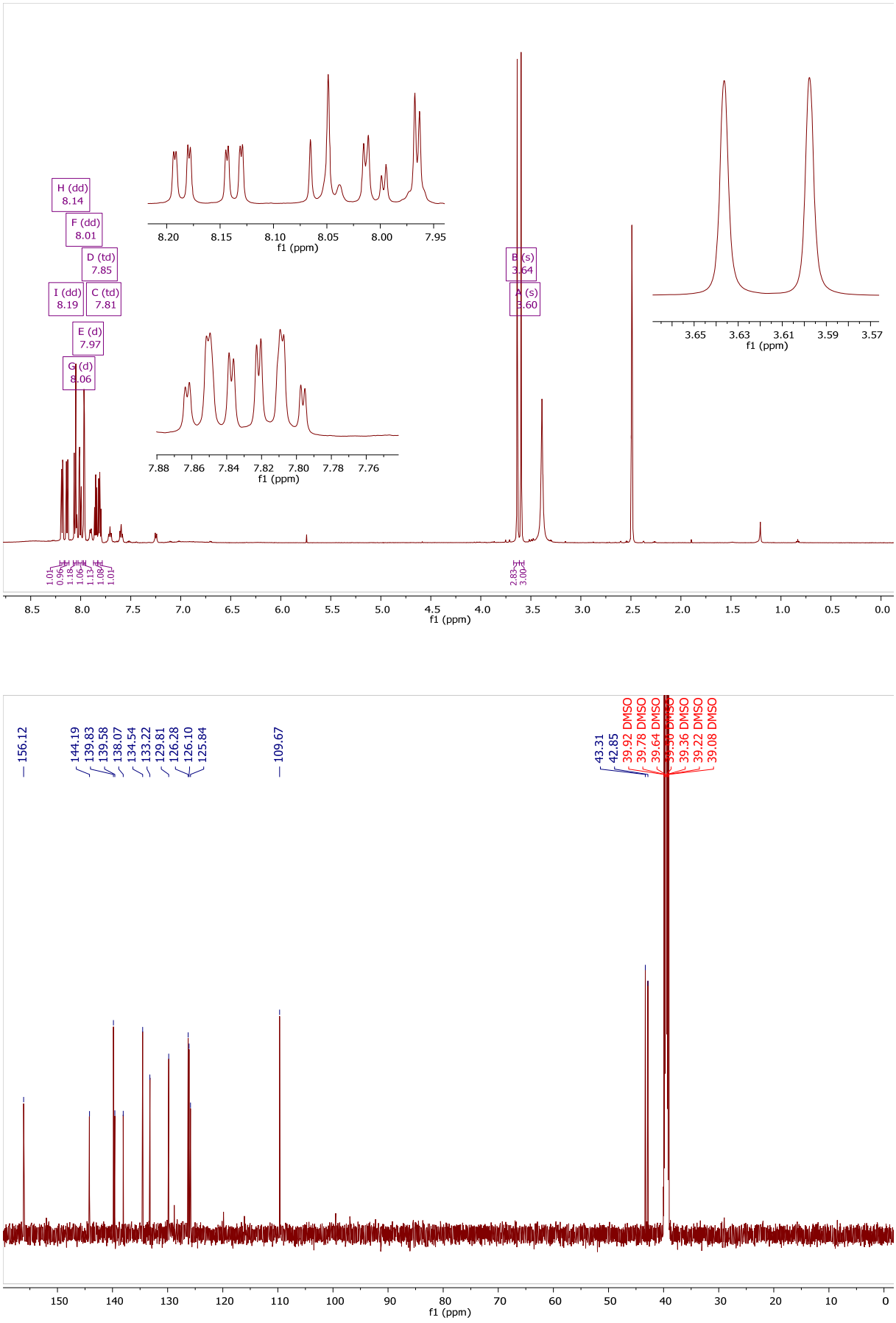

Figure 3.10. The ^{1}H NMR and ^{13}C NMR spectra of analogue **1**.

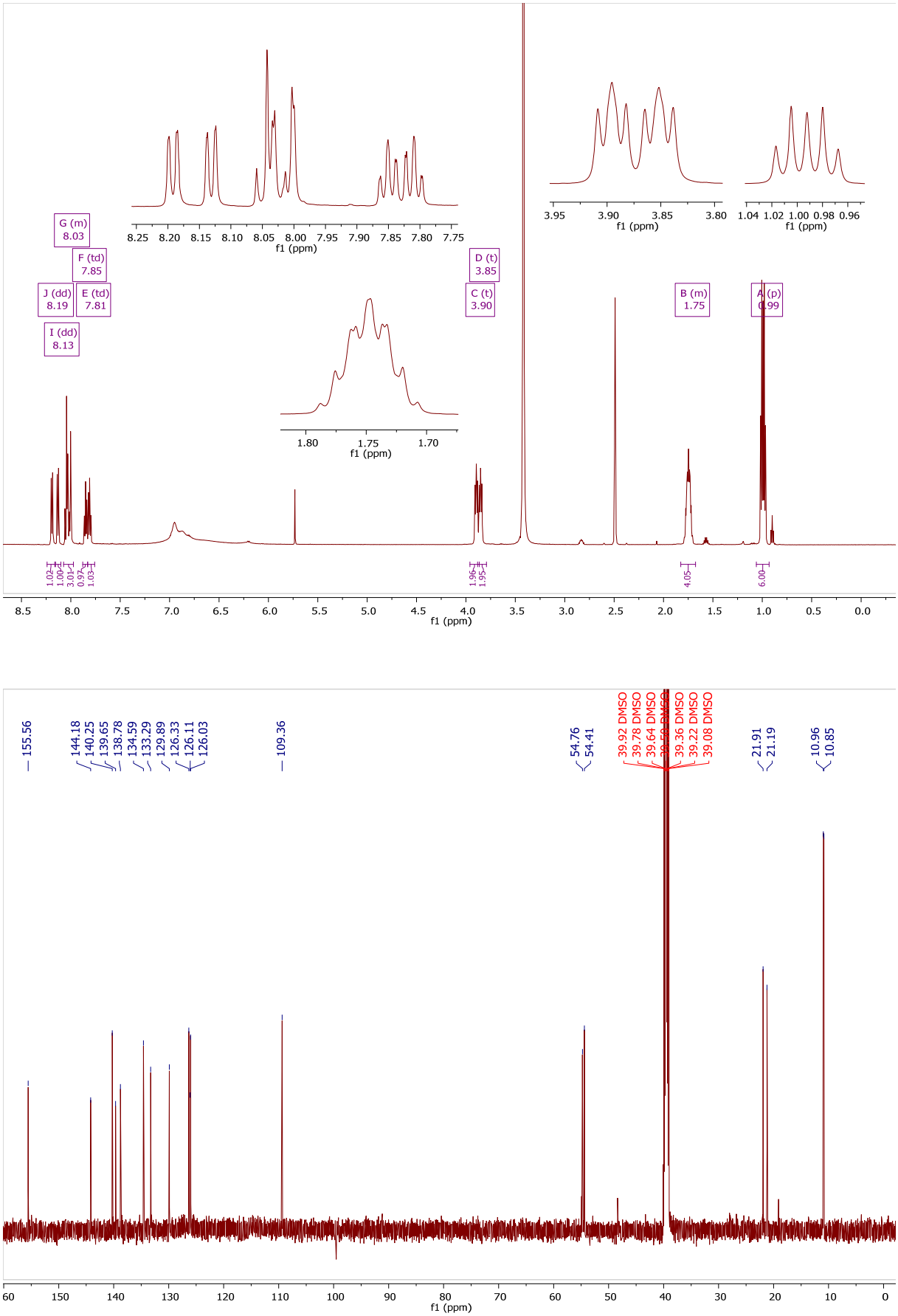

Figure 3.11. The ^{1}H NMR and ^{13}C NMR spectra of analogue **2**.

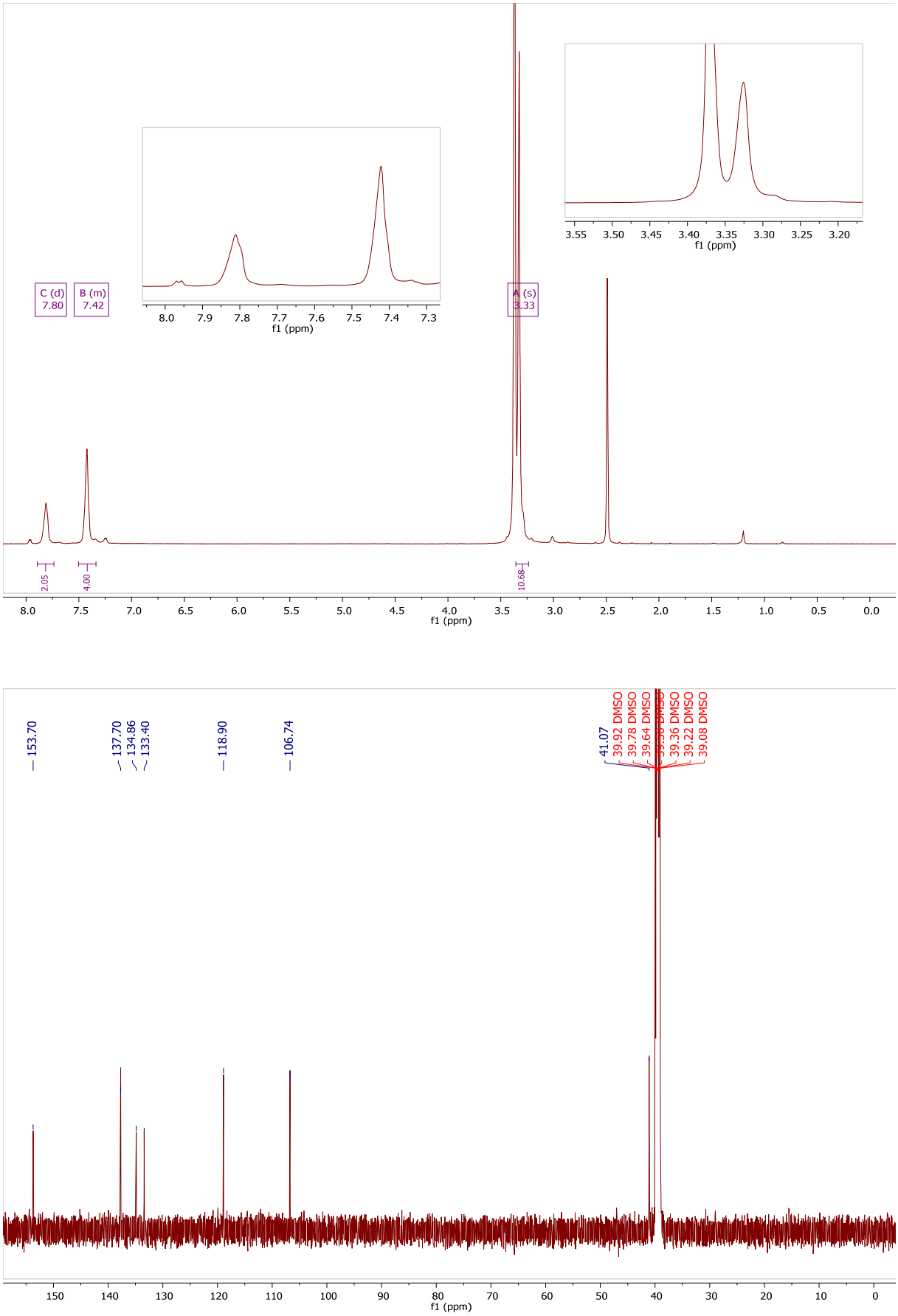

Figure 3.12. The ^{1}H NMR and ^{13}C NMR spectra of MB.

Notation of NMR spectra:

Table 3.3. The notations of the NMR spectra of MB and MB analogues **1**–**2**.

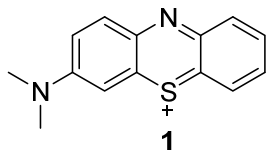 **1**	**^{1}H NMR** (600 MHz, DMSO-d6) δ 8.19 (dd, J = 8.0, 1.5 Hz, 1H), 8.14 (dd, J = 8.0, 1.4 Hz, 1H), 8.06 (d, J = 10.0 Hz, 1H), 8.01 (dd, J = 10.0, 2.6 Hz, 1H), 7.97 (d, J = 2.6 Hz, 1H), 7.85 (td, J = 7.6, 1.5 Hz, 1H), 7.81 (td, J = 7.2, 1.5 Hz, 1H), 3.64 (s, 3H), 3.60 (s, 3H). **^{13}C NMR** (151 MHz, DMSO-d6) δ 156.1, 144.2, 139.8, 139.6, 138.1, 134.5, 133.2, 129.8, 126.3, 126.1, 125.84, 109.7, 43.3, 42.9.
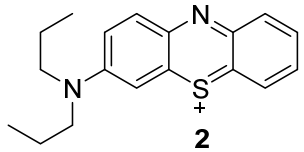 **2**	**^{1}H NMR** (600 MHz, DMSO-d6) δ 8.19 (dd, J = 8.1, 1.5 Hz, 1H), 8.13 (dd, J = 8.0, 1.5 Hz, 1H), 8.07 – 7.97 (m, 3H), 7.85 (td, J = 7.6, 1.5 Hz, 1H), 7.81 (td, J = 7.6, 1.5 Hz, 1H), 3.90 (t, J = 7.9 Hz, 2H), 3.85 (t, J = 8.2 Hz, 2H), 1.83 – 1.68 (m, 4H), 0.99 (p, J = 7.3 Hz, 6H). **^{13}C NMR** (151 MHz, DMSO-d6) δ 155.6, 144.2, 140.3, 139.7, 138.8, 134.6, 133.3, 129.9, 126.3, 126.1, 126.03, 109.4, 54.8, 54.4, 21.9, 21.2, 11.0, 10.9.
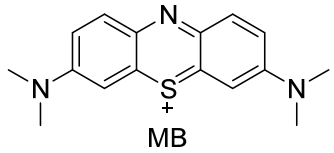 MB	**^{1}H NMR** (600 MHz, DMSO-d6) δ 7.80 (m, 2H), 7.50 – 7.34 (m, 4H), 3.33 (s, 12H). **^{13}C NMR** (151 MHz, DMSO-d6) δ 153.7, 137.7, 134.9, 133.4, 118.9, 106.7, 41.1.

Correlation between the structures and the NMR spectra:

The following tables (Tables 3.4–3.7) provide correlation between the NMR spectra and the structures of MB and the MB analogues **1**–**2**. As shown, both the ^{1}H NMR and ^{13}C NMR spectra correlated with the structures with respect to integration values, multiplicity, chemical shifts and number of signals. Based on the NMR data, it may thus be concluded that the structures of the MB analogues correspond to those provided in this dissertation.

Table 3.4. The correlation between the NMR spectra and the structure of MB

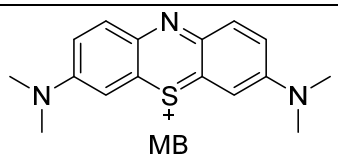

MB

^{1}H NMR	^{13}C NMR
• The methyl (CH_3) protons correspond to the signal at 3.33 ppm (The signal integrates for 12 protons). • The aromatic protons correspond to the two signals at 7.50–7.34 and 7.80 ppm (The signals integrate for 4 protons and 2 protons, respectively).	• The methyl carbons are represented by the signal at 41.1 ppm. • The aromatic carbons are represented by the signals at 153.7, 137.7, 134.9, 133.4, 118.9 and 106.7 ppm.
DEPT-45	
• The aromatic CH carbons are represented by seven signals at 137.7, 118.9 and 106.7 ppm. • The methyl (CH_3) carbons are represented by the signal at 41.1 ppm.	

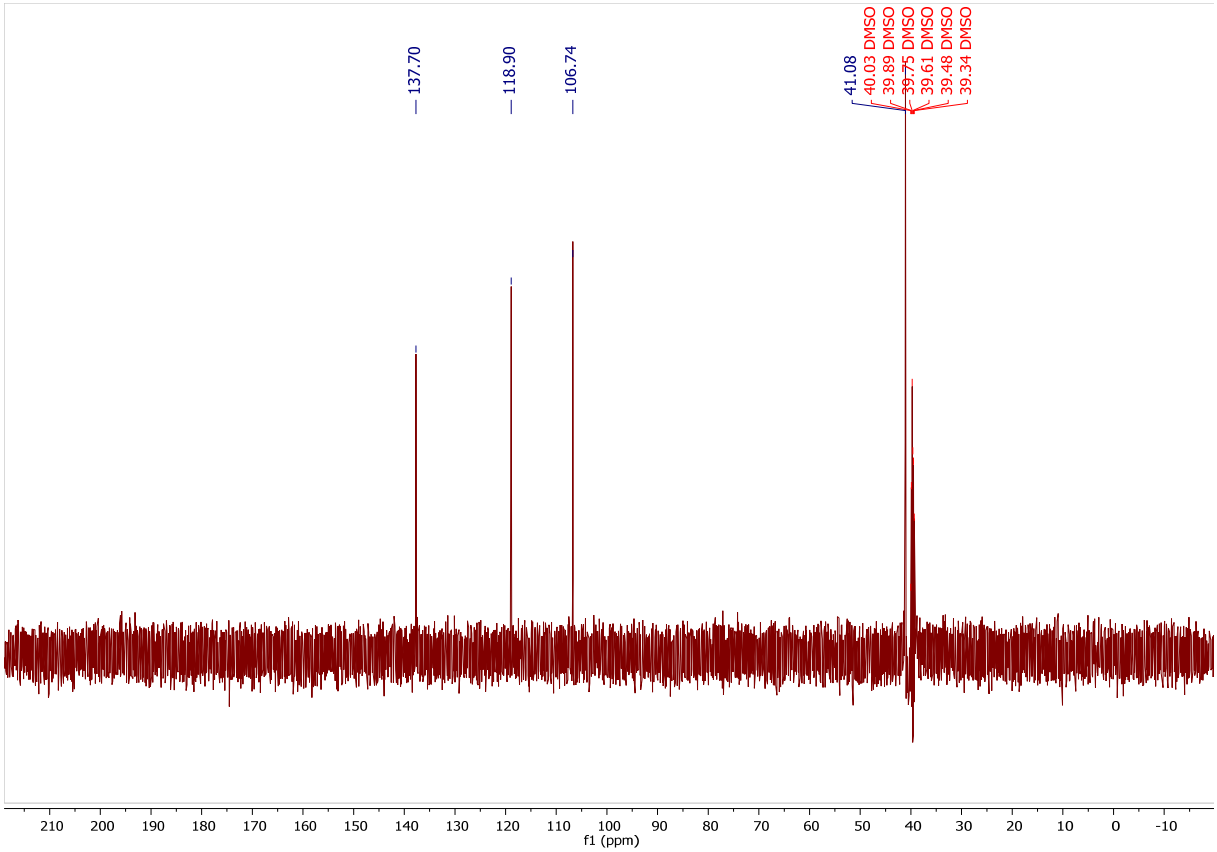

Figure 3.13. The DEPT-45 spectrum of MB.

Table 3.5. The correlation between the NMR spectra and the structure of **1**.

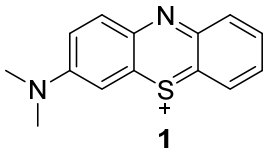

1

^{1}H NMR	^{13}C NMR
• The methyl (CH_3) protons correspond to the two singlets at 3.64 and 3.60 ppm (The signals integrate for 3 protons each). • The aromatic protons correspond to two triplet of doublets (7.81 and 7.85 ppm), two doublets (8.06 and 7.97 ppm) and three doublet of doublets (8.19, 8.14 and 8.01 ppm) (These signals integrate for 7 protons).	• The methyl ($\underline{C}H_3$) carbons are represented by the signals at 43.3 and 42.9 ppm. • The aromatic carbons are represented by twelve signals at 156.1, 144.2, 139.8, 139.6, 138.1, 134.5, 133.2, 129.8, 126.3, 126.1, 125.84 and 109.7 ppm.
DEPT-45	
• The aromatic CH carbons are represented by seven signals at 139.8, 134.5, 133.2, 129.8, 126.3, 126.1 and 109.7 ppm. • The methyl (CH_3) carbons are represented by two signals at 43.3 and 42.9 ppm.	

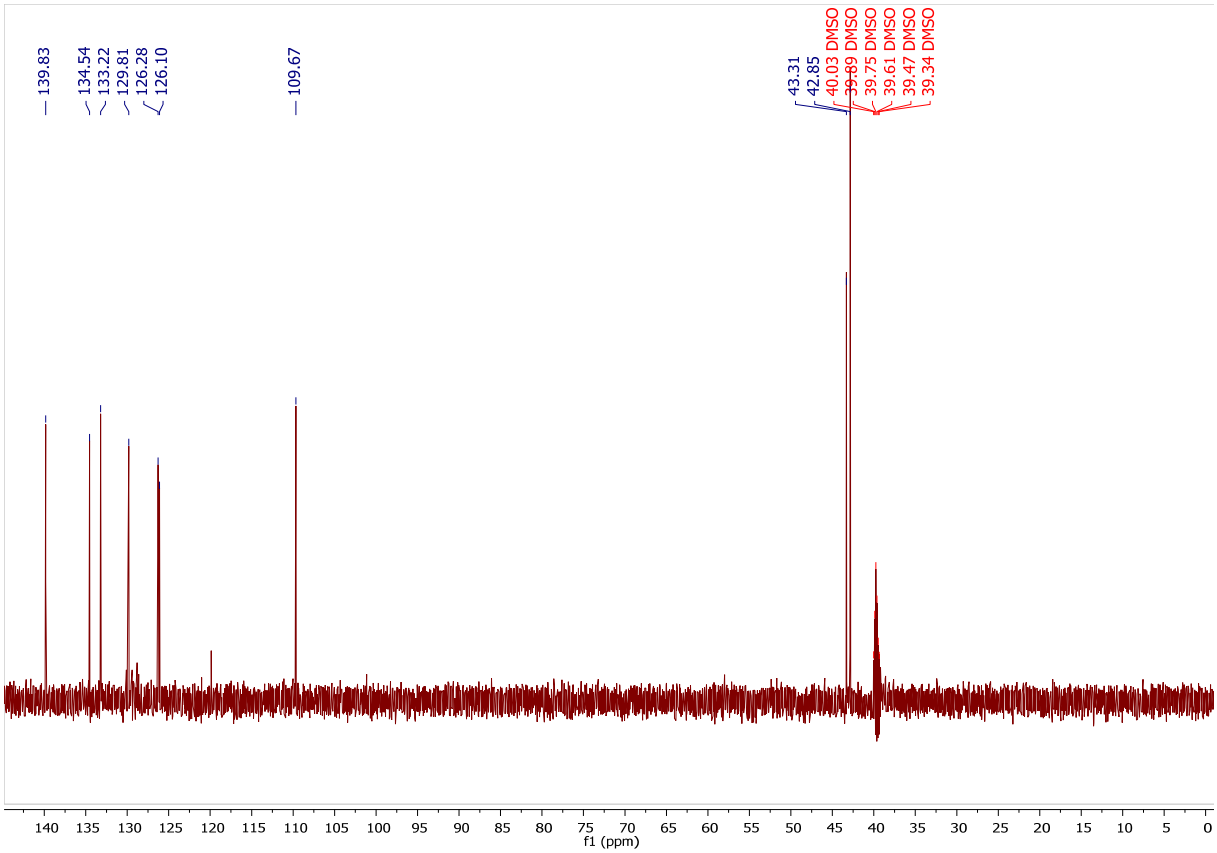

Figure 3.14. The DEPT-45 spectrum of **1**.

Table 3.6. The correlation between the NMR spectra and the structure of **2**.

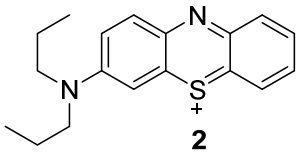

2

^{1}H NMR	**^{13}C NMR**
• The methyl (CH_3) protons correspond to the pentet at 0.99 ppm (The signal integrates for 6 protons). • The methylene (CH_3-$\underline{C}H_2$) protons correspond to the multiplet at 1.83–1.68 ppm (The signal integrates for 4 protons). • The methylene (N-$\underline{C}H_2$) protons correspond to the two triplets at 3.90 and 3.85 ppm (Each signal integrates for 2 protons). • The aromatic protons correspond to two triplet of doublets (7.81 and 7.85 ppm), a multiplet (8.07 – 7.97 ppm), and two doublet of doublets (8.19 and 8.13 ppm) (These signals integrate for 7 protons).	• The methyl ($\underline{C}H_3$) carbons are represented by the signals at 11.0 and 10.9 ppm. • The methylene (CH_3-$\underline{C}H_2$) carbons are represented by the signals at 21.9 and 21.2 ppm. • The methylene (N-$\underline{C}H_2$) carbons are represented by the signals at 54.8 and 54.4 ppm. • The aromatic carbons are represented by twelve signals at 155.6, 144.2, 140.3, 139.7, 138.8, 134.6, 133.3, 129.9, 126.3, 126.1, 126.03 and 109.4 ppm.
DEPT-135	
• The aromatic CH carbons are represented by seven signals at 140.3, 134.6, 133.3, 129.9, 126.3, 126.1 and 109.4 ppm. • The methyl (CH_3) carbons are represented by two signals at 11.0 and 10.9 ppm. • The methylene (CH_2) carbons are represented by four signals at 54.8, 54.4, 21.9 and 21.2 ppm.	

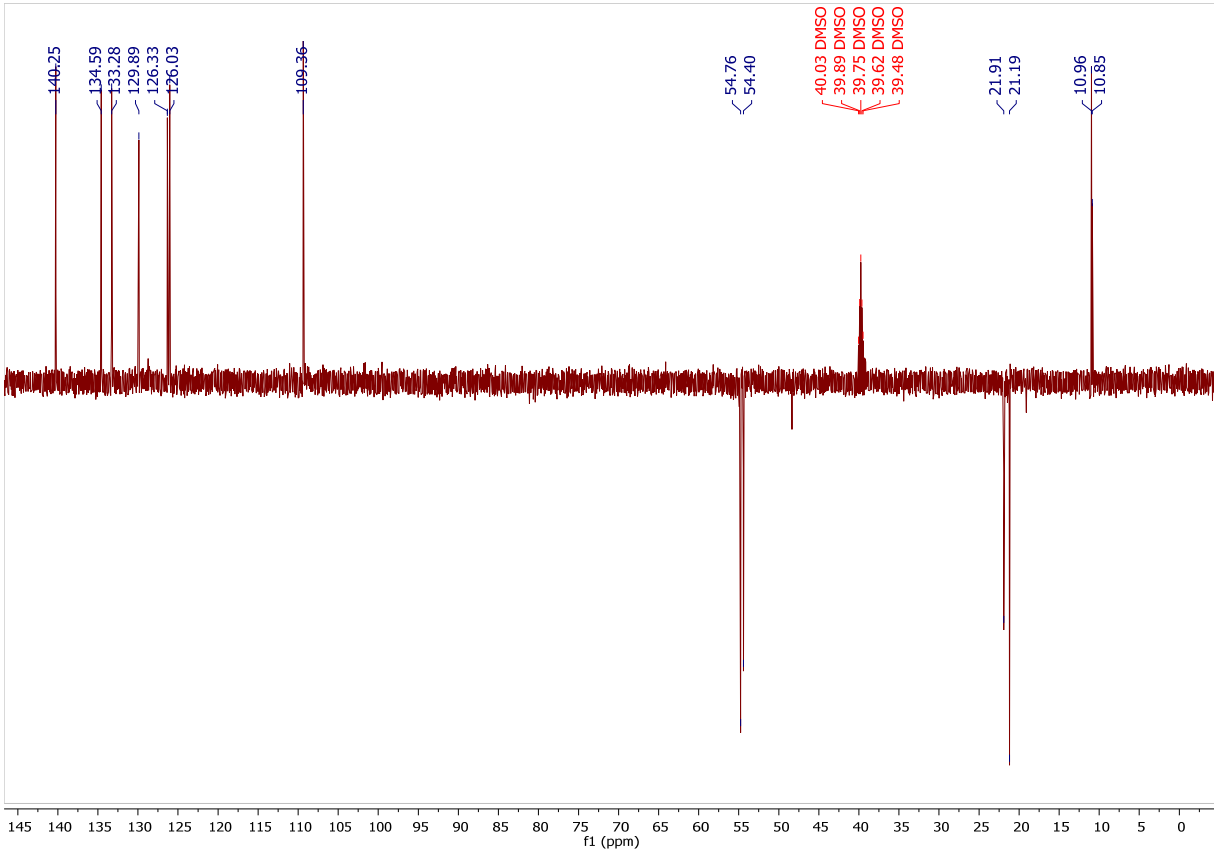

Figure 3.15. The DEPT-135 spectrum of **2**.

3.5.4 Melting points

The melting points of MB and MB analogues **1**–**2** were recorded and are given in Table 3.7. The results of the DSC show that the onset of melting for compound **1** is at 143.91 °C, but the melting occurs with degradation. For compound **2** the structural water is lost at 100.87 °C and melting occurs at 118.51 °C. The melting event is followed by degradation.

Table 3.7. The melting points of MB analogues **1**–**2**.

	Melting point (°C)
1	143.91 (melting with degradation)
2	118.51

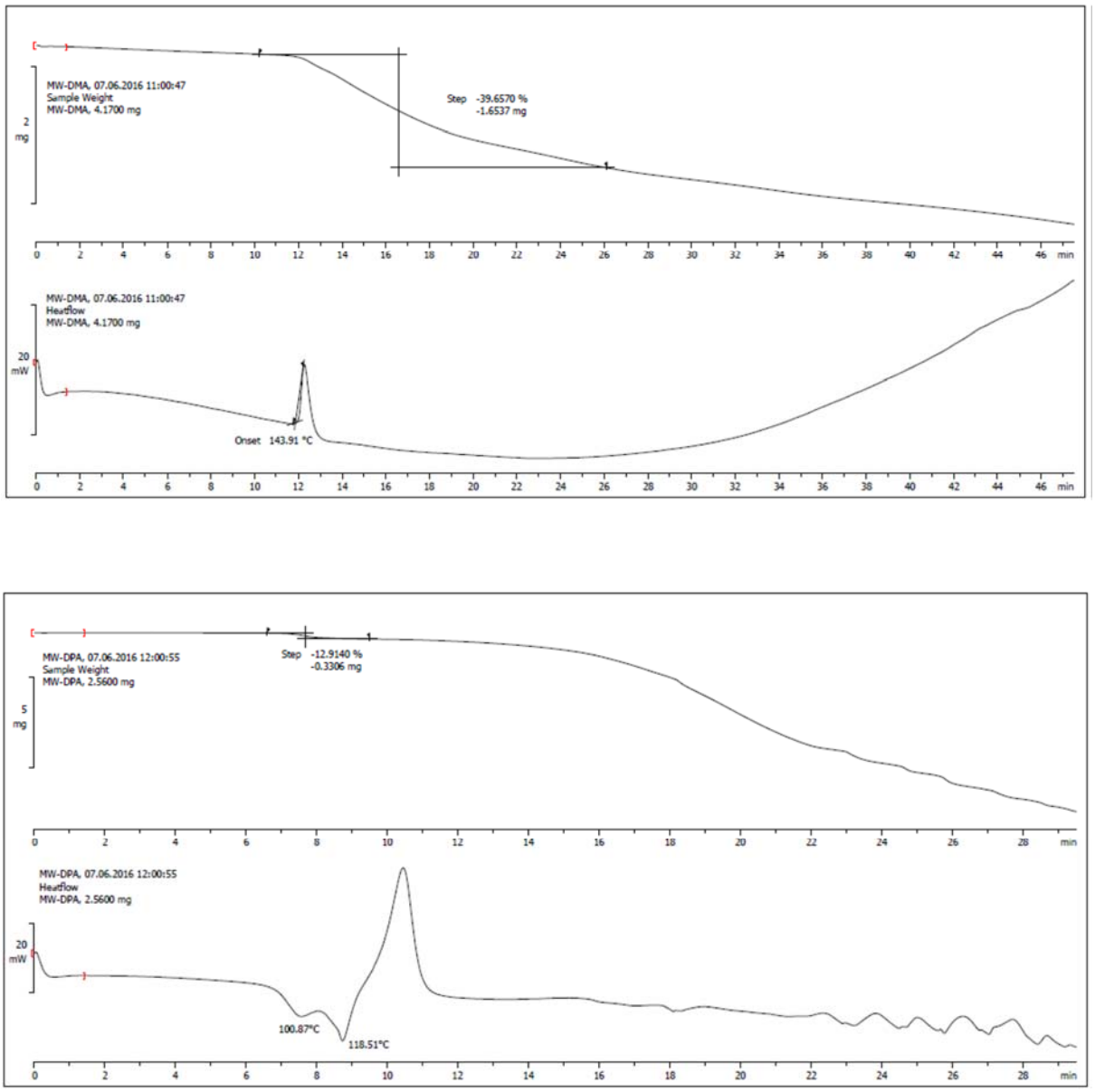

Figure 3.16. The DSC traces of compounds **1** (top) and **2** (bottom), respectively.

3.6 Conclusion

Using the protocol by Strekowski *et al*. (1993) this study has successfully synthesized two MB analogues. The analogues were characterised by NMR and MS, which corresponded with the proposed structures. In this respect, the integration values, multiplicities, chemical shifts and number of signals recorded by NMR correlated with the structures of the MB analogues. The experimentally determined molecular weights also corresponded with the calculated values. Although the yields were relatively low, the MB analogues exhibited a high degree of purity as judged by TLC. Thus, it can be concluded that the proposed structures of MB analogues **1**–**2** correspond with the physical data. This study also attempted the synthesis of various other MB analogues. Among these is compound **3**. Although the TLC analysis showed only one spot, the structure could not be confirmed by NMR. This appears to be another limitation for the synthesis of MB analogues and often unambiguous NMR spectra are difficult to obtain. This argument is supported by the ^{1}H NMR spectra of MB, in which the multiplicity of the signals was not observed.

Chapter 4
Enzymology

4.1 Introduction

In this chapter the MB analogues that were synthesized, compounds **1** and **2**, will be examined as potential inhibitors of human MAO-A and MAO-B. As discussed, MB is a high potency MAO-A inhibitor, a property that is responsible for serotonin toxicity associated with the use of MB in the clinic. MB also is a MAO-B inhibitor, but with several orders of magnitude lower potency compared to MAO-A inhibition. MB has been demonstrated to be a MAO-A and MAO-B inhibitor with an IC_{50} value of 0.07 μM for MAO-A (Aeschlimann *et al*., 1996; Harvey *et al*., 2010) and an IC_{50} value of 4.37 μM for MAO-B (Harvey *et al*., 2010; Ramsay *et al*., 2007). Several methods for measuring *in vitro* MAO activity have been reported. In this study, the determination of IC_{50} values of the synthetic analogues was done by fluorescence spectrophotometry. In this protocol, kynuramine is used as nonspecific MAO-A/B substrate. Kynuramine is oxidised by both MAO-A and MAO-B to ultimately yield 4-hydroxyquinoline, a fluorescent compound (Strydom *et al*., 2010). With fluorescence spectrophotometry, the formation of 4-hydroxyquinoline can be readily measured. From the MAO activity measurements in the presence of various concentrations of the test inhibitors, dose-response curves will be constructed from which the IC_{50} values will be calculated.

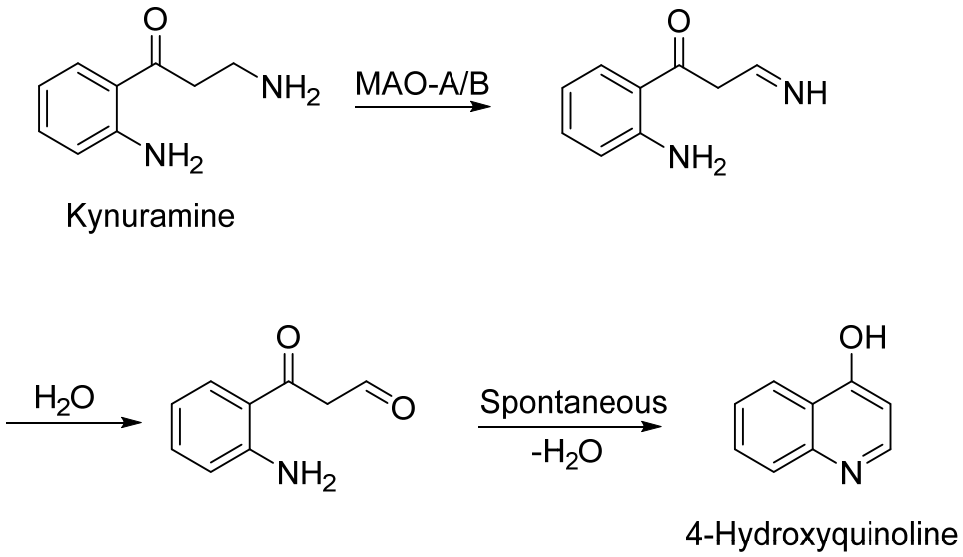

Figure 4.1. The oxidation of kynuramine by the MAOs to yield 4-hydroxyquinoline (Strydom *et al*., 2010).

4.2 Aims of this chapter

The main objective of this study is to determine if the synthesized MB analogues, compounds **1** and **2**, are inhibitors of human MAO-A and MAO-B. For this purpose the IC_{50} values will be measured and compared to those reported for MB. In addition, the reversibility of MAO inhibition by the synthetic analogues will be investigated by dialysis studies while the mode of inhibition will be investigated by constructing Lineweaver-Burk plots.

The following are the aims of this chapter:

- To evaluate the MAO-A and MAO-B inhibitory properties of the synthetic MB analogues, **1** and **2** by measuring IC_{50} values. These values will be compared to those reported for MB.
- To determine if **1** and **2** inhibits the human MAOs reversibility by conducting dialysis studies.
- To determine the mode of human MAO inhibition by **1** and **2** by the construction of Lineweaver-Burk plots.

4.3 Materials

Fluorescence measurements: A Varian Cary Eclipse fluorescence spectrophotometer (Agilent Technologies, Santa Clara, USA) was used for fluorometric measurements.

Chemicals: Kynuramine dihydrobromide, 4-hydroxyquinoline, (*R*)-deprenyl and pargyline were obtained from Sigma-Aldrich (St. Louis, MO, USA).

MAO enzymes: Insect cell microsomes containing recombinant human MAO-A (5 mg/ml) and MAO-B (5 mg/ml) were obtained from Sigma-Aldrich.

Data analysis: The sigmoidal dose-response curves to determine the IC_{50} values were constructed with a Graphpad Prism 5 software package (GraphPad, San Diego, CA, USA). All data analysis was done with the Graphpad Prism 5 software package.

Consumables and general chemicals: White polypropylene 96-well microtiter plates, potassium phosphate (K_2HPO_4/KH_2PO_4), DMSO, KCl, sucrose and NaOH were obtained from Merck (Merck, Darmstadt, Germany). To prepare all buffers, Milli-Q deionised water (Millipore) was used.

Dialysis: Slide-A-Lyzer dialysis cassettes (molecular weight cut-off at 10 000, sample volume capacity of 0.5–3 ml) were obtained from Thermo Scientific (Thermo Scientific, Waltham, MA, USA).

4.4 The determination of IC_{50} values

To determine the inhibition potencies of the synthetic MB analogues, **1** and **2**, IC_{50} values were measured. For this purpose sigmoidal dose-response curves were constructed from which the IC_{50} values were estimated. This study used the recombinant human MAO-A and MAO-B enzymes as enzyme sources. The mixed MAO-A/B substrate, kynuramine, served as substrate for both MAO enzymes.

4.4.1 Method

Figure 4.2 provides a summary for the method followed to determine IC_{50} values:

- All reactions were carried out in white 96-well microtiter plates (Eppendorf). The final volume of the enzymatic reactions was 200 µl.
- Potassium phosphate buffer (100 mM, made isotonic with KCl) at pH 7.4 served as reaction buffer.
- The enzyme reactions contained the following:
    - The MAO-A/B mixed substrate, kynuramine (50 µM).
    - Different inhibitor concentrations spanning at least 3 orders of magnitude (0.0003–100 µM).
    - DMSO as co-solvent (4%). The inhibitors were prepared in DMSO and added to the reactions to yield a final DMSO concentration of 4%.
    - The reactions were initiated with the addition of MAO-A or MAO-B (0.0075 mg protein/ml)
- The reactions were incubated for 20 min at 37 ºC in a convection oven.
- The reactions were subsequently terminated with the addition of 80 µl NaOH (2 N).
- The concentrations of 4-hydroxyquinoline formed in the reactions were measured by fluorescence spectrophotometry (λ_{ex} = 310; λ_{em} = 400 nm) (Novaroli *et al*., 2005).
- A linear calibration curve was constructed using authentic 4-hydroxyquinoline (0.047–1.56 µM). This curve was used to quantify the 4-hydroxyquinoline formed in the enzyme reactions. The enzyme catalytic rates were expressed as nmol 4-hydroxyquinoline formed/ min.mg protein.
- The enzyme catalytic rates were fitted to the one site competition model incorporated into the Prism 5 software package (GraphPad). The IC_{50} values were determined in triplicate and are expressed as mean ± standard deviation (SD).

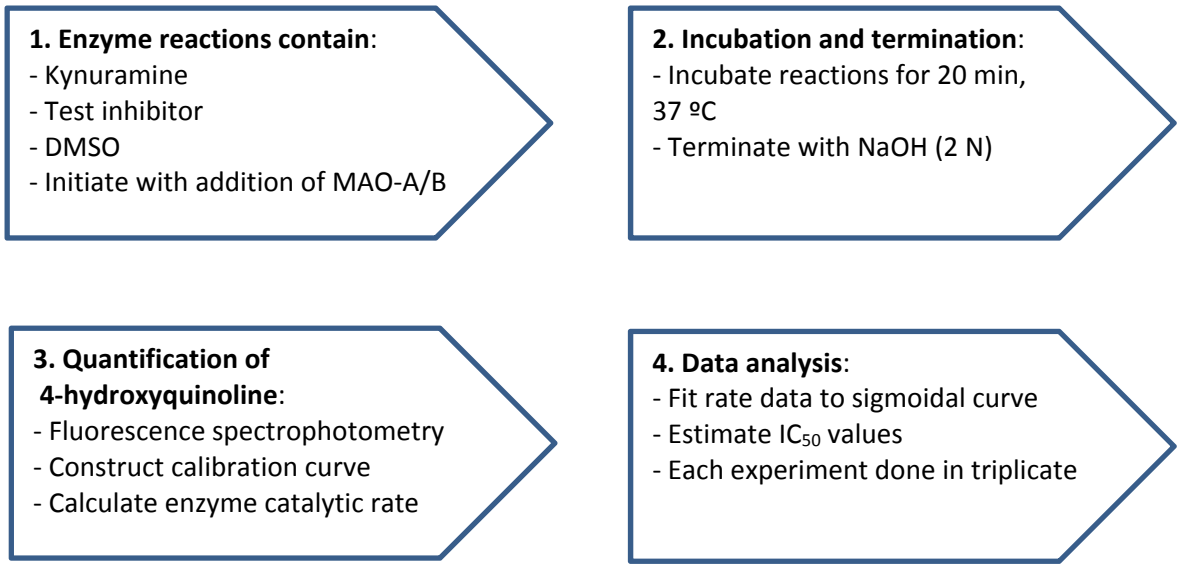

Figure 4.2. A summary of the method followed to determine IC_{50} values.

4.4.2 Results

General comments: An example of a linear calibration curve of fluorescence intensity versus 4-hydroxyquinoline concentration is given in Figure 4.3. As shown, fluorescence intensity versus 4-hydroxyquinoline concentration yields a high degree of linearity over the relevant range of this study (R^2 > 0.99). In this study, sigmoidal dose–response curves (enzyme catalytic rate versus logarithm of inhibitor concentration) were constructed in triplicate and the IC_{50} values were estimated from these graphs. The sigmoidal dose–response curves obtained will be given with the discussion of the results.

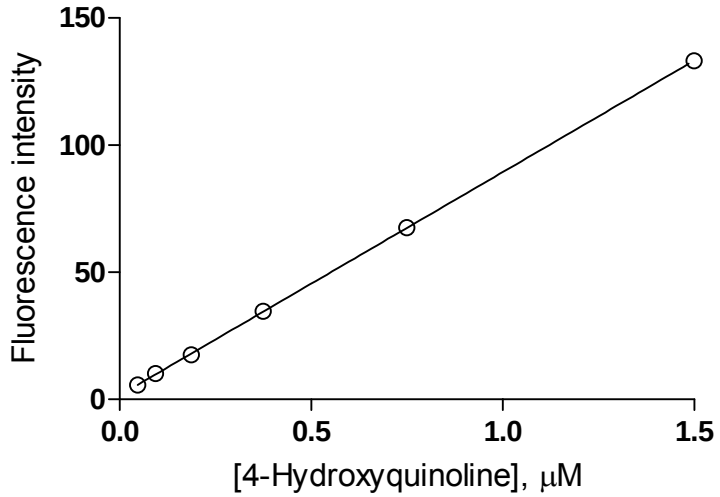

Figure 4.3. An example of a linear calibration curve of fluorescence intensity versus 4-hydroxyquinoline concentration.

Inhibition of MAO-A:

The sigmoidal dose–response curves for the inhibition of human MAO-A are given in Figures 4.4 and 4.5. The results show that compounds **1** and **2** inhibits MAO-A with IC_{50} values of 0.361 ± 0.007 μM and 0.728 ± 0.031 μM, respectively. Compared to MB, which exhibits an IC_{50} value of 0.07 μM for the inhibition of MAO-A (Aeschlimann *et al*., 1996; Harvey *et al*., 2010), these compounds are relatively weaker MAO-A inhibitors. As will be discussed at the end of this Chapter, this has implications for adverse effects associated with MB, most notably the cheese reaction and serotonin toxicity. Even though compounds **1** and **2** are less potent as MAO-A inhibitors than MB, they may still be regarded as MAO-A inhibitors and are in fact more potent inhibitors than toloxatone a clinically used MAO-A inhibitor which displays an IC_{50} value of 3.92 μM under identical experimental conditions to this study (Petzer *et al*., 2013). The observation that **2** is approximately twofold less potent as a MAO-A inhibitor than **1**, suggests that increasing the size of the dialkylamine side chain (as seen with **2**) lowers inhibition potency. Larger MB analogues may thus be less well accommodated in the MAO-A active site. The observation that MB is a higher potency MAO-A inhibitor than compounds **1** and **2** is not well understood on a molecular level. It is however clear that monosubstitution leads to lower MAO-A inhibition compared to the disubstituted MB.

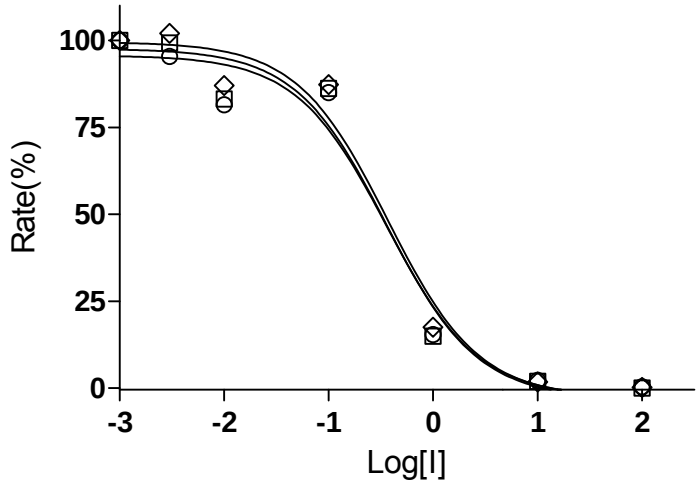

Figure 4.4. Sigmoidal dose–response curves for the inhibition of human MAO-A by compound **1** (three replicate determinations).

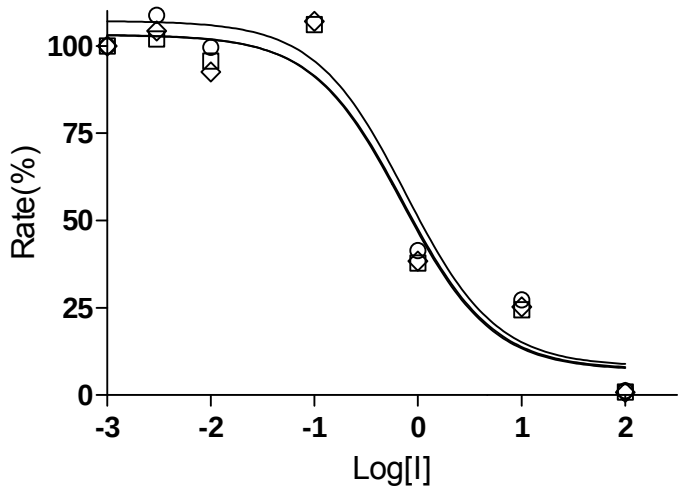

Figure 4.5. Sigmoidal dose–response curves for the inhibition of human MAO-A by compound **2** (three replicate determinations).

Inhibition of MAO-B:

The sigmoidal dose–response curves for the inhibition of human MAO-B are given in Figures 4.6 and 4.7. The results show that compounds **1** and **2** inhibit MAO-B with IC_{50} values of 0.105 ± 0.020 μM and 1.16 ± 0.128 μM, respectively. Compared to MB, which exhibits an IC_{50} value of 4.37 μM for the inhibition of MAO-B (Harvey *et al*., 2010; Ramsay *et al*., 2007), these compounds are relatively more potent MAO-B inhibitors. Compound **1,** in particular, is a potent MAO-B inhibitor and exhibits a similar IC_{50} value to the reference MAO-B inhibitor, lazabemide, which displays an IC_{50} value of 0.091 μM under identical experimental conditions to this study (Petzer *et al*., 2013). The observation that **2** is approximately 11-fold less potent as a MAO-B inhibitor than **1**, suggests that increasing the size of the dialkylamine side chain (as seen with **2**) lowers inhibition potency. This trend is similar to that observed for MAO-A. Larger MB analogues may thus be less well accommodated in the MAO-B active site. This point of view is supported by the report that azure B (IC_{50} = 0.968 μM), a metabolite of MB, is a more potent MAO-B inhibitor than MB (Petzer *et al*., 2012). Azure B is the N-demethylated metabolite of MB and thus possesses less steric bulk than MB. The presence of the second dimethylamine side chain in the structure of MB is expected to enhance steric bulk compared to compound **1** with only one dimethylamine side chain. This enhanced steric bulk may explain the lower MAO-B inhibition potency of MB compared to **1**. Also of interest, while MB is a highly selective MAO-A inhibitor, compound **1** is selective for MAO-A over the MAO-B isoform. Compound **2**, in turn, is a MAO-A selective inhibitor, but displays much less selectivity than MB.

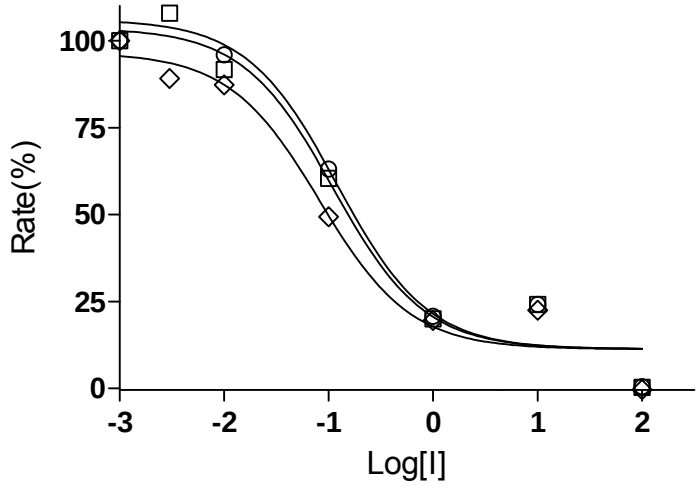

Figure 4.6. Sigmoidal dose–response curves for the inhibition of human MAO-B by compound **1** (three replicate determinations).

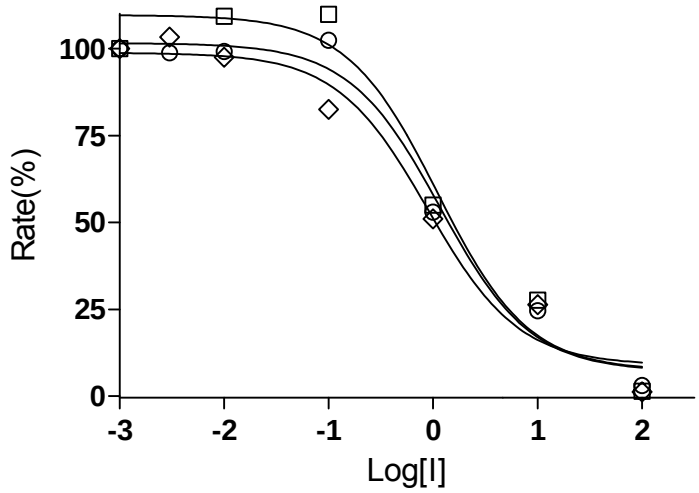

Figure 4.7. Sigmoidal dose–response curves for the inhibition of human MAO-B by compound **2** (three replicate determinations).

Table 4.1. The IC_{50} values for the inhibition of human MAO-A and MAO-B by compounds **1** and **2**. The reported values for MB are also given.

	IC_{50} (μM)[a]		SI[b]
	MAO-A	MAO-B	
1	0.361 ± 0.007	0.105 ± 0.020	3.44
2	0.728 ± 0.031	1.16 ± 0.128	0.63
MB	0.07[c]	4.37[c]	0.016

[a] All values are expressed as the mean ± standard deviation (SD) of triplicate determinations.

[b] Selectivity index (SI) = IC_{50}(MAO-A)/IC_{50}(MAO-B).

[c] Values from references (Aeschlimann *et al*., 1996; Harvey *et al*., 2010; Ramsay *et al*., 2007).

4.5 The reversibility of MAO inhibition

MAO inhibitors may be categorised as MAO-A selective, MAO-B selective and MAO-A/B non-selective inhibitors. MAO inhibitors may also be categorised as irreversible and reversible inhibitors. Reversibility of MAO inhibition is an important consideration since irreversible MAO-A inhibitors are used with caution in the clinic. Irreversible MAO-A inhibitors may cause a serious hypertensive response when taken with dietary tyramine (Da Prada *et al*., 1988). Tyramine is metabolised in the intestine by MAO-A which reduces systemic tyramine concentrations. The irreversible inhibition of MAO-A thus enhances the entry of tyramine into the systemic circulation and since tyramine induces the release of norepinephrine from peripheral neurons, a potentially dangerous increase in blood pressure may occur (Da Prada *et al*., 1988). Reversible MAO-A inhibitors do not cause tyramine-induced hypertension (Bonnet, 2003; Provost *et al*., 1992). MAO-B selective inhibitors, whether acting reversibly or irreversibly, are considered safe in this regard and do not potentiate tyramine-induced adverse effects. Since compounds **1** and **2** are good potency MAO-A inhibitors with IC_{50} values in the submicromolar region, it is of interest to determine the reversibility of MAO-A inhibition. Since MB is a reversible MAO-A inhibitor, it may be expected that compounds **1** and **2** would also act as reversible MAO-A inhibitors (Ramsay *et al*., 2007). This study will also investigate the reversibility of MAO-B inhibition by compounds **1** and **2**.

4.5.1 Method

The reversibility of the MAO inhibition by compounds **1** and **2** was examined by dialysis (Petzer *et al*., 2013). Figure 4.8 provides a summary for the method followed for the dialysis studies:

Dialysis of test inhibitors:

- Mixtures of MAO-A or MAO-B (0.03 mg/ml) and the test inhibitor, at a concentration of 4 × IC_{50} were prepared to a volume of 0.8 ml. The inhibitors were prepared in DMSO and added to the reactions to yield a final DMSO concentration of 4%.
- The buffer for these studies was potassium phosphate buffer (100 mM, pH 7.4) containing 5% sucrose.
- The mixtures were preincubated for 15 min at 37 °C and were subsequently placed in the Slide-A-Lyzer dialysis cassettes.
- The mixtures were dialysed at 4 °C in 80 ml of the buffer. The dialysis buffer was replaced with fresh buffer at 3 h and 7 h after the start of dialysis. Dialysis was carried out for 24 h in total.

Control reactions:

- As positive controls, MAO-A and MAO-B were preincubated in the presence of the irreversible inhibitors, pargyline and (R)-deprenyl, respectively. The concentrations of pargyline [IC_{50}(MAO-A) = 13 μM] (Strydom *et al*., 2012) and (R)-deprenyl [IC_{50}(MAO-B) = 0.079 μM] (Petzer *et al*., 2012) employed were equal to 4 × IC_{50} for the inhibition of MAO-A and MAO-B, respectively. These mixtures were dialysed as above.
- As negative control, MAO-A and MAO-B were preincubated in the absence of inhibitor. These mixtures were dialysed as above.
- Mixtures of the MAO-A and MAO-B and the test inhibitor were also maintained at 4 °C for 24 h, and were not dialysed.

MAO activity measurements:

- After 24 h of dialysis, samples of the dialysis mixtures (250 μl) were diluted twofold with the addition of kynuramine (250 μl) to yield an inhibitor concentration of 2 × IC_{50}, and a kynuramine concentration of 50 μM.
- These reactions (0.5 ml) were incubated for 20 min at 37 ºC.
- The reactions were terminated with the addition of 400 μl NaOH (2 N) and 1000 μl water.

- The concentrations of 4-hydroxyquinoline formed in the reactions were measured by fluorescence spectrophotometry (λ_{ex} = 310; λ_{em} = 400 nm) (Novaroli *et al*., 2005). For this purpose a 3.5 ml quartz cuvette (pathlength 10 × 10 mm) was employed.
- A linear calibration curve was constructed using authentic 4-hydroxyquinoline (0.047–1.56 μM). This curve was used to quantify the 4-hydroxyquinoline formed in the enzyme reactions. The enzyme catalytic rates were expressed as nmol 4-hydroxyquinoline formed/ min.mg protein.
- The dialysis experiments were carried out in triplicate and the MAO catalytic rates are expressed as mean ± SD.

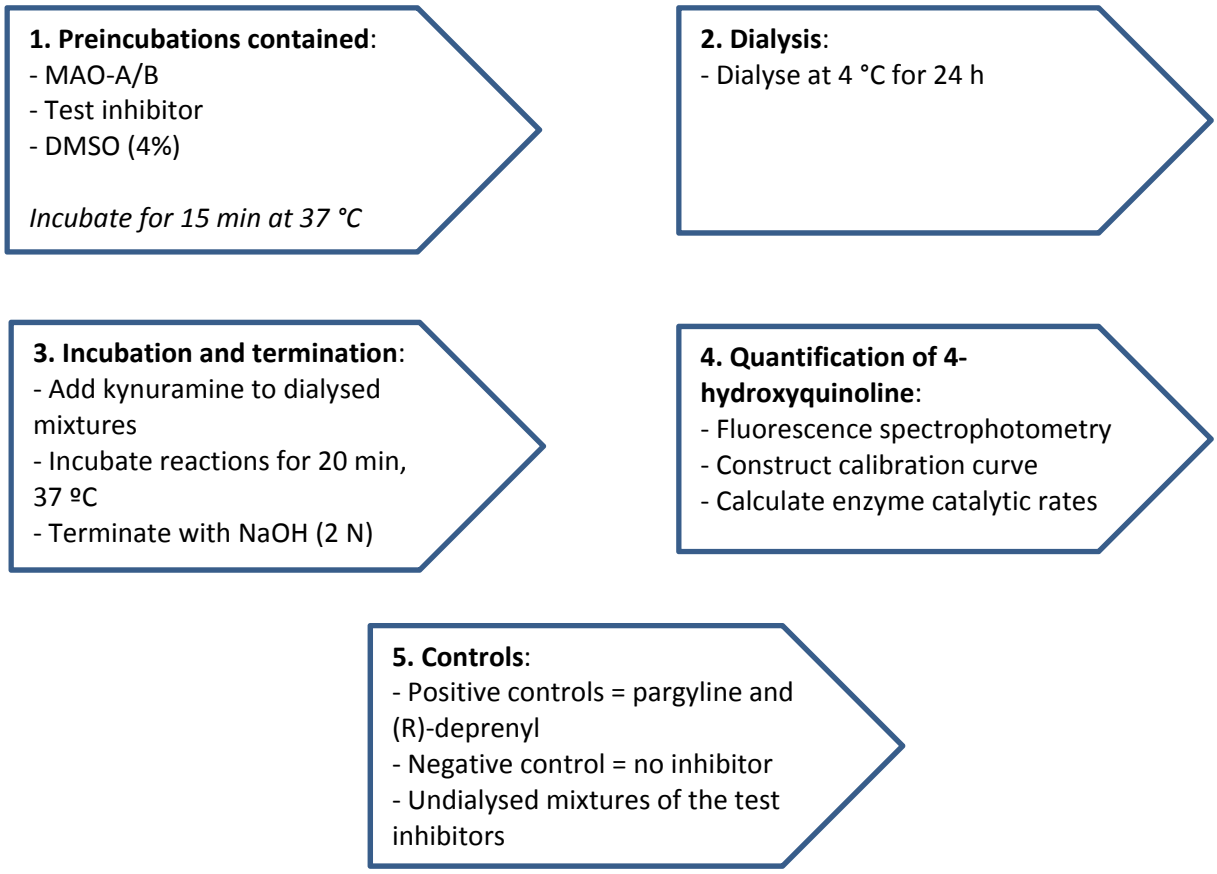

Figure 4.8. A summary of the method followed for the dialysis studies.

4.5.2 Results

In this study, the reversibility of MAO-A and MAO-B inhibition by MB analogues **1** and **2** were examined by dialysis. To determine if **1** and **2** are reversible inhibitors of the MAOs, the test inhibitors (at concentrations of 4 × IC_{50}) were incubated with MAO-A and MAO-B for a period of 15 min and subsequently dialysed for 24 h. The residual MAO catalytic activities were measured and compared to the MAO activities of the negative control, which consisted of dialysis experiments carried out in the absence of the test inhibitor. For reversible inhibition, it is expected that following dialysis of enzyme–inhibitor mixtures, enzyme activity will recover to levels equivalent to those of the control values (100%). As shown in Figure 4.9, after dialysis of mixtures of MAO-A and **1**, the MAO-A activity is completely recovered with the catalytic activity at 110% of the negative control value (recorded in the absence of inhibitor). In contrast, the MAO-A activity of undialysed mixtures of MAO-A and **1** is only 22% of the negative control value. This result shows that **1** interacts reversibly with MAO-A. After similar treatment and dialysis of mixtures of MAO-A and pargyline, an irreversible MAO-A inhibitor, the enzyme activity is not recovered, with the residual enzyme activity at a level of only 0.9% of the negative control value.

Figure 4.9 shows that after dialysis of mixtures of MAO-B and **1**, the MAO-B activity is also recovered with the catalytic activity at 90% of the negative control value (recorded in the absence of inhibitor). In contrast, the MAO-B activity of undialysed mixtures of MAO-B and **1** is only 32% of the negative control value. This result shows that **1** interacts reversibly with MAO-B. After similar treatment and dialysis of mixtures of MAO-B and (R)-deprenyl, an irreversible MAO-B inhibitor, the enzyme activity is not recovered, with the residual enzyme activity at a level of only 2.1% of the negative control value.

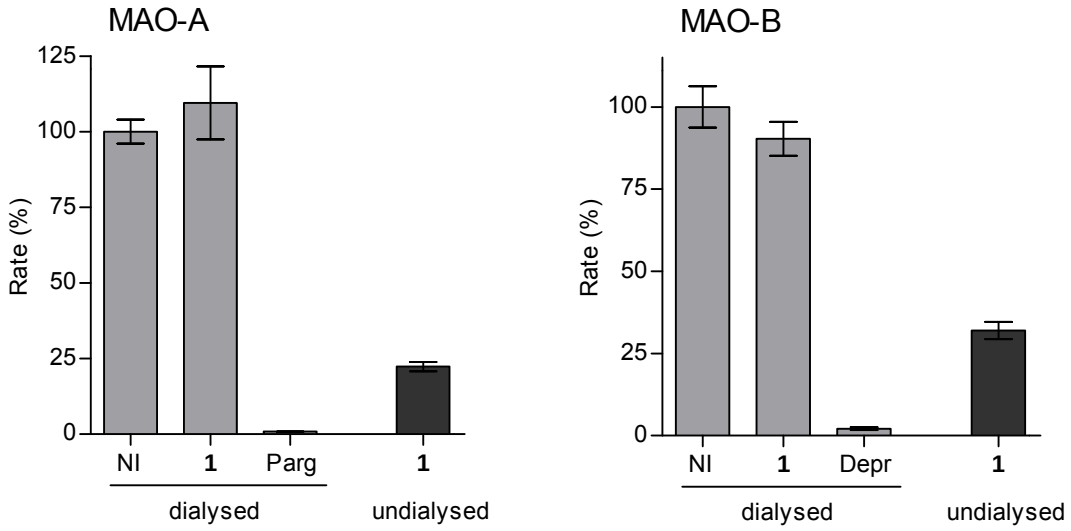

Figure 4.9. The reversibility of inhibition of human MAO-A and MAO-B by compound **1**. The MAO enzymes and **1** were preincubated for 15 min, dialysed for 24 h and the residual enzyme activities were measured (**1**–dialysed). The enzymes were similarly preincubated in the absence (NI–dialysed) and presence of the irreversible inhibitors, pargyline (Parg–dialysed) or (R)-deprenyl (Depr–dialysed), and dialysed. For comparison, the residual MAO activities of undialysed mixtures of the MAOs with **1** are also shown (**1**–undialysed).

As shown in Figure 4.10, after dialysis of mixtures of MAO-A and **2**, the MAO-A activity is also completely recovered with the catalytic activity at 100% of the negative control value (recorded in the absence of inhibitor). In contrast, the MAO-A activity of undialysed mixtures of MAO-A and **2** is only 30% of the negative control value. This result shows that **2** interacts reversibly with MAO-A.

Figure 4.10 shows that after dialysis of mixtures of MAO-B and **2**, the MAO-B activity is recovered with the catalytic activity at 77% of the negative control value (recorded in the absence of inhibitor). In contrast, the MAO-B activity of undialysed mixtures of MAO-B and **2** is only 33% of the negative control value. This result shows that **2** most likely interacts reversibly with MAO-B, but dialysis does not completely restore enzyme activity. A possible explanation for this is that **2** may exhibit some degree of tight-binding to MAO-B.

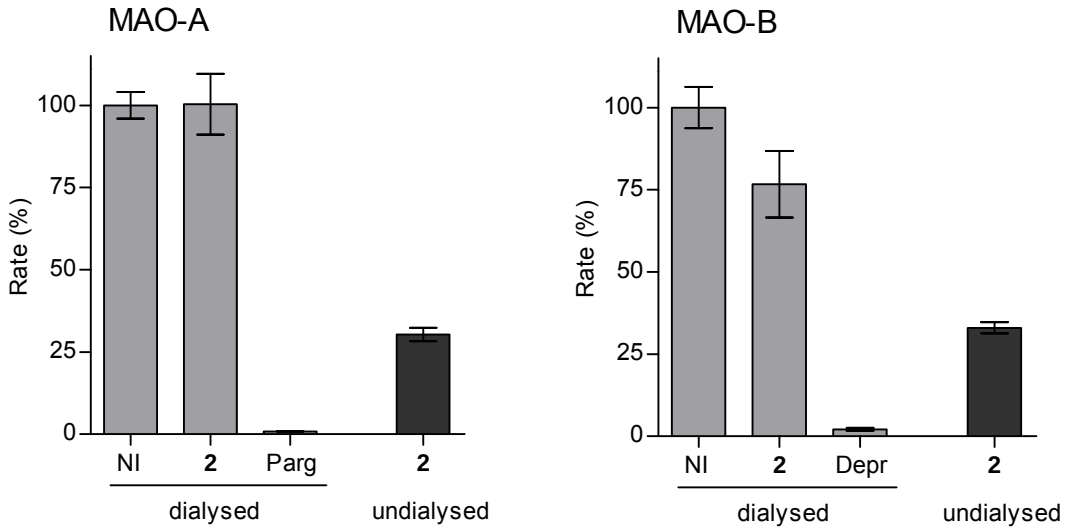

Figure 4.10. The reversibility of inhibition of human MAO-A and MAO-B by compound **2**. The MAO enzymes and **2** were preincubated for 15 min, dialysed for 24 h and the residual enzyme activities were measured (**2**–dialysed). The enzymes were similarly preincubated in the absence (NI–dialysed) and presence of the irreversible inhibitors, pargyline (Parg–dialysed) or (R)-deprenyl (Depr–dialysed), and dialysed. For comparison, the residual MAO activities of undialysed mixtures of the MAOs with **2** are also shown (**2**–undialysed).

4.6 Lineweaver-Burk plots and K_i value determinations

To investigate the modes of MAO-A and MAO-B inhibition by compounds **1** and **2**, sets of Lineweaver-Burk plots for the inhibition of each MAO isoform were constructed. Each set of Lineweaver-Burk plots was constructed by measuring MAO activity at 8 different kynuramine concentrations (15–250 μM), in the absence of inhibitor, and presence of five different concentrations of the test inhibitor. With this study it will be determined if compounds **1** and **2** are competitive inhibitors of the MAOs. Furthermore, the enzyme-inhibitor dissociation constants (K_i values) for the reversible interaction of compounds **1** and **2** with the MAOs will be measured.

4.6.1 Method

Figure 4.11 provides a summary for the method followed for the construction of Lineweaver-Burk plots:

- All reactions were carried out in 1.5 ml microcentrifuge tubes. The final volume of the enzymatic reactions was 0.5 ml.

- Potassium phosphate buffer (100 mM, made isotonic with KCl) at pH 7.4 served as reaction buffer.
- The enzyme reactions contained the following:
    - The MAO-A/B mixed substrate kynuramine at 8 different concentrations (15–250 µM)
    - The following six inhibitor concentrations: 0 × $IC_{50,}$ ¼ × IC_{50}, ½ × IC_{50}, ¾ × IC_{50}, 1 × IC_{50} and 1¼ × IC_{50}
    - DMSO as co-solvent (4%). The inhibitors were prepared in DMSO and added to the reactions to yield a final DMSO concentration of 4%
    - The reactions were initiated with the addition of MAO-A or MAO-B (0.015 mg protein/ml)
- These reactions (0.5 ml) were incubated for 20 min at 37 ºC in a waterbath.
- The reactions were terminated with the addition of 400 µl NaOH (2 N) and 1000 µl water.
- The concentrations of 4-hydroxyquinoline formed in the reactions were measured by fluorescence spectrophotometry (λ_{ex} = 310; λ_{em} = 400 nm) (Novaroli *et al*., 2005). For this purpose a 3.5 ml quartz cuvette (pathlength 10 × 10 mm) was employed.
- A linear calibration curve was constructed using authentic 4-hydroxyquinoline (0.047–1.56 µM). This curve was used to quantify the 4-hydroxyquinoline formed in the enzyme reactions. The enzyme catalytic rates were expressed as nmol 4-hydroxyquinoline formed/ min.mg protein.
- The Lineweaver-Burk plots were constructed with the Prism 5 software package.
- The K_i values were estimated by global (shared) fitting of the inhibition data to the Michaelis-Menten equation using the Prism 5 software package. The K_i values may also be estimated from a plot of the slopes of the Lineweaver-Burke plots versus inhibitor concentration (x-axis intercept equals $–K_i$).

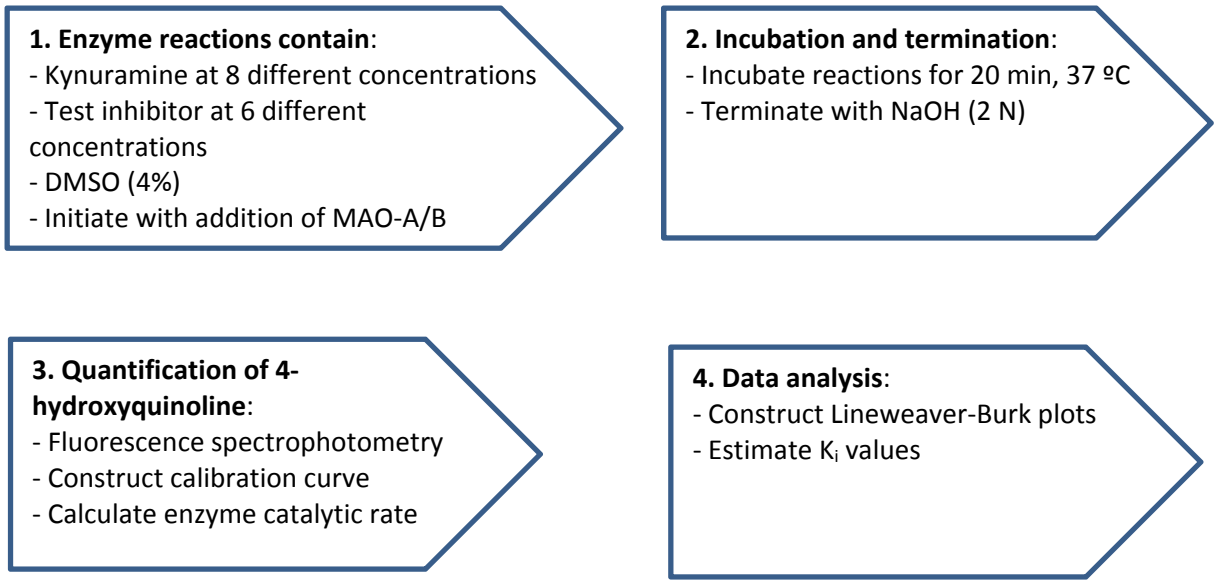

Figure 4.11. A summary of the method followed for the construction of Lineweaver-Burk plots.

4.6.2 Results

The Lineweaver-Burk plots for the inhibition of MAO-A by compound **1** is shown in Figure 4.12. For the inhibition of MAO-A, the lines of the Lineweaver-Burk plots are linear, but intersect on the x-axis. For competitive inhibition, the lines are, however, expected to intersect on the y-axis indicating that V_{max} remains unchanged with increasing concentrations of the competitive inhibitor, while the apparent K_m increases. The observation that the lines intersect on the x-axis is indicative of non-competitive inhibition where the apparent K_m remains unchanged with increasing concentrations of the non-competitive inhibitor, while V_{max} decreases. The decrease in V_{max} is also apparent from the Michaelis-Menten graphs illustrated in Figure 4.13, which shows that V_{max} decreases with increasing concentrations of the inhibitor. These data suggests that compound **1** is not a competitive MAO-A inhibitor, but exhibit kinetics more related to non-competitive inhibition. A non-competitive inhibitor usually binds reversibly to a different site from the active site, where the substrate binds. With the inhibitor bound the substrate is converted at a slower rate to product compared to when no inhibitor is bound. The K_i value for non-competitive inhibition of MAO-A by **1** was determined by global (shared) fitting of the inhibition data to the Michaelis-Menten equation using the Prism 5 software package. This value is listed in Table 4.1 and was found to be 0.280 ± 0.018 μM.

For the inhibition of MAO-B by compound **1**, the set of Lineweaver-Burk plots obtained fitted neither classical competitive nor non-competitive inhibition. The data are thus presented in Figure 4.13 as the corresponding Michaelis-Menten plots. As for the inhibition of MAO-A by **1**,

V_{max} decreases with increasing concentrations of the inhibitor. An estimation of the K_i for non-competitive inhibition yields a value of 0.058 ± 0.0027 μM.

For the inhibition of MAO-A and MAO-B by compound **2**, the sets of Lineweaver-Burk plots obtained also did not fit classical competitive or non-competitive inhibition. The Michaelis-Menten plots are presented in Figure 4.14 and show that for the inhibition of MAO-A and MAO-B by **2**, V_{max} decreases with increasing concentrations of the inhibitor. An estimation of the K_i values for non-competitive inhibition yields 0.581 ± 0.015 μM for MAO-A and 1.03 ± 0.057 μM for MAO-B.

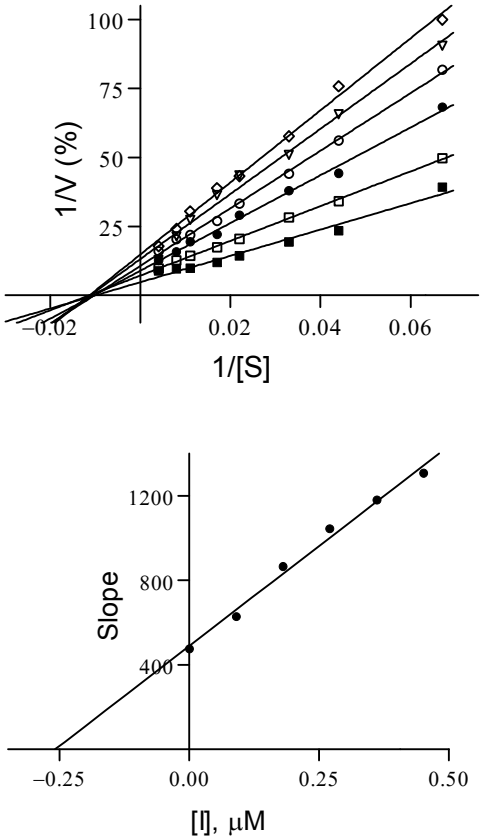

Figure 4.12. Lineweaver-Burk plots for the inhibition of human MAO-A in the absence (filled squares) and presence of various concentrations of **1**. The concentrations of **1** used were equal to ¼ × IC_{50}, ½ × IC_{50}, ¾ × IC_{50}, 1 × IC_{50} and 1¼ × IC_{50}. These graphs show the slopes of the Lineweaver-Burk plots versus inhibitor concentration.

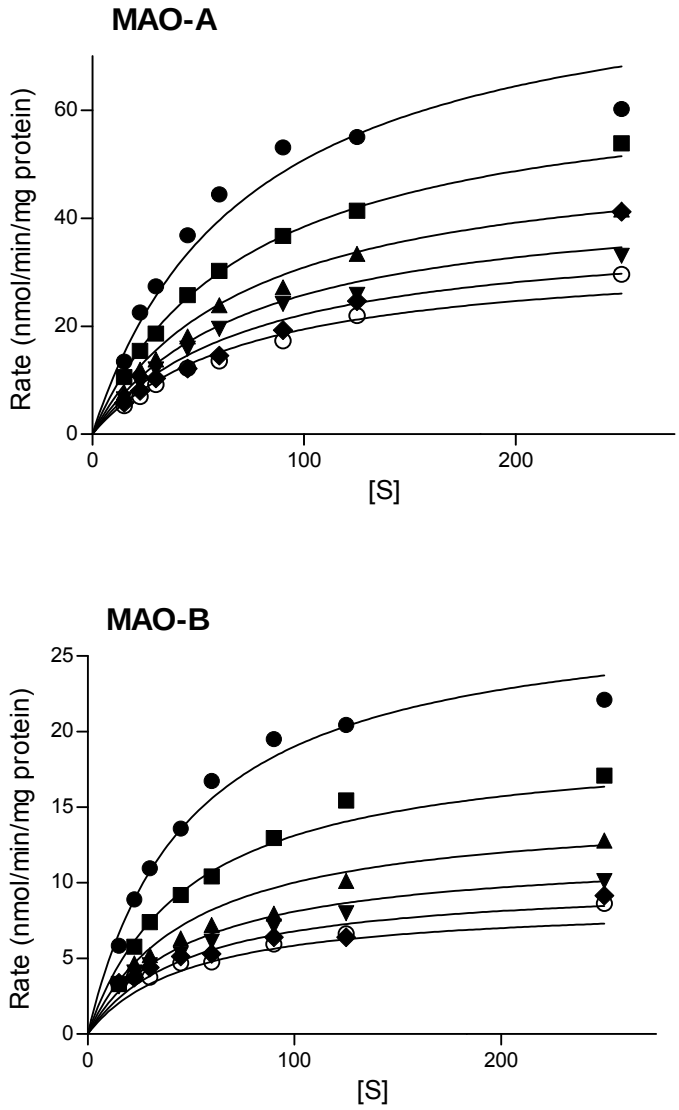

Figure 4.13. Michaelis-Menten plots for the catalytic rates of human MAO-A and MAO-B in the absence (filled circles) and presence of various concentrations of **1**. The concentrations of **1** used were equal to ¼ × IC_{50}, ½ × IC_{50}, ¾ × IC_{50}, 1 × IC_{50} and 1¼ × IC_{50}.

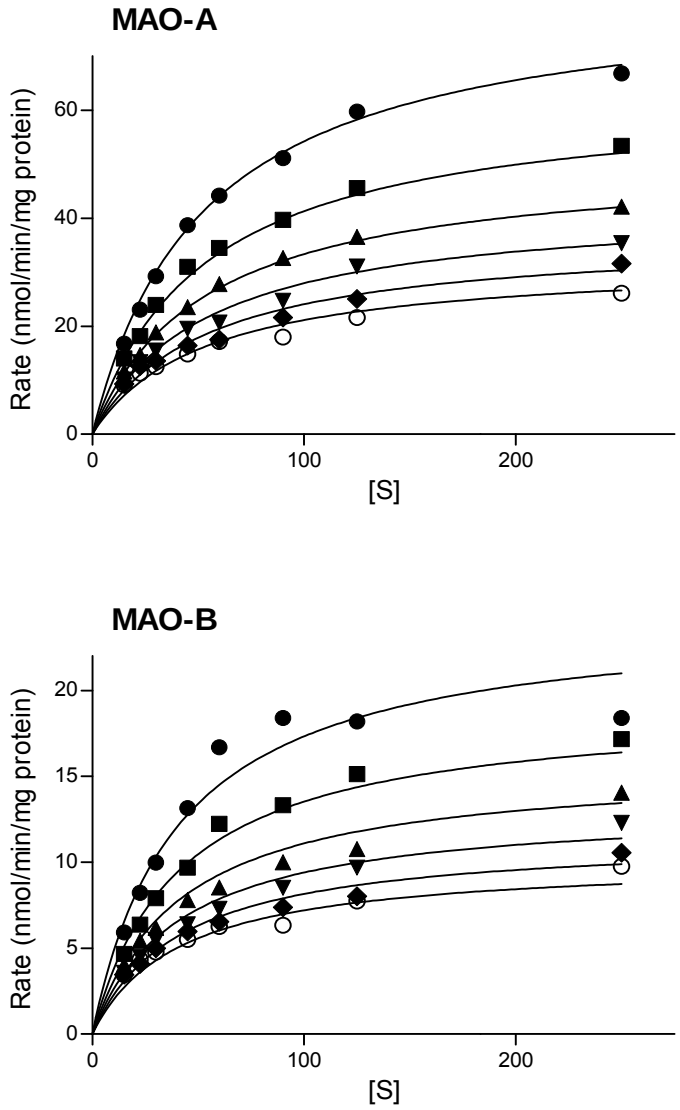

Figure 4.14. Michaelis-Menten plots for the catalytic rates of human MAO-A and MAO-B in the absence (filled circles) and presence of various concentrations of **2**. The concentrations of **2** used were equal to ¼ × IC_{50}, ½ × IC_{50}, ¾ × IC_{50}, 1 × IC_{50} and 1¼ × IC_{50}.

Table 4.2. The K_i values (non-competitive) for the inhibition of human MAO-A and MAO-B by compounds **1** and **2**.

	K_i (μM)[a]		SI[b]
	MAO-A	MAO-B	
1	0.280 ± 0.018	0.058 ± 0.0027	4.83
2	0.581 ± 0.015	1.03 ± 0.057	0.56
MB	0.027[c]		

[a] All values are expressed as the mean ± standard deviation (SD).

[b] Selectivity index (SI) = K_i(MAO-A)/K_i(MAO-B).

[c] Value from reference (Ramsay *et al*., 2007).

4.7 Conclusion

This chapter evaluated the MAO inhibition properties of the synthetic MB analogues, **1** and **2**. From the IC_{50} values it is clear that **1** is a more potent MAO-A and MAO-B inhibitor compared to **2**. Compounds **1** and **2** are, however, significantly weaker as MAO-A inhibitors compared to MB, but display more potent inhibition of the MAO-B isoform compared to MB. The MB analogues were also found to be reversible MAO inhibitors, although **2** may exhibit some tight-binding to MAO-B. The reversible mode of MAO inhibition is similar to that reported for MB (Ramsay *et al*., 2007). Reversible MAO-A inhibitors do not cause tyramine-induced hypertension, and it may thus be concluded that the MB analogues should possess a good safety profile in this regard (Bonnet, 2003; Provost *et al*., 1992). Interestingly, the Lineweaver-Burk plots constructed for the inhibition of the MAOs by **1** and **2** are not typical of competitive inhibition. For the inhibition of MAO-A by **1**, the Lineweaver-Burk plots are indicative of non-competitive inhibition. For all compounds, V_{max} for MAO-A and MAO-B is suppressed with increasing inhibitor concentration. Although this dissertation cannot unequivocally state that inhibition is non-competitive, it is clear that MAO inhibition by **1** and **2** is not classical competitive. Although some elements of the kinetic analysis are consistent with non-competitive inhibition, the docking study will clearly show that **1** and **2** fit within the MAO-A and MAO-B active sites (Chapter 5). This finding argues against the non-competitive mode of inhibition since non-competitive inhibitors does not bind in the substrate binding cavity.

Chapter 5
Molecular modelling

5.1 Introduction

In the previous chapter it was shown that the MB analogues, **1** and **2**, are MAO inhibitors. In spite of their structural similarities, MB and compounds **1** and **2** exhibit different potencies and specificities for the MAO isoforms. For example, compound **1** is a highly potent MAO-B inhibitor, while MB and **2** are only moderately potent as MAO-B inhibitors. Also, MB is a much more potent inhibitor of MAO-A than either **1** or **2**. To provide more insight into these findings, this chapter explores possible binding orientations of these compounds in MAO-A and MAO-B by using molecular modelling. An overview of the structures of MAO-A and MAO-B will, however, firstly be given as background to this chapter.

5.2 Background to the structures of MAO

MAO B:

The X-ray crystal structure of human MAO-B was first reported in 2002 (Binda *et al*., 2002). The structure showed that the FAD cofactor is covalently bound to the MAO protein via an 8α-thioether linkage to Cys397 and that the MAO-B protein is bound via the C-terminal α-helix to the mitochondrial outer membrane. This α-helix consists of 32 amino acids and protrudes perpendicularly into the phospholipid bilayer of the mitochondrial membrane, thus anchoring the enzyme (Binda *et al*., 2002).

Figure 5.1. The structure of human MAO-B. The FAD is shown in magenta while the co-crystallised ligand, safinamide, is shown in yellow. The C-terminal α-helix is at the bottom of the structure (Binda *et al*., 2007).

To reach the active site of the enzyme, a substrate molecule must pass by a protein loop at the entrance to the active site. The active site of MAO-B consists of two cavities, the “entrance cavity” and the “substrate cavity”, which are separated by the side chain Ile199. This residue thus serves as a “gate” between the two cavities and may rotate from the cavity space to allow for fusion of the two cavities into a single large space. This fusion occurs when large cavity spanning compounds bind to MAO-B. The other residues that define the border between the two cavities are Leu171, Phe168 and Tyr326. The entrance cavity has a volume of 290 $Å^3$ while the substrate cavity has a volume of 420 $Å^3$. The amine functional group of a substrate is recognised at the back of the active site by an aromatic cage, which is formed by residues Tyr398, Tyr435 and the isoalloxazine ring system of the FAD. The side chains of Tyr398 and Tyr435 are orientated perpendicular to the plane of the flavin ring (Binda *et al*, 2002).

MAO-A:

The X-ray crystal structure of MAO-A shows that, similar to MAO-B, the FAD cofactor is covalently bound to the MAO protein. For MAO-A, this linkage is to Cys406. The MAO-A protein is also bound to the mitochondrial outer membrane via the C-terminal α-helix (Son *et al*., 2008). The similar structures of MAO-A and MAO-B are to be expected since these

enzymes are approximately 70% identical on the amino acid sequence level (Shih *et al*., 1999).

Figure 5.2. The structure of human MAO-A. The FAD is shown in magenta while the co-crystallised ligand, harmine, is shown in yellow. The C-terminal α-helix is at the bottom of the structure (Son *et al*., 2008).

In contrast to human MAO-B, MAO-A has a single substrate binding cavity which is much smaller, shorter and wider. The MAO-A active site has a volume of 550 $Å^3$. As for MAO-B, the amine functional group of a substrate is recognised at the back of the active site by an aromatic cage, which is formed by residues Tyr407, Tyr444 and FAD ring system. The side chains of Tyr407 and Tyr444 are also orientated perpendicular to the plane of the flavin ring, which is similar to MAO-B (Son *et al*., 2008).

Differences in active site residues between MAO-A and MAO-B are responsible for the different substrate and inhibitor specificities of the two isoforms. Most notably, Phe208 in MAO-A is a relatively large residue which restricts the binding of larger compounds to MAO-A. Ile199 is the homologous residue (to Phe208) in MAO-B and since its side chain has a smaller volume than the Phe208 side chain, Ile199 is able to rotate from the active site to allow larger inhibitors to bind to the fused entrance and substrate cavities (Son *et al*., 2008). Also, Tyr326 in MAO-B imposes a restriction on certain orientations that compounds may adopt. In

MAO-A the homologous residue is Ile335. Because of its smaller size, compounds may adopt certain orientations in MAO-A which is not possible in MAO-B (Son *et al*., 2008).

5.3 Aims of this chapter

The objective of this chapter is to gain insight into the potential binding orientations of compounds **1** and **2** in the active sites of human MAO-A and MAO-B.

The following are the aims of this chapter:

- To dock harmine and safinamide into active site models of human MAO-A and MAO-B, respectively, and to compare the binding orientations to those of the co-crystallised ligands in the corresponding X-ray crystal structures.
- To dock MB into active site models of human MAO-A and MAO-B and further analyse the binding interactions by dynamics simulation.
- To dock compounds **1** and **2** into active site models of human MAO-A and MAO-B, and to compare the binding orientations to that of MB.

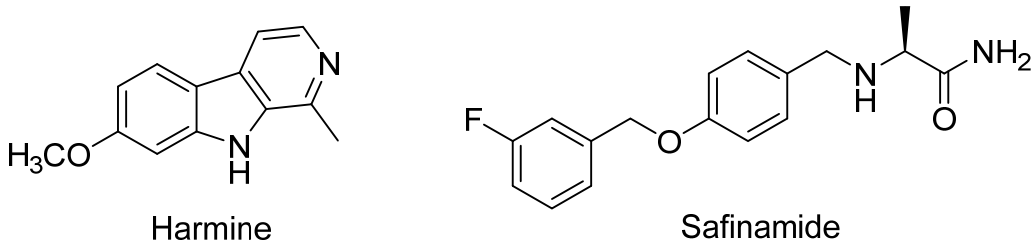

Figure 5.3. The structures of harmine and safinamide (Son *et al*., 2008).

5.4 Materials and methods

5.4.1 Materials

- For the docking studies, the Windows-based Discovery Studio 3.1 software package (Accelrys, San Diego, CA, USA) was used, applying the default values and conditions (unless otherwise specified).
- The reported X-ray crystal structures of human MAO-A (PDB code 2Z5X) (Son *et al*., 2008) and human MAO-B (PDB code 2V5Z) (Binda *et al*., 2007) served as protein models. These models were obtained from the Brookhaven Protein Data Bank. In these structures MAO-A is complexed with harmine while safinamide serves as co-crystallised ligand for MAO-B.
- The illustrations were prepared with Discovery Studio 3.1.

5.4.2 Docking procedure

Docking of a structure into a receptor model involves three steps namely, (a) protein preparation, (b) construction of the ligands and (c) docking of the ligands into the receptor model. These steps are illustrated in Figure 5.4 and detailed below.

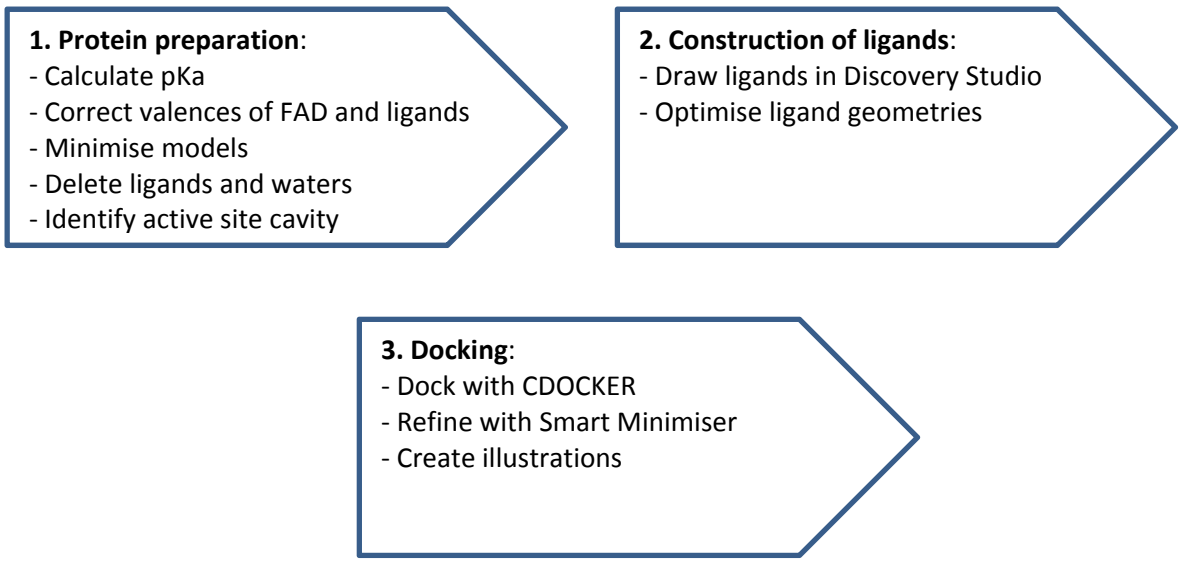

Figure 5.4. An illustration of the docking procedure.

Protein preparation:

- The models were prepared for the docking simulations by firstly calculating the pKa values and protonation states (at pH 7.4) of the ionisable amino acids. Based on these calculations hydrogen atoms were added.
- The FAD cofactors were set to the oxidised state and after verifying that the valences of the FAD cofactors and co-crystallised ligands (harmine and safinamide) are correct, the Momany and Rone CHARMm force field was applied to the models.
- A fixed atom constraint was applied to the peptide backbone and employing the Smart Minimizer algorithm (maximum steps, 5000), the models were energy minimised. For this procedure the implicit generalized Born solvation model with molecular volume was used.
- The backbone constraints as well as co-crystallised ligands were removed and the active site cavities were identified by analysing the cavities present in the proteins.
- All waters were subsequently removed from the protein models, with the exception of HOH 710, 718 and 739 in MAO-A, and HOH 1155, 1170 and 1351 in the A-chain of MAO-B. These waters are located in the active sites of the MAOs and are considered to be conserved.

Construction of ligands:

- The structures of the ligands were drawn in Discovery Studio and their geometries were briefly optimised using a Dreiding-like force field (5000 iterations). For the purpose of this step, the ligands were harmine, safinamide, MB and compounds **1** and **2**.
- After submitting the inhibitor structures to the Prepare Ligands protocol, atom potential types and partial charges were assigned with the Momany and Rone CHARMm force field.

Docking:

- The ligands were docked into the MAO models with the CDOCKER algorithm, allowing for ten random conformations for each inhibitor. For the docking procedure, the heating target temperature was set to 700 K and full potential mode was used.
- Finally, the docking orientations were refined using *in situ* ligand minimisation with the Smart Minimizer algorithm.

5.4.3 Molecular dynamics simulation

The dynamics simulation was carried out with the standard dynamics cascade provided in Discovery Studio. For this purpose the highest ranked docking solution for MB (as docked into MAO-B) was subjected to a short molecular dynamics simulation (500 ps). The following is an overview of the protocol, which is also given in Figure 5.5.

- The prepared protein models from the docking studies were used as starting points. Fixed atom constraints were applied to the backbone of the protein model and the residues that are further than 5 Å from the docked ligand.
- Using the standard dynamics cascade, the interaction of MB with MAO-B was studied. The first two steps of the cascade consisted of a steepest descent minimisation (maximum steps, 2500) followed by a conjugate gradient minimisation (maximum steps, 2500; RMS gradient, 0.01).
- Heating consisted of 2000 steps (time step, 0.001 ps) from 50 K to 300 K, and equilibration of the system was allowed for 10000 steps (time step, 0.001 ps).
- The production run was carried out for 500 000 steps (time step, 0.001 ps) in the NVT ensemble, applying the SHAKE algorithm to all bonds involving hydrogen atoms. The equations for motion were integrated with the Leapfrog Verlet algorithm. The implicit generalized Born solvation model with simple switching was used during the dynamics calculations. The conformation of the complex was saved every 1 ps, yielding 500 frames.

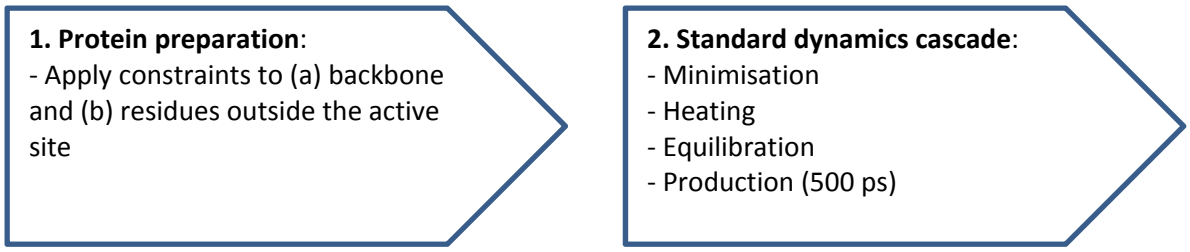

Figure 5.5. An illustration of the steps of the molecular dynamics simulation.

5.5 Results

5.5.1 MAO-A docking results

Harmine docked into MAO-A:

As shown in Figure 5.6, harmine docks into the MAO-A active site with a similar orientation to that observed in the X-ray crystal structure, with the pyridine nitrogen directed towards the FAD. The docked orientation of harmine exhibits a root-mean-square deviation (RMSD) value of only 1.20 Å from the orientation of the co-crystallised ligand. The docked harmine is placed slightly (approximately 1.32 Å) further form the FAD compared to the position of the co-crystallised ligand. Based on the similarity of both binding orientation and position of the docked and co-crystallised ligands, it may be concluded that the docking protocol is suitable for docking ligands into an active site model of MAO-A. The docking results show that harmine undergoes a π–π interaction with Tyr444, one of the amino acids that defines the aromatic sandwich in the MAO-A active site.

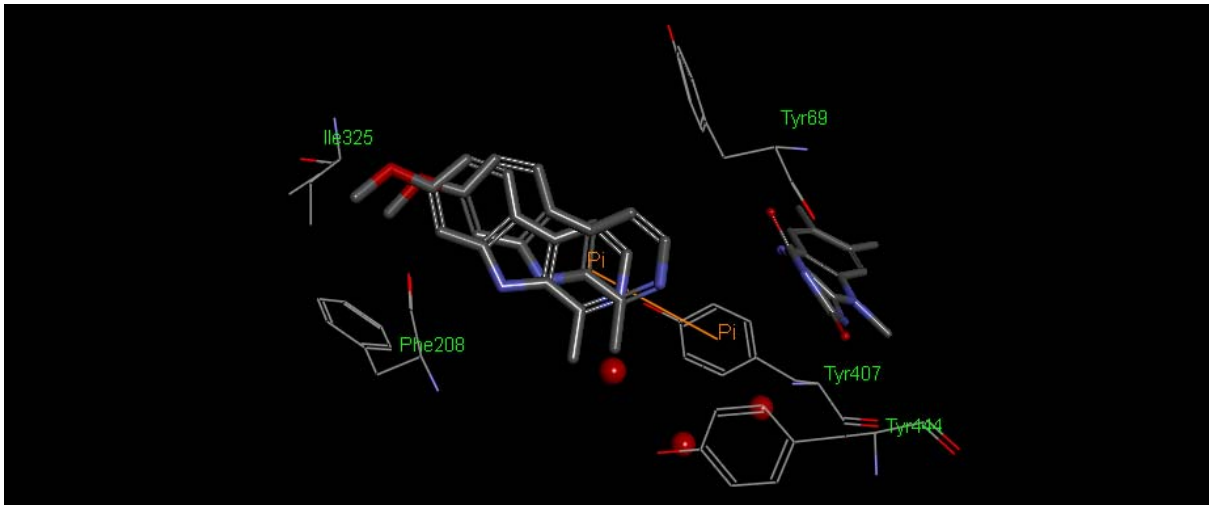

Figure 5.6. The docked binding orientation of harmine in MAO-A compared to the orientation of harmine in the X-ray crystal structure.

MB docked into MAO-A:

As shown in Figure 5.7, MB docks into the MAO-A active site with a similar orientation to harmine and binds at approximately the same distance from the FAD as harmine. MB forms a π–π interaction with Tyr407, also one of the amino acids that define the aromatic sandwich in the MAO-A active site. Furthermore, the charged thiazine sulphur of MB undergoes a π–cation interaction with the phenyl ring of Phe208. In this respect, the thiazine sulphur is directed to the bottom of the active site, in the direction of Phe208.

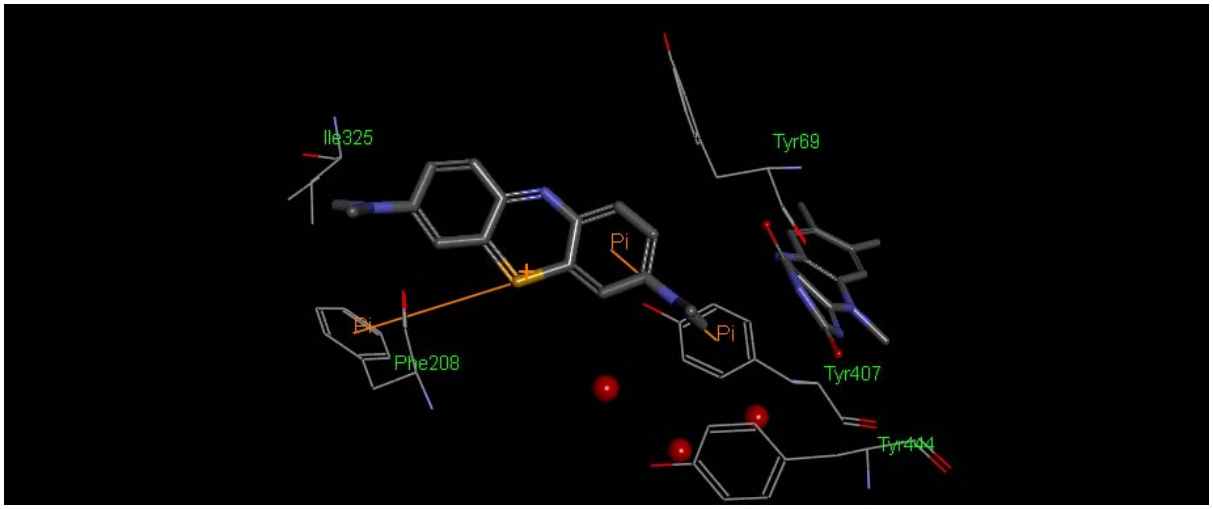

Figure 5.7. The docked binding orientation of MB in MAO-A.

*Compound **1** docked into MAO-A:*

As shown in Figure 5.8, compound **1** docks into the MAO-A active site with a similar orientation to MB. Also, similar to MB, compound **1** forms a π–π interaction with Tyr407. Compound **1** binds closer to the FAD than MB, and as a result the π–cation interaction with the phenyl ring of Phe208 is not observed. For **1** the thiazine sulphur is also directed to the bottom of the active site, in the direction of Phe208. Interestingly, the dimethylamine group of **1** is directed away from the FAD, which makes it possible for this compound to approach closer to the FAD than MB. The projection of the dimethylamine group away from the FAD is to be expected since the region in front of the FAD is relatively polar compared to the rest of the active site and the region where the hydrophobic dimethylamine group binds.

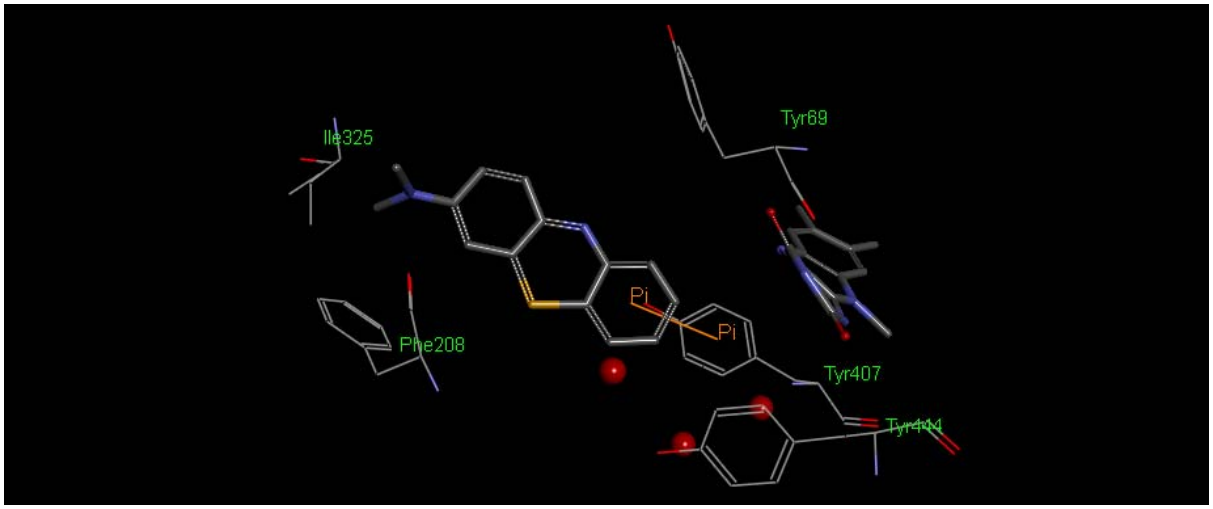

Figure 5.8. The docked binding orientation of compound **1** in MAO-A.

*Compound **2** docked into MAO-A:*

As shown in Figure 5.9, compound **2** docks into the MAO-A active site with the thiazine sulphur directed to the top of the active site, in the direction of Tyr69. This is opposite to the orientations observed for MB and compound **1**. Compound **2** thus has the ability to form a π–cation interaction with the phenyl ring of Phe69. As observed for harmine, compound **2** undergoes a π–π interaction with Tyr444. The opposite orientation of **2** compared to MB and **1** is most likely due to steric limitation imposed by Phe208. The phenyl ring of this residue may undergo structural overlap with the dipropylamine group should compound **2** have bound with a similar orientation to MB and **1**. As with compound **1**, compound **2** binds closer to the FAD than MB, a placement made possible by the projection of the dipropylamine group away from the FAD. This orientation is also to be expected since the hydrophobic dimethylamine group would preferably bind in the apolar region and not in front of the FAD, the most polar area of the MAO-A active site.

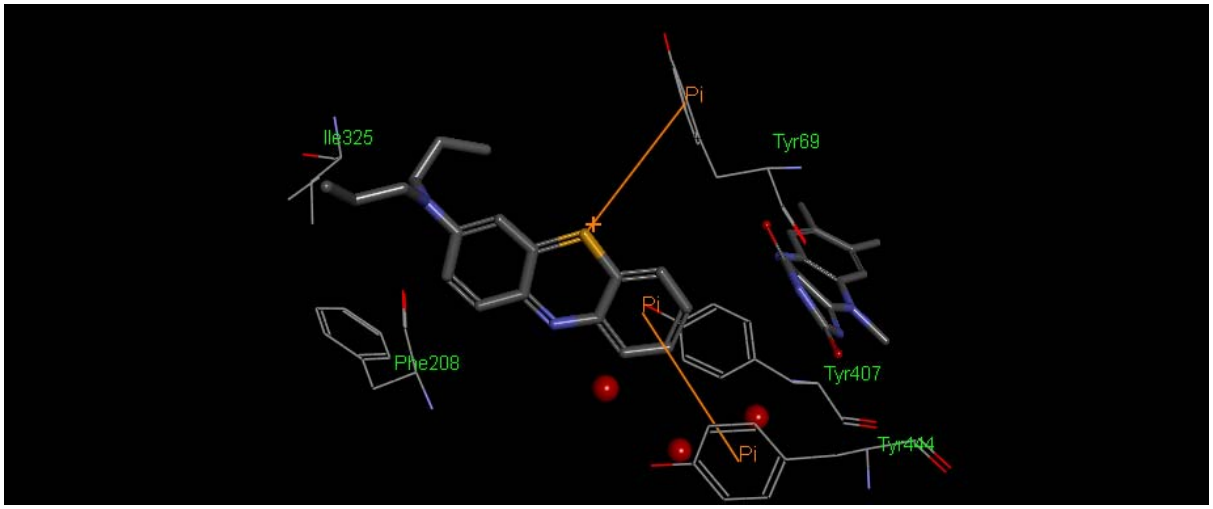

Figure 5.9. The docked binding orientation of compound **2** in MAO-A.

5.5.2 MAO-B docking results

Safinamide docked into MAO-B:

As shown in Figure 5.10, the orientation by which safinamide docks into the MAO-B active site is virtually superimposable on the orientation observed in the X-ray crystal structure. The docked orientation of safinamide exhibits a RMSD value of only 0.44 Å from the orientation of the co-crystallised ligand. Based on the similarity of the orientation and position of the docked and co-crystallised ligands, it may be concluded that the docking protocol is suitable for docking ligands into an active site model of MAO-B. Safinamide binds in the MAO-B active site with the amide functional group placed in proximity to the FAD, which is considered to be the polar region of the MAO-B active site. Here the amide oxygen undergoes hydrogen bonding with a water molecule. The fluorobenzyloxy side chain of safinamide, in turns, binds towards the entrance of the cavity, which is a hydrophobic region. The fluorobenzyloxy side chain extends well beyond Ile199, the gate residue between the entrance and substrate cavities of MAO-B. It may thus be concluded that safinamide spans both cavities of MAO-B.

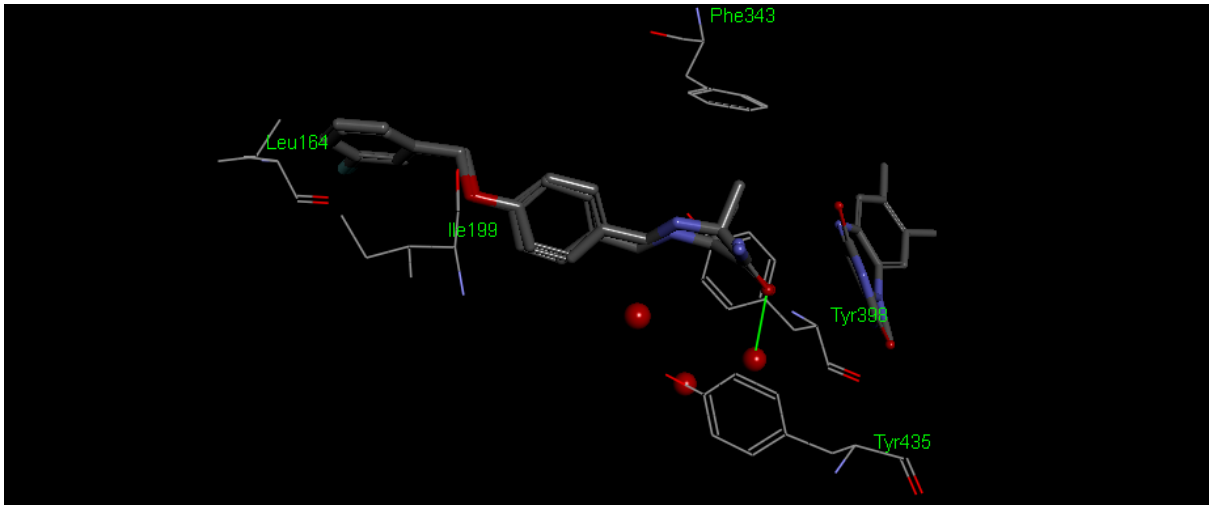

Figure 5.10. The docked binding orientation of safinamide in MAO-B compared to the orientation of safinamide in the X-ray crystal structure.

MB docked into MAO-B:

As shown in Figure 5.11, MB docks into the MAO-B active site with the thiazine sulphur directed to the top of the active site, in the direction of Phe343. This is opposite to the orientation observed for MB in MAO-A. MB forms a π–π interaction with Tyr435, one of the amino acids that define the aromatic sandwich in the MAO-B active site. Because of its smaller size compared to safinamide, MB does not extend as deep into the entrance cavity of MAO-B, with only the dimethylamine establishing contacts in the entrance cavity. Support for the accuracy of the docking simulation comes from the structure of MB in complex with human MAO-B, which bears the double mutation I199A-Y326A (PDB code: 3ZYX). Although the structure differs for native MAO-B in the mutations of key residues in the active site, the orientation of MB is the same to the docked orientations with respect to the thiazine sulphur, which is also directed to the top of the cavity (Figure 5.12).

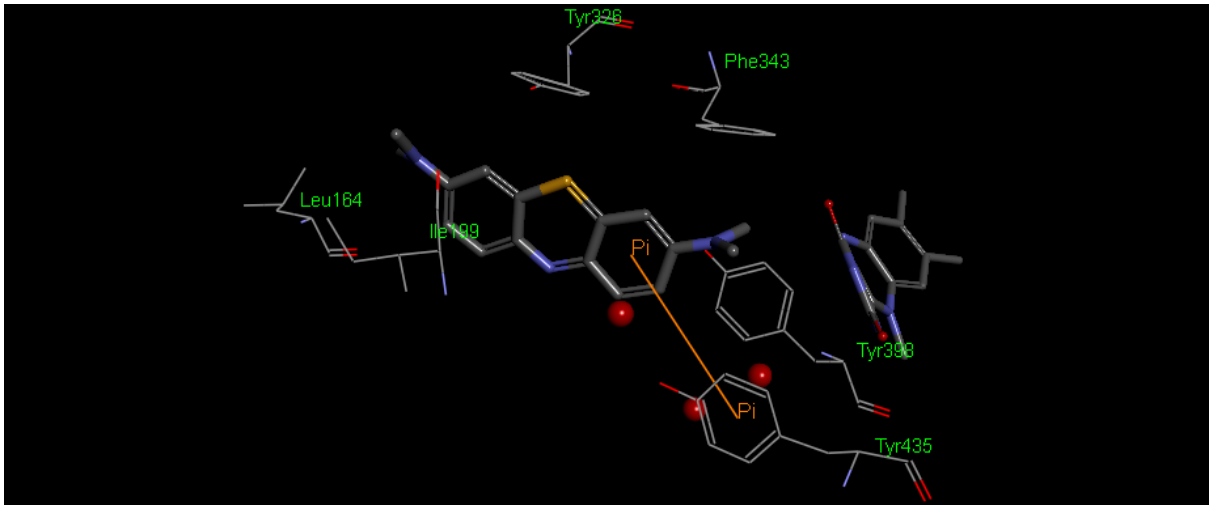

Figure 5.11. The docked binding orientation of MB in MAO-B.

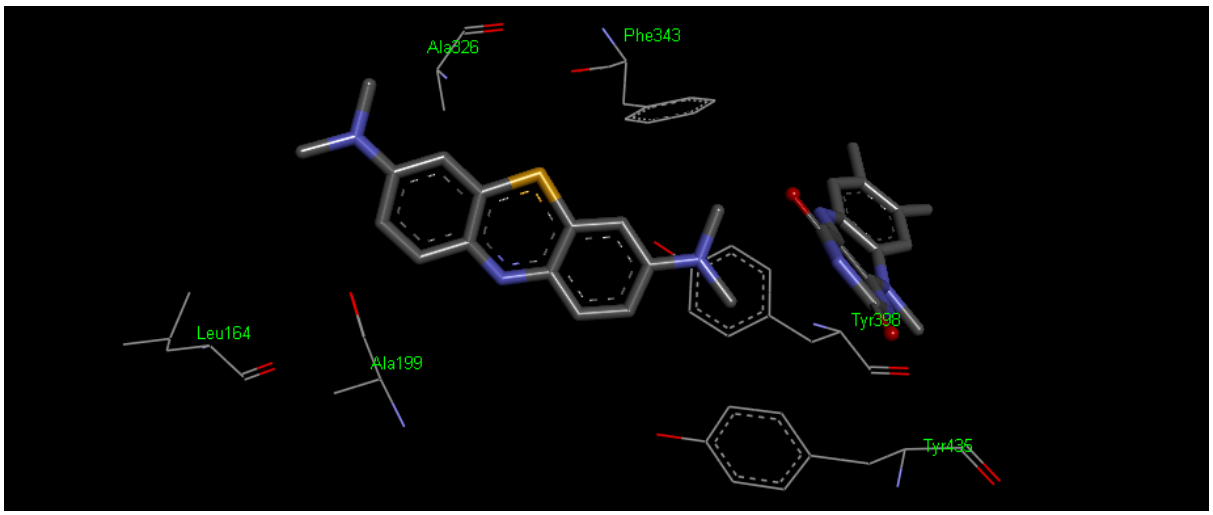

Figure 5.12. The binding orientation of MB in a crystal structure of human MAO-B which bears the double mutation I199A-Y326A (PDB code: 3ZYX).

*Compound **1** docked into MAO-B:*

As shown in Figure 5.13, compound **1** docks into the MAO-B active site with a similar orientation to that observed in MAO-A and the thiazine sulphur is thus directed to the bottom of the active site, in the opposite direction of Phe343. This orientation is opposite that observed for MB in MAO-B. Interestingly, compound **1** binds distant from the FAD, which enables the establishment of a π–cation interaction with the phenyl ring of Tyr326. The dimethylamine group also projects deeper into the entrance cavity than observed for MB, and it may be argued that compound **1** establishes more productive Van der Waals interactions with the MAO-B entrance cavity that MB.

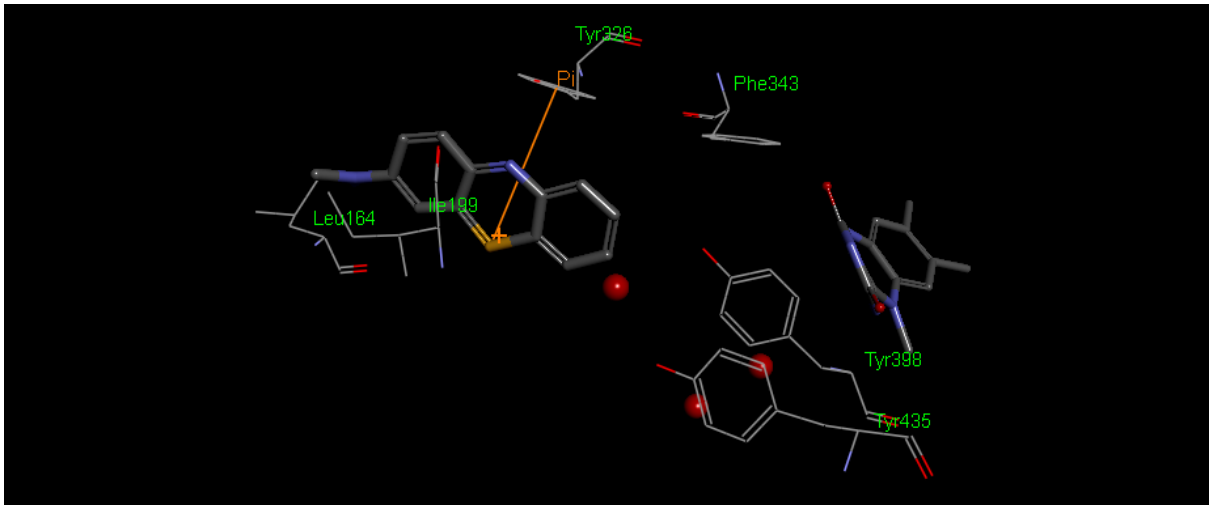

Figure 5.13. The docked binding orientation of compound **1** in MAO-B.

*Compound **2** docked into MAO-B:*

As shown in Figure 5.14, compound **2** docks into the MAO-B active site with a similar orientation to that observed in MAO-A and the thiazine sulphur is thus directed to the top of the active site, in the direction of Phe343. This orientation is similar to that observed for MB in MAO-B. Also similar to MB, compound **2** forms a π–π interaction with Tyr435, one of the amino acids that define the aromatic sandwich in the MAO-B active site. The dipropylamine group projects deep into the entrance cavity and possibly establishes Van der Waals interactions with the hydrophobic space of the MAO-B entrance cavity. Interestingly, compound **2** binds closer to the FAD than compound **1**.

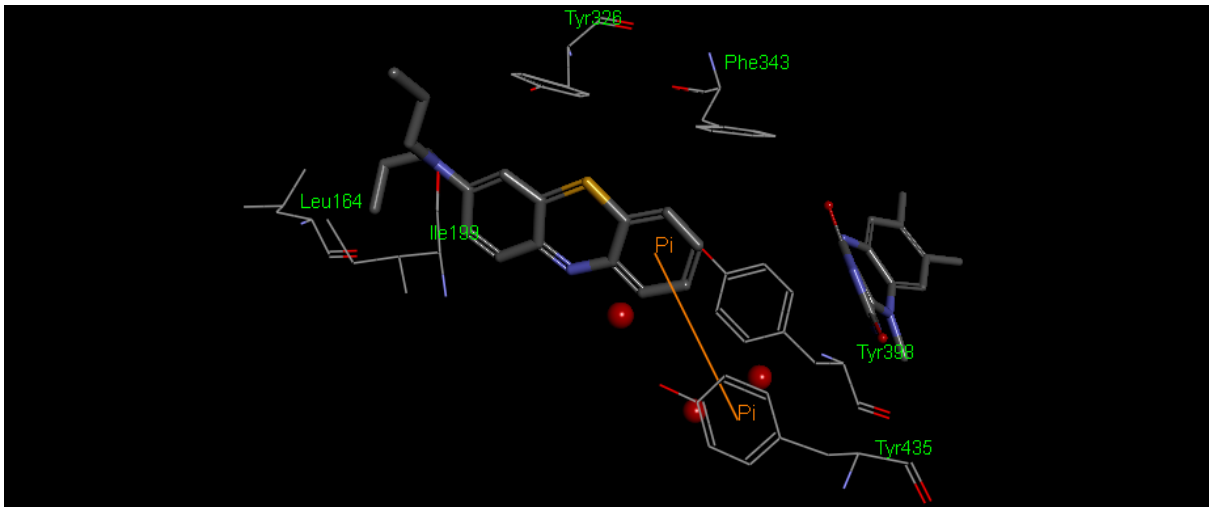

Figure 5.14. The docked binding orientation of compound **2** in MAO-B.

5.5.3 Molecular dynamics simulation

The orientation of a ligand in a protein binding site as determined by docking represents only a single pose in time. A ligand is, to a certain degree, free to move in the binding site and in doing so, interactions may break while new interactions are formed. To study this, a molecular dynamics simulation is performed during which the ligand is allowed to move around in the active site. For this study the trajectory of MB in MAO-B was investigated for 500 ps, recording a frame every 1 ps. MB was selected since experimental evidence supports the docked pose predicted by CDOCKER. As mentioned, the structure of MB in complex with human MAO-B, which bears the double mutation I199A-Y326A (PDB code: 3ZYX) is similar to the docked structure of MB in complex with human MAO-B.

The aim of this study was to:

- Determine the relative importance of each interaction between MB and MAO-B as determined in the docking study
- To determine if new interactions are formed as MB moves within the MAO-B active site
- To determine the relative freedom of movement of MB within the MAO-B active site

An analysis of the trajectory of MB shows that its orientation and placement in the MAO-B active site is relatively stable with an average RMSD from the initial docked orientation of 1.44 ± 0.32 Å. As mentioned, in the docked structure, MB forms a π–π interaction with Tyr435, one of the amino acids that define the aromatic sandwich in the MAO-B active site. Also MB does not extend as deep into the entrance cavity of MAO-B, with only the dimethylamine establishing contacts in the entrance cavity. In the trajectory, the π–π interaction between MB and Tyr435 is maintained for 138 frames (of a total of 500 frames), which demonstrates the importance of this interaction in the stabilisation of MB. In 64 frames, a π–π interaction between MB and Tyr398 also occur which shows that the aromatic cage residues (Tyr398 and Tyr435) collaborate to stabilise the structure of MB. Of much significance, however, is the finding that a π–cation interaction occurs between the thiazine sulphur of MB and Tyr326 in 480 frames, indicating that interaction is maintained almost throughout the trajectory of MB in the MAO-B active site. This interaction therefore is responsible for the relatively little movement of MB in the active site and Tyr326 may be viewed as anchor that restricts MB's movement.

No hydrogen bonding is observed between MB and MAO-B. The major interacting residues are given in Table 5.1, with the interaction energies (kcal/mol) as well as the average

percentage contribution to total interaction energy (%) of each residue. The most prominent Van der Waals interactions of MB with MAO-B thus occur with Ile171, Ile199, Gln206, Tyr326, Tyr398, Tyr435 and the FAD. These interactions contribute to on average 37.7% of the total interaction energy between MB and the MAO-B active site. Among these interactions, the Van der Waals interaction between Ile199 and MB is most productive and contributes 12.2% of the total interaction energy. Based on this analysis it may be concluded that MB is not only stabilised by the π–π interaction (with Tyr435) found in the docking study, but also by Van der Waals interactions (most notably with Ile199) and π–cation interactions (with Tyr326). It is noteworthy that the most productive interactions (Table 5.1) occur with residues in the substrate cavity and gating residues (Ile199), showing that MB does not appreciably protrude into the entrance cavity of MAO-B.

Table 5.1. The interaction energies between key MAO-B residues and MB.

	Interaction energy (kcal/mol)	**Average contribution to total interaction energy (%)**
Ile171	–3.95 ± 0.83	10.4%
Ile199	–4.64 ± 0.61	12.2%
Gln206	–2.94 ± 0.68	7.7%
Tyr326	–2.82 ± 0.31	7.4%
Tyr398	–2.12 ± 0.35	5.6%
Tyr436	–2.06 ± 0.46	5.4%
FAD	–2.75 ± 0.62	7.2%

All values are expressed as the mean ± SD of 500 frames.

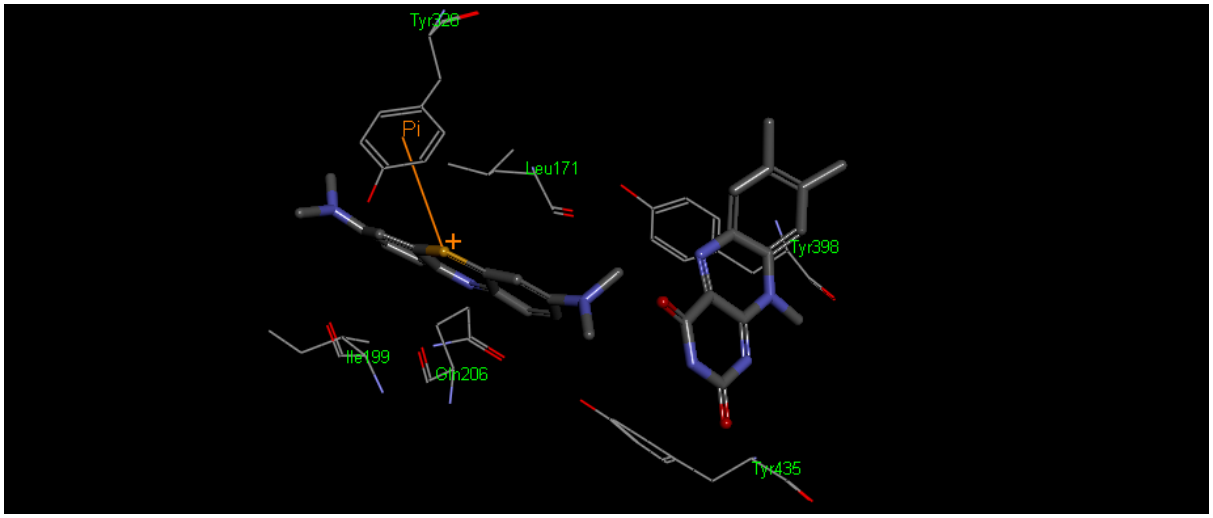

Figure 5.15. An orientation of MB in MAO-B, showing the π–cation interaction with Tyr326.

5.6 Summary

As mentioned at the beginning of this chapter, MB and compounds **1** and **2** exhibit different potencies and specificities for the MAO isoforms. Compound **1** is a highly potent MAO-B inhibitor, while MB and **2** are only moderately potent as MAO-B inhibitors. Also, MB is a much more potent inhibitor of MAO-A than either **1** or **2**. The modelling study showed that **2** is a particularly weak MAO-A inhibitor since a steric limitation on the dipropylamine group is imposed by Phe208. This compound thus binds with a different orientation compared to MB and **1**, which are more potent MAO-A inhibitors than **2**. MB, in turn, forms a π–cation interaction with the phenyl ring of Phe208 which may explain its potent MAO-A inhibition compared to **1**. Compound **1** approaches close to the FAD, which reduces the possibility of this π–cation interaction.

The results also show that MB docks into MAO-B with a similar orientation to that observed in the complex of MB with human MAO-B, which bears the double mutation I199A-Y326A. This provides good evidence of the accuracy of the docking study. Of note was the finding that compound **1** binds distant from the FAD compared to MB, and thus projects deeper into the entrance cavity to establish more productive Van der Waals interactions with the MAO-B entrance cavity than MB. This may explain the higher potency MAO-B inhibition of **1** compared to MB. A dynamics simulation showed that a π–cation interaction occurs between the thiazine sulphur of MB and Tyr326 in MAO-B. This interaction most likely acts as an anchor that restricts MB's movement in MAO-B. This study also showed that van der Waals interactions of the substrate cavity and gating residues are important for inhibitor stabilisation.

Chapter 6
Conclusion

6.1 Background

As discussed in the Introduction, MB is a known inhibitor of MAO-A with an *in vitro* IC_{50} value of 0.07 μM (Harvey *et al*., 2010; Ramsay *et al*., 2007). MB also inhibits the MAO-B isoform, but with lower potency compared to MAO-A. MB thus exhibits an IC_{50} value of 4.37 μM for the inhibition of MAO-B (Harvey *et al*., 2010). Since MAO-A inhibition is a well-established mechanism of action for the MAO inhibitor class of antidepressants, MB may, at least in part, exert an antidepressant action by inhibition of MAO-A. Indeed, MB exhibits promising antidepressant (Harvey *et al*., 2010) and anxiolytic (Eroğlu & Cağlayan, 1997) activity in pre-clinical models and clinical trials. The MAO-B inhibition component of MB's pharmacological profile, in turn, may find application in the treatment of Parkinson's disease. MAO-B inhibitors are established therapy for Parkinson's disease and are thought to act by elevating central dopamine levels.

6.2 Rationale of this study

While MB possesses an excellent safety profile, in combination with serotonergic agents such as serotonin reuptake inhibitors, MB can induce ST, which is a direct result of its ability to potently inhibit MAO-A. It may therefore be advantageous to "design-out" the MAO-A inhibition properties of MB in order to improve its safety profile. This study has synthesized two new derivatives of MB and characterised their *in vitro* interactions with recombinant human MAO-A and MAO-B.

6.3 Aims have been reached

Synthesis:

Using the protocol by Strekowski *et al*. (1993) this study has successfully synthesized two MB analogues, compounds **1** and **2**. The analogues were characterised by NMR and MS, which corresponded with the proposed structures. Both compounds are monosubstituted MB analogues. This study concludes that the synthetic protocol used is effective for only certain amine substrates, and that monosubstituted MB analogues are more readily obtained than disubstituted MB analogues.

IC_{50} values for the inhibition of the MAOs:

This study finds that compounds **1** and **2** inhibits MAO-A with IC_{50} values of 0.361 μM and 0.728 μM, respectively. Compared to MB, which exhibits an IC_{50} value of 0.07 μM for the inhibition of MAO-A, these compounds are relatively weaker MAO-A inhibitors (Aeschlimann *et al*., 1996; Harvey *et al*., 2010). Compounds **1** and **2** inhibit MAO-B with IC_{50} values of 0.105 μM and 1.16 μM, respectively. Compared to MB, which exhibits an IC_{50} value of 4.37 μM for the inhibition of MAO-B, these compounds are relatively more potent MAO-B inhibitors (Harvey *et al*., 2010; Ramsay *et al*., 2007). Compound **1**, in particular, is a potent MAO-B inhibitor and exhibits a similar IC_{50} value to the reference MAO-B inhibitor, lazabemide, which displays an IC_{50} value of 0.091 μM under identical experimental conditions to this study (Petzer *et al*., 2013).

Reversibility of MAO inhibition:

Employing dialysis, it was found that the synthesized MB analogues are reversible MAO inhibitors, although **2** may exhibit some tight-binding to MAO-B. Since reversible MAO-A inhibitors do not cause tyramine-induced hypertension, it may be concluded that the MB analogues should possess a good safety profile in this regard (Bonnet, 2003; Provost *et al*., 1992).

Lineweaver-Burk and Michaelis-Menten plots:

It was interesting to find that the Lineweaver-Burk plots constructed for the inhibition of the MAOs by **1** and **2** are not typical of competitive inhibition. For the inhibition of MAO-A by **1**, the Lineweaver-Burk plots are indicative of non-competitive inhibition. For all compounds, V_{max} for MAO-A and MAO-B is suppressed with increasing inhibitor concentration. A molecular explanation for this behaviour is not apparent, particularly when considering that MB exhibits a competitive mode of MAO-A inhibition (Ramsay *et al*., 2007).

6.4 Hypothesis

As hypothesized, the synthesized MB analogues act as inhibitors of human MAO-A and MAO-B. Compounds such as **1** that potently inhibit both MAO-A and MAO-B would be applicable for the treatment of Parkinson's disease where depression is a comorbidity. The observation that MAO-A inhibition is reversible reduces the possibility of tyramine-induced hypertension. For MAO-A inhibition, ST may, however, still occur.

It was found that **2** is approximately twofold less potent as a MAO-A inhibitor than **1**. This suggests that increasing the size of the dialkylamine side chain (as seen with **2**) lowers inhibition potency and larger MB analogues may thus be less well accommodated in the MAO-

A active site. The observation that MB is a higher potency MAO-A inhibitor than compounds **1** and **2** is not well understood on a molecular level. It is however clear that monosubstitution leads to lower MAO-A inhibition compared to the disubstitution of MB. The observation that **2** is approximately 11-fold less potent as a MAO-B inhibitor than **1**, suggests that increasing the size of the dialkylamine side chain (as seen with **2**) also lowers MAO-B inhibition potency. This trend is similar to that observed for MAO-A. Larger MB analogues may be less well accommodated in the MAO-B active site.

Chapter 7
Bibliography

Abi-Gerges, N., Eschenhagen, T., Hove-Madsen, L., Fischmeister, R. & Mery, P.F. 1997. Methylene blue is a muscarinic antagonist in cardiac myocytes. *Molecular pharmacology,* 52(3):482-490.

Aeschlimann, C., Cerny, T. & Küpfer, A. 1996. Inhibition of (mono)amine oxidase activity and prevention of ifosfamide encephalopathy by methylene blue. *Drug metabolism and disposition,* 24(12):1336-1339.

Ajithkumar, T., Parkinson, C., Shamshad, F. & Murray, P. 2007. Ifosfamide encephalopathy. *Clinical oncology,* 19(2):108-114.

Akoachere, M., Buchholz, K., Fischer, E., Burhenne, J., Haefeli, W.E., Schirmer, R.H. & Becker, K. 2005. *In vitro* assessment of methylene blue on chloroquine-sensitive and -resistant *Plasmodium falciparum* strains reveals synergistic action with artemisinins. *Antimicrobial agents and chemotherapy,* 49(11):4592-4597.

Albert, M., Lessin, M.S. & Gilchrist, B.F. 2003. Methylene blue: Dangerous dye for neonates. *Journal of pediatric surgery,* 38(8):1244-1245.

Alici-Evcimen, Y. & Breitbart, W.S. 2007. Ifosfamide neuropsychiatric toxicity in patients with cancer. *Psycho-oncology,* 16(10):956-960.

Amara, S.G. & Kuhar, M.J. 1993. Neurotransmitter transporters: Recent progress. *Annual review of neuroscience,* 16:73-93.

Atamna, H., Nguyen, A., Schultz, C., Boyle, K., Newberry, J., Kato, H. & Ames, B.N. 2008. Methylene blue delays cellular senescence and enhances key mitochondrial biochemical pathways. *FASEB journal,* 22(3):703-712.

Bach, K.K., Lindsay, F.W., Berg, L.S. & Howard, R.S. 2004. Prolonged postoperative disorientation after methylene blue infusion during parathyroidectomy. *Anesthesia and analgesia,* 99(5):1573-1574.

Barbosa, P. & Peters, T.M. 1971. The effects of vital dyes on living organisms with special reference to methylene blue and neutral red. *The histochemical journal,* 3(1):71-93.

Bennett, M.C., Diamond, D.M., Stryker, S.L., Parks, J.K. & Parker Jr., W.D. 1992. Cytochrome oxidase inhibition: A novel animal model of Alzheimer's disease. *Journal of geriatric psychiatry and neurology,* 5(2):93-101.

Bernstein, H.-G,Stanarius, A., Baumann, B., Henning, H., Krell, D., Danos, P., Falkai, P. & Bogerts, B. 1998. Nitric oxide synthase-containing neurons in the human hypothalamus: Reduced number of immunoreactive cells in the paraventricular nucleus of depressive patients and schizophrenics. *Neuroscience,* 83(3):867-875.

Binda, C., Newton-Vinson, P., Hubálek, F., Edmondson, D.E. & Mattevi, A. 2002. Structure of human monoamine oxidase B, a drug target for the treatment of neurological disorders. *Nature structural biology,* 9(1):22-26.

Binda, C., Wang, J., Pisani, L., Caccia, C., Carotti, A., Salvati, P., Edmondson, D.E. & Mattevi, A. 2007. Structures of human monoamine oxidase B complexes with selective noncovalent inhibitors: Safinamide and coumarin analogs. Journal of medicinal chemistry, 50(23):5848-5852.

Bongard, R.D., Krenz, G.S., Linehan, J.H., Roerig, D.L., Merker, M.P., Widell, J.L. & Dawson, C.A. 1994. Reduction and accumulation of methylene blue by the lung. *Journal of applied physiology,* 77(3):1480-1491.

Bonnet, U. 2003. Moclobemide: Therapeutic use and clinical studies. *CNS drug reviews,* 9(1):97-140.

Brink, C.B., Clapton, J.D., Eagar, B.E. & Harvey, B.H. 2008. Appearance of antidepressant-like effect by sildenafil in rats after central muscarinic receptor blockade: Evidence from behavioural and neuro-receptor studies. *Journal of neural transmission,* 115(1):117-125.

Brunton, L.L., Chabner, B.A. & Knollman, B.C. 2010. Goodman & Gillman's: The pharmacological basis of therapeutics. 12th ed. New York: McGraw-Hill.

Buchholz, K., Schirmer, R.H., Eubel, J.K., Akoachere, M.B., Dandekar, T., Becker, K. & Gromer, S. 2008. Interactions of methylene blue with human disulfide reductases and their orthologues from *Plasmodium falciparum*. *Antimicrobial agents and chemotherapy,* 52(1):183-191.

Caro H. 1877. Engl. Pat. 3751. 9/10.

Cawein, M., Behlen II, C.H., Lappat, E.J. & Cohn, J.E. 1964. Hereditary diaphorase deficiency and methemoglobinemia. *Archives of internal medicine,* 113(4):578-585.

Cheng, K.K. 1954. Intra-arterial injection of methylene blue for staining nerve endings in striated muscles. *Nature,* 173(4402):492-493.

Clifton 2nd, J. & Leikin, J.B. 2003. Methylene blue. *American journal of therapeutics,* 10(4):289-291.

Coulibaly, B., Zoungrana, A., Mockenhaupt, F.P., Schirmer, R.H., Klose, C., Mansmann, U., Meissner, P.E. & Müller, O. 2009. Strong gametocytocidal effect of methylene blue-based combination therapy against falciparum malaria: A randomised controlled trial. *PLoS ONE,* 4(5):e5318.

Culo, F., Sabolovic, D., Somogyi, L., Marušic, M., Berbiguier, N. & Galey, L. 1991. Anti-tumoral and anti-inflammatory effects of biological stains. *Agents and actions,* 34(3-4):424-428.

Da Prada, M., Zürcher, G., Wüthrich, I. & Haefely, W.E. 1988. On tyramine, food, beverages and the reversible MAO inhibitor moclobemide. *Journal of neural transmission, supplement,* 26:31-56.

Dawson, T.M. & Snyder, S.H. 1994. Gases as biological messengers: Nitric oxide and carbon monoxide in the brain. *Journal of neuroscience,* 14(9):5147-5159.

Deiana, S., Harrington, C.R., Wischik, C.M. & Riedel, G. 2009. Methylthioninium chloride reverses cognitive deficits induced by scopolamine: Comparison with rivastigmine. *Psychopharmacology,* 202(1-3):53-65.

Delport, A., Harvey, B.H., Petzer, A. & Petzer, J.P. 2014. Azure B and a synthetic structural analogue of methylene blue, ethylthioninium chloride, present with antidepressant-like properties. *Life sciences,* 117(2):56-66.

Di Cataldo, A., Astuto, M., Rizzo, G., Bertuna, G., Russo, G. & Incorpora, G. 2009. Neurotoxicity during ifosfamide treatment in children. *Medical science monitor,* 15(1):CS22-CS25.

Dioni, W. 2011. The use of “Brillant Blue #1” as a nuclear dye useful for amateur microscopists, and notes on Fast Green FCF. http://www.microscopy-uk.org.uk/mag/indexmag.html?http://www.microscopy-uk.org.uk/mag/artmay11/wd-Brilliant-Blue-1.html Date of access: 30 Jan. 2017.

DiSanto, A.R. & Wagner, J.G. 1972. Pharmacokinetics of highly ionized drugs. II. methylene blue--absorption, metabolism, and excretion in man and dog after oral administration. *Journal of pharmaceutical sciences,* 61(7):1086-1090.

Do Nascimento, T.S., Pereira, R.O., De Mello, H.L. & Costa, J. 2008. Methemoglobinemia: From diagnosis to treatment. *Revistabrasileira de anestesiologia,* 58(6):651-664.

Edmondson, D.E., DeColibus, L., Binda, C., Li, M. & Mattevi, A. 2007. New insights into the structures and functions of human monoamine oxidases A and B. *Journal of neural transmission,* 114(6):703-705.

Eroğlu, L. & Çağlayan, B. 1997. Anxiolytic and antidepressant properties of methylene blue in animal models. *Pharmacological research*, 36(5):381-385.

Felgenträger, A., Maisch, T., Dobler, D. & Späth, A. 2013. Hydrogen bond acceptors and additional cationic charges in methylene blue derivatives: Photophysics and antimicrobial efficiency. *BioMed research international,* 2013. doi:10.1155/2013/482167.

Finberg, J.P.M., Takeshima,T., Johnston,J.M. & Commissiong,J.W. 1998. Increased survival of dopaminergic neurons by rasagiline, a monoamine oxidase B inhibitor. *Neuroreport*, 9(4):703-707.

Flockhart, D.A. 2012. Dietary restrictions and drug interactions with monoamine oxidase inhibitors: An update. Journal of clinical psychiatry, 73:17-24.

Gardner, A., Johansson, A., Wibom, R., Nennesmo, I., Von Döbeln, U., Hagenfeldt, L. & Hällström, T. 2003. Alterations of mitochondrial function and correlations with personality traits in selected major depressive disorder patients. *Journal of affective disorders,* 76(1-3):55-68.

Garthwaite, J. 1991. Glutamate, nitric oxide and cell-cell signalling in the nervous system. Trends in neurosciences, 14(2):60-67.

Garthwaite, J., Garthwaite, G., Palmer, R.M.J. & Moncada, S. 1989. NMDA receptor activation induces nitric oxide synthesis from arginine in rat brain slices. *European journal of pharmacology: Molecular pharmacology,* 172(4-5):413-416.

Ghaemi, S.N., Lenox, M.S. & Baldessarini, R.J. 2001. Effectiveness and safety of long-term antidepressant treatment in bipolar disorder. *Journal of clinical psychiatry,* 62(7):565-569.

Giacobini, E. 2003. Cholinesterases: New roles in brain function and in Alzheimer's disease. *Neurochemical research*, 28(3-4):515-522.

Gillman, P.K. 2011. Advances pertaining to the pharmacology and interactions of irreversible nonselective monoamine oxidase inhibitors. Journal of clinical psychopharmacology, 31:66-74.

Glover, V., Sandler, M., Grant, E., Rose, F.C., Orton, D., Wilkinson, M. & Stevens, D. 1977. Transitory decrease in platelet monoamine-oxidase activity during migraine attacks. *The lancet,* 309(8008):391-393.

Gonzalez-Lima, F. & Bruchey, A.K. 2004. Extinction memory improvement by the metabolic enhancer methylene blue. *Learning and memory,* 11(5):633-640.

Gonzalez-Lima, F., Valla, J. & Matos-Collazo, S. 1997. Quantitative cytochemistry of cytochrome oxidase and cellular morphometry of the human inferior colliculus in control and Alzheimer's patients. Brain research, 752(1-2):117-126.

Gorman, S.A., Bell, A.L., Griffiths, J., Roberts, D. & Brown, S.B. 2006. The synthesis and properties of unsymmetrical 3,7-diaminophenothiazin-5-ium iodide salts: Potential photosensitisers for photodynamic therapy. *Dyes and pigments,* 71(2):153-160.

Grieg, N.H., Kamal, M.A., Jabir, N.R., Tabrez, S., Nasim, F.H., Abuzenadah, A.M. & Aliev, G. 2014. Chapter 6 - specific cholinesterase inhibitors: A potential tool to assist in management of Alzheimer disease. (*In* Choudhary, A.I., *ed*. Drug design and discovery in Alzheimer's disease. UK: Bentham Science Publishers Ltd. p. 366-386).

Griscavage, J.M., Fukuto, J.M., Komori, Y. & Ignarro, L.J. 1994. Nitric oxide inhibits neuronal nitric oxide synthase by interacting with the heme prosthetic group. role of tetrahydrobiopterin in modulating the inhibitory action of nitric oxide. *Journal of biological chemistry,* 269(34):21644-21649.

Harkin, A.J., Bruce, K.H., Craft, B. & Paul, I.A. 1999. Nitric oxide synthase inhibitors have antidepressant-like properties in mice: 1. Acute treatments are active in the forced swim test. *European journal of pharmacology,* 372(3):207-213.

Harvey, B.H. 1996. Affective disorders and nitric oxide: A role in pathways to relapse and refractoriness? *Human psychopharmacology,* 11(4):309-319.

Harvey, B.H. 2008. Is major depressive disorder a metabolic encephalopathy? *Human psychopharmacology: Clinical and experimental*, 23:371-384.

Harvey, B.H., Carstens, M.E. & Taljaard, J.J.F. 1994. Evidence that lithium induces a glutamatergic-nitric oxide-mediated response in rat brain. *Neurochemical research*, 19:469 474.

Harvey, B.H., Duvenhage, I., Viljoen, F., Scheepers, N., Malan, S.F., Wegener, G., Brink, C.B. & Petzer, J.P. 2010. Role of monoamine oxidase, nitric oxide synthase and regional brain monoamines in the antidepressant-like effects of methylene blue and selected structural analogues. *Biochemical pharmacology,* 80(10):1580-1591.

Harvey, B.H., Stein, D.J. & Emsley, R.A. 1999. The new-generation antipsychotics - integrating the neuropathology and pharmacology of schizophrenia. South African medical journal, 89(6):661-672.

Haynes, R.K., Chan, W.C., Wong, H.N., Li, K.Y., Wu, W.K., Fan, K.M., Sung, H.H., Williams, I.D., Prosperi, D., Melato, S., Coghi, P. & Monti, D. 2010. Facile oxidation of leucomethylene blue and dihydroflavins by artemisinins: Relationship with flavoenzyme function and antimalarial mechanism of action. *ChemMedChem,* 5(8):1282-1299.

Hibbs Jr., J.B., Taintor, R.R. & Vavrin, Z. 1987. Macrophage cytotoxicity: Role for L-arginine deiminase and imino nitrogen oxidation to nitrite. *Science,* 235(4787):473-476.

Holzgrabe, U., Kapková, P., Alptüzün, V., Scheiber, J. & Kugelmann, E. 2007. Targeting acetylcholinesterase to treat neurodegeneration. *Expert opinion on therapeutic targets,* 11(2):161-179.

Imaizumi, R., Omori, K., Unoki, A., Sano, K., Watari, Y., Namba, J. & Inui, K. 1959. Physiological significance of monoamine oxidase. *Japanese journal of pharmacology,* 887-95.

Kessler, R.C., Berglund, P., Demler, O., Jin, R., Merikangas, K.R. & Walters, E.E. 2005. Erratum: Lifetime prevalence and age-of-onset distributions of DSM-IV disorders in the national comorbidity survey replication. *Archives of general psychiatry,* 62(6):593-602.

Kouyaté, B., Sie, A., Yé, M., De Allegri, M. & Müller, O. 2007. The great failure of malaria control in Africa: A district perspective from Burkina Faso. *PLoS medicine,* 4(6):0997-1000.

Krass, M., Wegener, G., Vasar, E. & Volke, V. 2011. The antidepressant action of imipramine and venlafaxine involves suppression of nitric oxide synthesis. Behavioural brain research, 218(1):57-63.

Liebenberg, N., Harvey, B.H., Brand, L. & Brink, C.B. 2010. Antidepressant-like properties of phosphodiesterase type 5 inhibitors and cholinergic dependency in a genetic rat model of depression. *Behavioural pharmacology,* 21(5-6):540-547.

Lo, J.C.Y., Darracq, M.A. & Clark, R.F. 2014. A review of methylene blue treatment for cardiovascular collapse. *Journal of emergency medicine,* 46(5):670-679.

Lorke, D.E., Kalasz, H., Petroianu, G.A. & Tekes, K. 2008. Entry of oximes into the brain: A review. *Current medicinal chemistry,* 15(8):743-753.

Louters, L.L., Dyste, S.G., Frieswyk, D., TenHarmsel, A., Vander Kooy, T.O., Walters, L. & Whalen, T. 2006. Methylene blue stimulates 2-deoxyglucose uptake in L929 fibroblast cells. *Life sciences,* 78(6):586-591.

Lu, Y.T., Arai, C., Ge, J.F., Ren, W.S., Kaiser, M., Wittlin, S., Brun, R., Lu, J.M. & Ihara, M. 2011. Synthesis and in vitro antiprotozoal activities of water-soluble, inexpensive phenothiazinium chlorides. *Dyes and pigments,* 89(1):44-48.

Luna-Muñoz, J., Peralta-Ramirez, J., Chávez-Macías, L., Harrington, C.R., Wischik, C.M. & Mena, R. 2008. Thiazin red as a neuropathological tool for the rapid diagnosis of Alzheimer's disease in tissue imprints. *Acta neuropathologica,* 116(5):507-515.

Mayer, B., Brunner, F. & Schmidt, K. 1993. Inhibition of nitric oxide synthesis by methylene blue. *Biochemical pharmacology,* 45(2):367-374.

McCord, J.M. & Fridovich, I. 1969. The utility of superoxide dismutase in studying free radical reactions. I. Radicals generated by the interaction of sulfite, dimethyl sulfoxide, and oxygen. *Journal of biological chemistry,* 244(22):6056-6063.

Moncada, S., Palmer, R.M.J. & Higgs, E.A. 1991. Nitric oxide: Physiology, pathophysiology, and pharmacology. *Pharmacological reviews,* 43(2):109-142.

Moore, P.K. & Handy, R.L.C. 1997. Selective inhibitors of neuronal nitric oxide synthase - is no NOS really good NOS for the nervous system? *Trends in pharmacological sciences,* 18(6):204-211.

Mudher, A. & Lovestone, S. 2002. Alzheimer's disease - do tauists and baptists finally shake hands? *Trends in neurosciences,* 25(1):22-26.

Müller, T. 1996. Supravital uptake of methylene blue by dendritic cells within stratified squamous epithelia: A light and electron microscope study. *Biotechnic and histochemistry,* 71(2):96-101.

Müller, T. 1998. Methylene blue supravital staining: An evaluation of its applicability to the mammalian brain and pineal gland. *Histology and histopathology,* 13(4):1019-1026.

Müller, T. 2000. Supravital methylene blue staining of piloneural complexes of common fur hair follicles in the rat. *Biotechnic and histochemistry,* 75(6):245-250.

Narsapur, S.L. & Naylor, G.J. 1983. Methylene blue. A possible treatment for manic depressive psychosis. *Journal of affective disorders,* 5(2):155-161.

Naylor, G.J., Martin, B., Hopwood, S.E. & Watson, Y. 1986. A two-year double-blind crossovertrial of the prophylactic effect of methylene blue in manic-depressive psychosis. *Biological psychiatry*, 21:915-920.

Naylor, G.J., Smith, A.H.W. & Conelly, P. 1987. A controlled trial of methylene blue in severe depressive illness. *Biological psychiatry*, 22:657-659.

Necula, M., Breydo, L., Milton, S., Kayed, R., Van Der Veer, W.E., Tone, P. & Glabe, C.G. 2007. Methylene blue inhibits amyloid aβ oligomerization by promoting fibrillization. *Biochemistry,* 46(30):8850-8860.

Nordberg, A. 2006. Emerging biology of the cholinergic system across the spectrum of Alzheimer's disease. International psychogeriatrics, 18(5):S3-S16.

Novaroli, L., Reist, M., Favre, E., Carotti, A., Catto, M. & Carrupt, P. 2005. Human recombinant monoamine oxidase B as reliable and efficient enzyme source for inhibitor screening. Bioorganic & medicinal chemistry, 13(22):6212-6217.

Ohlow, M.J. & Moosmann, B. 2011. Phenothiazine: The seven lives of pharmacology's first lead structure. *Drug discovery today,* 16(3-4):119-131.

Oosthuizen, F., Wegener, G. & Harvey, B.H. 2005. Nitric oxide as inflammatory mediator in post-traumatic stress disorder (PTSD): evidence from an animal model. *Neuropsychiatric disease and treatment,* 12:109-123.

Oxenkrug, G.F., Sablin, S.O. & Requintina, P.J. 2007. Effect of methylene blue and related redox dyes on monoamine oxidase activity; rat pineal content of N-acetylserotonin, melatonin, and related indoles; and righting reflex in melatonin-primed frogs. *Annals of the New York academy of sciences,* 1122:245-252.

Oz, M., Isaev, D., Lorke, D.E., Hasan, M., Petroianu, G. & Shippenberg, T.S. 2012. Methylene blue inhibits function of the 5-HT transporter. *British journal of pharmacology,* 166(1):168-176.

Oz, M., Lorke, D.E. & Petroianu, G.A. 2009. Methylene blue and Alzheimer's disease. Biochemical pharmacology, 78(8):927-932.

Oz, M., Lorke, D.E., Hasan, M. & Petroianu, G.A. 2011. Cellular and molecular actions of methylene blue in the nervous system. *Medicinal research reviews,* 31(1):93-117.

Pålhagen, S., Heinonen, E.H., Hägglund, J., Kaugesaar, T., Kontants, H., Mäki-Ikola, O., Palm, R. & Turunen, J. 1998. Selegiline delays the onset of disability in de novo parkinsonian patients. Neurology, 51(2):520-525.

Palmer, R.M.J., Ferrige, A.G. & Moncada, S. 1987. Nitric oxide release accounts for the biological activity of endothelium-derived relaxing factor. *Nature,* 327(6122):524-526.

Peter, C., Hongwan, D., Küpfer, A. & Lauterburg, B.H. 2000. Pharmacokinetics and organ distribution of intravenous and oral methylene blue. *European journal of clinical pharmacology,* 56(3):247-250.

Petzer, A., Harvey, B.H. & Petzer, J.P. 2014. The interactions of azure B, a metabolite of methylene blue, with acetylcholinesterase and butyrylcholinesterase. Toxicology and applied pharmacology, 274(3):488-493.

Petzer, A., Harvey, B.H., Wegener, G. & Petzer, J.P. 2012. Azure B, a metabolite of methylene blue, is a high-potency, reversible inhibitor of monoamine oxidase. *Toxicology and applied pharmacology,* 258(3):403-409.

Petzer, A., Pienaar, A. & Petzer, J.P. 2013. The inhibition of monoamine oxidase by esomeprazole. Drug research, 63(9):462-467.

Pfaffendorf, M., Bruning, T.A., Batink, H.D. & Van Zwieten, P.A. 1997. The interaction between methylene blue and the cholinergic system. *British journal of pharmacology,* 122(1):95-98.

Provost, J.C.,Funck-Brentano, C., Rovei, V., D'Estanque, J., Ego, D. & Jaillon, P. 1992. Pharmacokinetic and pharmacodynamic interaction between toloxatone, a new reversible monoamine oxidase-A inhibitor, and oral tyramine in healthy subjects. *Clinical pharmacology and therapeutics,* 52(4):384-393.

Querfurth, H.W. & LaFerla, F.M. 2010. Alzheimer's disease. *New England journal of medicine,* 362(4):329-344.

Ramsay, R.R., Dunford, C. & Gillman, P.K. 2007. Methylene blue and serotonin toxicity: Inhibition of monoamine oxidase A (MAO A) confirms a theoretical prediction. *British journal of pharmacology,* 152(6):946-951.

Rana, A.Q., Qureshi, A.R.M., Rahman, L., Jesudasan, A., Hafez, K.K. & Rana, M.A. 2016. Association of restless legs syndrome, pain, and mood disorders in Parkinson's disease. *International journal of neuroscience,* 126(2):116-120.

Reif, A., Strobel, A., Jacob, C.P., Herterich, S., Freitag, C.M., Töpner, T., Mössner, R., Fritzen, S., Schmitt, A. & Lesch, K.P. 2006. A NOS-III haplotype that includes functional polymorphisms is associated with bipolar disorder. *International journal of neuropsychopharmacology,* 9(1):13-20.

Rojas, J.C., Bruchey, A.K. & Gonzalez-Lima, F. 2012. Neurometabolic mechanisms for memory enhancement and neuroprotection of methylene blue. *Progress in neurobiology,* 96(1):32-45.

Salaris, S.C., Babbs, C.F. & Voorhees III, W.D. 1991. Methylene blue as an inhibitor of superoxide generation by xanthine oxidase. A potential new drug for the attenuation of ischemia/reperfusion injury. *Biochemical pharmacology,* 42(3):499-506.

Schirmer, R.H., Adler, H., Pickhardt, M. & Mandelkow, E. 2011. “Lest we forget you — methylene blue …”. 2011. Neurobiology of aging, 32(12):2325.e7-2325.e16.

Schirmer, R.H., Coulibaly, B., Stich, A., Scheiwein, M., Merkle, H., Eubel, J., Becker, K., Becher, H., Müller, O., Zich, T., Schiek, W. & Kouyaté, B. 2003. Methylene blue as an antimalarial agent. *Redox report,* 8(5):272-275.

Schneider, F., Lutun, P., Hasselmann, M., Stoclet, J.C. & Tempé, J.D. 1992. Methylene blue increases systemic vascular resistance in human septic shock - preliminary observations. *Intensive care medicine,* 18(5):309-311.

Scott, A. & Hunter Jr., F.E. 1966. Support of thyroxine-induced swelling of liver mitochondria by generation of high energy intermediates at any one of three sites in electron transport. *Journal of biological chemistry,* 241(5):1060-1066.

Shih, J.C., Chen, K. & Ridd, M.J. 1999. Monoamine oxidase: From genes to behavior. Annual review of neuroscience, 22:197-217.

Singh, R., Vinayagam, S. & Vajifdar, H. 2012. Methemoglobinemia as a result of accidental lacquer thinner poisoning. *Indian journal of critical care medicine,* 16(1):44-47.

Son, S.-Y., Ma, J., Kondou, Y., Yoshimura, M., Yamashita, E. & Tsukihara, T. 2008. Structure of human monoamine oxidase A at 2.2-Å resolution: The control of opening the entry for substrates/inhibitors. Proceedings of the national academy of sciences of the United States of America, 105(15):5739-5744.

Strekowski, L., Hou, D.-F.,Wydra, R.L. & Schinazi, R.F. 1993. A synthetic route to 3-(dialkylamino)phenothiazin-5-ium salts and 3,7- disubstituted derivatives containing two different amino groups. *Journal of heterocyclic chemistry,* 30(6):1693-1696.

Strydom, B., Malan, S.F., Castagnoli Jr., N., Bergh, J.J. & Petzer, J.P. 2010. Inhibition of monoamine oxidase by 8-benzyloxycaffeine analogues. Bioorganic and medicinal chemistry, 18(3):1018-1028.

Sullivan, K. 2008. A survey of community awareness of Alzheimer's disease: What are the common misconceptions? *International journal of geriatric psychiatry,* 23(12):1320-1322.

Suzuki, E., Yagi, G., Nakaki, T., Kanba, S. & Asai, M. 2001. Elevated plasma nitrate levels in depressive states. *Journal of affective disorders,* 63:221-224.

Sweet, G. & Standiford, S.B. 2007. Methylene-blue-associated encephalopathy. *Journal of the american college of surgeons,* 204(3):454-458.

Taniguchi, S., Suzuki, N., Masuda, M., Hisanaga, S.,Iwatsubo, T., Goedert, M. & Hasegawa, M. 2005. Inhibition of heparin-induced tau filament formation by phenothiazines, polyphenols, and porphyrins. *Journal of biological chemistry,* 280(9):7614-7623.

Tardivo, J.P., Del Giglio, A., De Oliveira, C.S., Gabrielli, D.S., Junqueira, H.C., Tada, D.B., Severino, D., De FátimaTurchiello, R. & Baptista, M.S. 2005. Methylene blue in photodynamic therapy: From basic mechanisms to clinical applications. *Photodiagnosis and photodynamic therapy,* 2(3):175-191.

Tariot, P.N., Cohen, R.M., Sunderland, T., Newhouse, P.A., Yount, D., Mellow, A.M., Weingartner, H., Mueller, E.A. & Murphy, D.L. 1987. L-deprenyl in Alzheimer's disease. Preliminary evidence for behavioral change with monoamine oxidase B inhibition. *Archives of general psychiatry,* 44(5):427-433.

Tretter, L., Horvath, G., Hölgyesi, A., Essek, F. & Adam-Vizi, V. 2014. Enhanced hydrogen peroxide generation accompanies the beneficial bioenergetic effects of methylene blue in isolated brain mitochondria. *Free radical biology and medicine,* 77317-330.

Vennerstrom, J.L., Makler, M.T., Angerhofer, C.K. & Williams, J.A. 1995. Antimalarial dyes revisited: Xanthenes, azines, oxazines and thiazines. *Antimicrobial agents and chemotherapy,* 39(12):2671-2677.

Volke, V., Wegener, G., Vasar, E. & Rosenberg, R. 1999. Methylene blue inhibits hippocampal nitric oxide synthase activity in vivo. *Brain research,* 826(2):303-305.

Wagner, S.J., Skripchenko, A., Robinette, D., Foley, J.W. & Cincotta, L. 1998. Factors affecting virus photoinactivation by a series of phenothiazine dyes. *Photochemistry and photobiology,* 67(3):343-349.

Wainwright, M. & Crossley, K.B. 2002. Methylene blue - A therapeutic dye for all seasons? *Journal of chemotherapy,* 14(5):431-443.

Wainwright, M., Meegan, K., Loughran, C. & Giddens, R.M. 2009. Phenothiazinium photosensitisers, part VI: Photobactericidal asymmetric derivatives. *Dyes and pigments,* 82(3):387-391.

Walter-Sack, I., Rengelshausen, J., Oberwittler, H., Burhenne, J., Mueller, O., Meissner, P. & Mikus, G. 2009. High absolute bioavailability of methylene blue given as an aqueous oral formulation. *European journal of clinical pharmacology,* 65(2):179-189.

Warth, A., Goeppert, B., Bopp, C., Schirmacher, P., Flechtenmacher, C. & Burhenne, J. 2009. Turquoise to dark green organs at autopsy. *Virchowsarchiv,* 454(3):341-344.

Wegener, G., Harvey, B.H., Bonefeld, B., Müller, H.K., Volke, V., Overstreet, D.H. & Elfving, B. 2010. Increased stress-evoked nitric oxide signalling in the flinders sensitive line (FSL) rat: A genetic animal model of depression. *International journal of neuropsychopharmacology,* 13(4):461-473.

Wegener, G., Volke, V. & Rosenberg, R. 2000. Endogenous nitric oxide decreases hippocampal levels of serotonin and dopamine in vivo. *British journal of pharmacology,* 130(3):575-580.

Wischik, C.M., Edwards, P.C., Lai, R.Y.K., Roth, M. & Harrington, C.R. 1996. Selective inhibition of Alzheimer disease-like tau aggregation by phenothiazines. *Proceedings of the national academy of sciences of the United States of America,* 93(20):11213-11218.

Wischik, C.M., Rickard, J.E., Harrington, C.R., Horsley, D., Storey, J.M.D., Marshall, C., Sinclair,J.P. & Wan Tan, H. 2006. Methods of chemical synthesis and purification of diaminophenothiazinium compounds including methylthioninium chloride. (Patent: US 2006/0287523 A1).

Wiseman, V., Kim, M., Mutabingwa, T.K. & Whitty, C.J.M. 2006. Cost-effectiveness study of three antimalarial drug combinations in Tanzania. *PLoS medicine,* 3(10):1844-1850.

Wong-Riley, M.T.T. 1989. Cytochrome oxidase: An endogenous metabolic marker for neuronal activity. *Trends in neurosciences,* 12(3):94-101.

Youdim, M.B.H. & Bakhle, Y.S. 2006. Monoamine oxidase: Isoforms and inhibitors in Parkinson's disease and depressive illness. *British journal of pharmacology*, 147:287.

Zhang, X., Rojas, J.C. & Gonzalez-Lima, F. 2006. Methylene blue prevents neurodegeneration caused by rotenone in the retina. *Neurotoxicity research,* 9(1):47-57.

Ziv, G. & Heavner, J.E. 1984. Permeability of the blood-milk barrier to methylene blue in cows and goats. *Journal of veterinary pharmacology and therapeutics,* 7(1):55-59.

Zoungrana, A., Coulibaly, B., Sié, A., Walter-Sack, I., Mockenhaupt, F.P., Kouyaté, B., Schirmer, R.H., Klose, C., Mansmann, U., Meissner, P. & Müller, O. 2008. Safety and efficacy of methylene blue combined with artesunate or amodiaquine for

uncomplicated falciparum malaria: A randomized controlled trial from Burkina Faso. *PLoS ONE*, 3(2):e1630.